Immobilization of gold nanoparticles for colourimetric detection of biofilms on surfaces

by

Sarah Ann LeBlanc

A thesis
presented to the University of Waterloo
in fulfillment of the
thesis requirement for the degree of
Master of Applied Science
in
Chemical Engineering

Waterloo, Ontario, Canada, 2015

AUTHOR'S DECLARATION

I hereby declare that I am the sole author of this thesis. This is a true copy of the thesis, including any required final revisions, as accepted by my examiners.

I understand that my thesis may be made electronically available to the public.

Abstract

Biofilms in contact lens cases amplify the risk of microbial and infiltrative keratitis, which can lead to severe eye damage and vision loss. A method warning users of biofilm contamination on the contact lens case surface is needed so they can discontinue use of the case to prevent related eye infections. Biosensors based on gold nanoparticles in solution are being explored as they can provide a simple colourimetric sensor response to bacteria. However, for consumer-level applications, gold nanoparticle-based biosensors need to be immobilized onto a surface to reduce potential health risks associated with nanomaterial exposure.

This thesis focuses on the development of an immobilized gold nanoparticle biosensor for the colourimetric detection of biofilms on surfaces. Development of the biosensor begins with controlling the deposition of gold nanoparticles onto the surface, as their immobilization state dictates the optical properties critical to the sensor performance. A literature review of the current methods to immobilize colloidal gold nanoparticles demonstrates that there are a variety of strategies to control the immobilization state. Building on current strategies, a new method to immobilize charged gold nanoparticles is explored through modification of the surface with weak polyelectrolytes. By varying the deposition pH of weak polyelectrolytes, the electrostatic immobilization of gold nanoparticles can be tuned from dispersed particles to large three-dimensional particle aggregates, producing a broad range of optical properties. The ability to modulate the immobilization state is dependent on the polyelectrolyte used as well as the particle size.

Using the developed method, an optimal immobilization state of the gold nanoparticles is used to create the colourimetric biosensor. Having populations of both single and small clusters of gold nanoparticles on the surface, a visible colour change from red to blue is produced with an increase in refractive index. This biosensor surface is capable of detecting biofilms from Gram-positive *Staphylococcus aureus* and Gram-negative *Achromobacter xylosoxidans* visually and through simple image analysis. Finally, the colourimetric biosensor was successfully integrated onto and capable of detecting the presence of biofilm on plastic substrates, including a commercial contact lens case.

This work demonstrates the capabilities of this immobilized gold nanoparticle biosensor as a new platform for the detection of biofilms on surfaces. In addition to biofilm detection in contact lens cases, this technology can be exploited for biofilm detection in healthcare, food services and water treatment industries.

Acknowledgements

First and foremost I thank my supervisor, Professor Frank Gu, for his continual advice, guidance and support throughout my research. I also extend my gratitude to my external mentor and collaborator, Professor Lyndon Jones, who provided guidance and resources to enable the success of my project.

I would like to acknowledge various research groups and individuals for providing help and resources throughout this research project. I am thankful to Lei Zhang from Professor Pu Chen's group for help with atomic force microscopy imaging, and BumSok (Brandon) Seo from Professor Ting Tsui's group for help with scanning electron microscopy imaging. I am also thankful to Brendan McDonald from Professor Boxin Zhao's group for help using the ultra violet ozone and contact angle analysis instruments. I acknowledge the help from Dr. Liyan Zhao from Professor Tong Leung's group for performing x-ray photoelectron spectroscopy analysis. I am especially grateful to Shih-Chung Wei and Professor Chii-Wann Lin for their insights and contribution to modeling of the gold nanoparticles.

I would like to extend my appreciation to all of the past and present members of the Frank Gu Research Group who have helped me along the way and made my time here enjoyable. I am especially grateful to graduated lab member Dr. Mohit Verma, and current graduate students Paul Chen, Jacob Rogowski, Shengyan (Sandy) Liu, Erin Bedford, Timothy Leshuk and Peter Lin.

Finally, I would like to recognize the financial support I received from the Natural Sciences and Engineering Research Council of Canada (NSERC) Alexander Graham Bell Canada Graduate Scholarship, 20/20 NSERC Opthalmic Materials Network, Waterloo Institute for Nanotechnology (WIN) Nanofellowship, and the University of Waterloo President's Graduate Scholarship.

Dedication

To my family and fiancé,

for their continual love and support throughout my education

Table of Contents

List of Figures

List of Tables

Chapter 1
Introduction

1.1 Overview

Over 125 million people worldwide wear contact lenses, with almost half using monthly reusable lenses. Of the reusable contact lens wearers, microbial contamination occurs in over 50% of contact lens cases.[1–3] Contact lens and contact lens case contamination of pathogenic organisms is known to greatly increase the risk of and cause microbial keratitis and infiltrative keratitis[3–5], which can result in vision loss. Furthermore, the prevalence of biofilms on the inside surfaces of contact lens cases has been widely demonstrated.[4,6] Biofilms pose an even greater risk to wearers because they are known to overcome the strategies used to prevent contamination by increasing the resistance of bacteria to disinfectant solutions[7–9], and rendering antimicrobial cases less effective.[10] As biofilms cannot be seen with the naked eye, a method warning users of biofilm contamination is needed so they can discontinue use of the contact lens case to prevent related eye infections.

Conventional methods to detect the presence of biofilm include the use of *ex situ* cell culture, dye staining, and imaging techniques.[11] These techniques require a trained technician in a laboratory environment to identify the presence of biofilm using specialized equipment or reagents. A simple point-of-care biosensor system for the detection of biofilm on surfaces is needed for consumer-level users. This biosensor should be simple for the untrained user, low in cost, and non-specific to allow detection of a variety of biofilms.

Nanotechnology has led to the advancement of many biosensor technologies. Properties such as increased surface are to volume ratio and nanoscale phenomenon provide many advantages over bulk materials. In particular, gold nanoparticles possess unique optical properties. Upon interaction with light, gold nanoparticles exhibit localized surface plasmon resonance through the coherent oscillation of conduction electrons in the nanoparticle. This allows their optical properties to be tuned by changing the particle size, shape, interparticle interactions, as well as the surrounding dielectric environment.[12] Gold nanoparticles have been employed in several strategies for the colourimetric detection of pathogenic bacteria.[13] In particular, led by Dr. Mohit Verma, our lab has developed a colourimetric biosensor based on unmodified gold nanostars for the detection and identification of pathogens.[14–16] This solution-based biosensor is capable of producing a visible colour change in the presence of planktonic bacteria, however is not capable of detecting biofilms. To eliminate exposure

of the sensor nanomaterial components to users and the environment, a surface-based biosensor is also desired.

This research project uses the unique optical properties gold nanoparticles to produce a surface-based colourimetric sensor for the detection of biofilms. A new method to immobilize the gold nanoparticles onto solid substrate is explored, studying how both the properties of the surface and particles affect the immobilization state and thus the optical properties of the surface. Using this method, an optimal immobilization state of the gold nanoparticles is used to create a novel detection mechanism producing a visible colour change on the surface in the presence of biofilm. Future research avenues based on this work include improving the durability of the immobilized nanoparticles and expanding the capabilities to different surfaces and types of biofilms for applications in healthcare, food services and water treatment.

1.2 Research Objectives

The overarching objective of this research is to develop a colourimetric biosensor for the detection of biofilm contamination on surfaces. The biosensor should be non-specific to different types of biofilms and low in cost. This research focuses on developing a biosensor based on the intrinsic properties of immobilized gold nanoparticles to produce a visual colour change on the surface in the presence of biofilm. The sensing ability of gold nanoparticles is dependent on their immobilization state, and can be determined through a versatile immobilization method. Furthermore, the immobilization method should be able to incorporate the biosensor onto a variety of surfaces including plastics used in contact lens cases. Non-specific detection of different biofilms is achieved through detecting their common properties, avoiding the use of biomolecules such as antibodies, keeping the sensor low-cost. The specific objectives for the project include:

1. Develop a method to control the immobilization state of colloidal gold nanoparticles on surfaces
    - Determine the effect of changing the surface properties to modulate the immobilization state
    - Study the effect of immobilizing gold nanoparticles with different sizes and shapes
2. Optimize the gold nanoparticle immobilization for the colourimetric detection of biofilms
    - Select the optimal immobilization state and characterize the detection mechanism
    - Test the ability to detect biofilms of both Gram-positive and Gram-negative bacteria

3. Demonstrate colourimetric detection of biofilm in a contact lens case
    - Integrate the sensor onto a plastic surface and onto a contact lens case
    - Validate the sensor capabilities on these surfaces

1.3 Thesis Outline

This thesis contains one chapter of literature review, two experimental research chapters, and a final chapter presenting the conclusions and recommendations of this work. Chapter 1 provides an introduction to the thesis, outlining the research motivation and specific objectives of the research project.

Chapter 2 reviews current literature containing methods to immobilize colloidal gold nanoparticles onto solid substrates. The review focuses on methods to control the immobilization state of the gold nanoparticles, highlighting techniques to modulate the properties of the surface, colloidal solution, as well as pre-patterning of the surface using microfabrication. Then, the optimal immobilization states of gold nanoparticles desired for specific applications are critically examined. The review acts as a guide to enable the smart design of methods to control the immobilization outcome of gold nanoparticles.

Chapter 3 explores a new method to control the immobilization of colloidal gold nanoparticles. By controlling the substrate properties, the immobilization state of the nanoparticles can be modulated from single disperse particles to large three-dimensional clusters. This chapter provides a simple single-layer immobilization strategy capable of providing a wide variety of immobilization states.

Chapter 4 uses the immobilization strategy presented in Chapter 3 to obtain an optimal gold nanoparticle immobilization state capable of producing a visible colour change of the surface. The detection mechanism is characterized on a glass surface using multilayer film formation, followed by biofilm detection of both Gram-positive and Gram-negative bacteria. Then, the sensor is integrated onto a plastic surface and contact lens case. This chapter provides proof-of-concept for the colourimetric detection of biofilms using an immobilized gold nanoparticle biosensor.

Finally, Chapter 5 summarizes the conclusions drawn from this research and presents recommendations for future work to improve upon and create new research avenues for this biosensor technology. Several recommended avenues include studying the stability of the immobilized nanoparticles as well as their potential to affect biofilm deposition and growth. To improve the biosensor for contact lens case applications, the sensor should be integrated onto a variety of other

plastic surfaces and tested with a larger library of ocular pathogens. Other research avenues based on this work include the detection of biofilms in the food processing and health care industries.

Chapter 2
Literature Review

2.1 Summary

Immobilized gold nanoparticles bring unprecedented advances to sensors based on surface plasmon resonance, surface-enhanced Raman scattering, and electrochemistry. The immobilization state of the gold nanoparticles on the surface is crucial to enable these applications and optimize performance. Here, we review the different strategies for immobilization of colloidal gold nanoparticles onto solid substrates with emphasis on controlling the immobilization state. This includes consideration of both the properties of the surface and colloid solution, in addition to microfabrication techniques used for pattern-directed immobilization. Then, we highlight the desired immobilization states optimal for each application. This review is intended to act as a guide in controlling the immobilization state of colloidal gold nanoparticles to facilitate the improvement of current devices and enable the smart design of new applications.

2.2 Introduction

In the past several decades, interest in immobilizing gold nanoparticles onto solid substrates has grown amongst researchers across fields of chemistry, materials science, optics, photonics and medicine. Compared to other metallic nanoparticles, gold nanoparticles offer the benefits of being the most chemically stable nanoparticle[17], and the facile reactivity of gold with biomolecules yields highly functional surfaces desired for analytical applications. Upon interaction with light, gold nanoparticles exhibit localized surface plasmon resonance (LSPR) enabling enhanced electromagnetic and optical properties over bulk substrates.[12] As the LSPR properties of gold nanoparticles is affected by the local environment as well as interparticle interactions, the immobilization state of gold nanoparticles on the surface dictates the particle-enhanced surface properties. Thus, the ability to control the immobilization outcome of gold nanoparticles is critical to obtain the desired surface properties.

A variety of methods exist to incorporate gold nanoparticles onto solid substrates, which can be classified into two categories: direct formation of nanoparticles on the surface, or deposition of colloidal nanoparticles onto the surface. Direct formation of gold nanoparticles on the surface involves the growth of gold nanoscale features through ion reduction[18], thermal evaporation[19], or electrodeposition[20] of gold on substrates that have been patterned through micro- or nano- fabrication techniques such as electron beam lithography.[21] These techniques are known to create precise

periodic arrays of nanoparticles, however they require specialized equipment and set-up, are restricted to small-area applications, and are expensive. Deposition of pre-formed colloidal gold nanoparticles offers an inexpensive alternative for incorporation of gold nanoparticles onto surfaces requiring no specialized equipment. This method takes advantage of widely-studied colloidal gold nanoparticle synthesis techniques to obtain desired shapes and sizes of gold nanoparticles in solution[14,22,23] with the flexibility to modify large-area surfaces. In addition to selecting the particle size and shape, varying the immobilization state provides multiple degrees of freedom to create a wide variety of gold nanoparticle-enhanced surfaces.

Several recent excellent reviews covering applications of metallic nanoparticle-modified surfaces for LSPR sensors[24], electrochemical sensors[25], and surface-enhanced Raman spectroscopy (SERS)[26,27] and general analytical applications[28] have outlined strategies for immobilization of colloidal gold nanoparticles. However, the effect of the different immobilization strategies and other deposition parameters on the final immobilization state on the particles was not explored. This review aims to cover the state-of-the-art strategies for immobilization of colloidal gold nanoparticles onto solid substrates with a focus on methods to control the deposition to obtain desired immobilization states. Then, the immobilization states desired for specific applications are critically reviewed, such that this article can act as a guide to select the optimal colloidal gold nanoparticle immobilization strategy and deposition parameters for selected applications.

2.3 Immobilization strategies

To control the immobilization of colloidal gold nanoparticles, there are three main factors that must be considered: (1) the properties of the immobilization surface, (2) the properties of the gold nanoparticles in solution, and (3) the interaction of the gold nanoparticles with the surface. The different strategies to modify surfaces to enable and control the immobilization of gold nanoparticles, as well as the interactions of gold nanoparticles with these surfaces are covered in this section. The most common and widely established strategies include the use of covalent, electrostatic, polymer brush, and sol-gel/polymer network immobilization (Figure 1). The effect of the properties of the gold nanoparticle solution on the deposition and immobilization of particles is covered in a subsequent section.

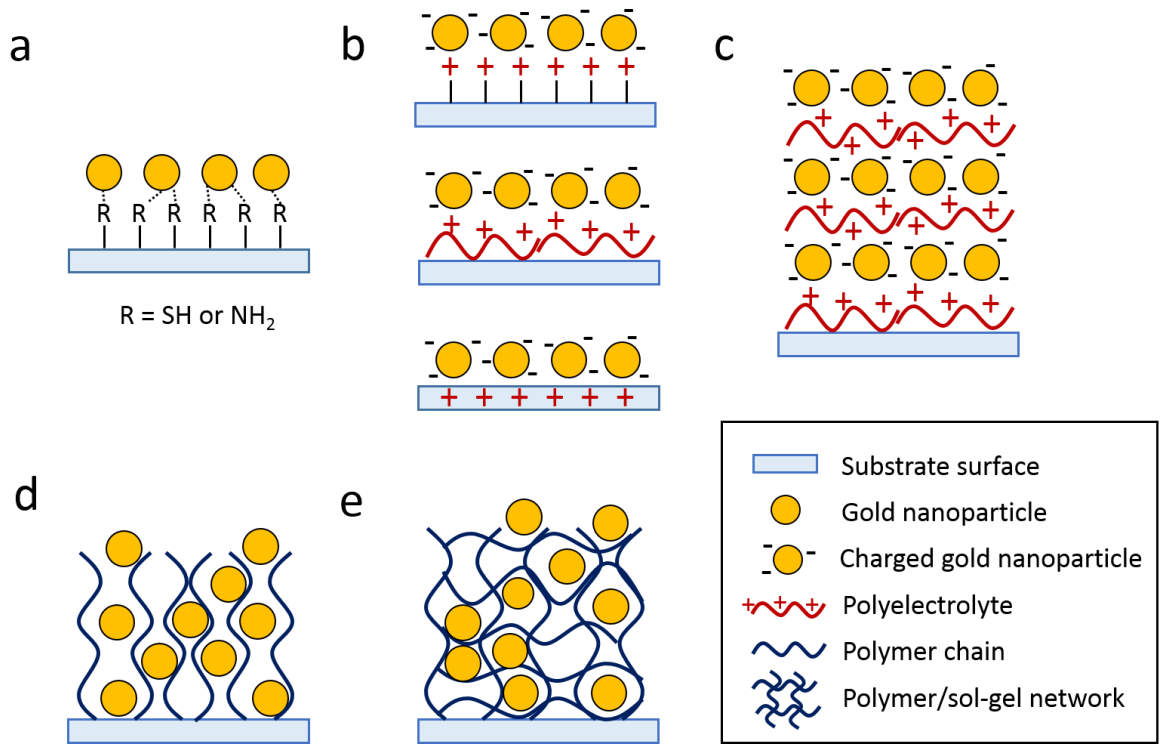

Figure 1. Schematics depicting the most common methods to immobilize colloidal gold nanoparticles onto solid substrates including: covalent immobilization (a), single layer electrostatic immobilization of charged particles (top: surface modified with charged molecule, middle: surface modified with polyelectrolyte, bottom: charged surface) (b), multilayer electrostatic immobilization (c), immobilization into a polymer brush (d), and immobilization into a sol-gel or polymer network (e).

2.3.1 Covalent immobilization

The most common strategy for immobilization of gold nanoparticles is through modification of the surface with molecules containing a thiol or amino moiety to covalently bond gold nanoparticles to the surface through their high affinity to gold (Figure 1a). Direct covalent binding of the surface to gold is advantageous as it allows the immobilization of both charged and uncharged particles, without the need for specific particle functionalization. The type of molecule used to bind the nanoparticles will depend on the substrate. For substrates terminated with hydroxyl groups on the surface, including glass, silicon containing an oxide layer and indium tin oxide (ITO), alkoxysilane compounds are primarily used to modify the surface via silanization. Thiol-terminated alkoxysilanes including 3-mercaptopropyltrimethoxysilane (MPTMS) [29–37] and 3-mercaptopropyltriethoxysilane (MPTES) [36,38], as well as amino-terminated 3-aminopropyltrimethoxysilane (APTMS)[39], 3-

aminopropyltriethoxysilane (APTES)[29,30,32,36,38,40] and *p*-aminophenyltrimethoxysilane (APhTMS)[33] have been used to covalently immobilize gold nanoparticles onto solid substrates. For substrates with different chemical functionality, bifunctional compounds including various dithiols[41–44], cysteamine[45,46] and mercaptohexylamine[47] have been successfully employed. In these covalent immobilization strategies, the modified substrate is typically submerged in the colloidal gold nanoparticle solution. Both the functionality of the linker molecule as well as the surface modification properties play an important role in determining the immobilization outcome.

Several studies have compared the covalent immobilization properties of gold nanoparticles using thiol-gold versus amine-gold interactions using similar alkoxysilane molecules. When immobilizing 14 nm citrate stabilized gold nanospheres onto an ITO surface modified with MPTMS or APTES, it was found that the APTES surface not only immobilizes a higher density of particles than MPTMS, but also favors particle aggregation.[32] The formation of island-type nanoparticle clusters on the APTES surface was attributed to electrostatic contributions from the amino-functional group. However, immobilizing non-charged 4.5 nm 1-dodecanethiol capped gold nanospheres, identical deposition characteristics were achieved on both MPTMS and APhTMS modified silicon surfaces.[33] These results suggest that amino-binding to gold nanoparticles has added sensitivity to electrostatic interactions only with charged particles, with the capability of inducing aggregation on the surface.

In addition to particle affinity towards the amino and thiol functionality, the variation in the grafting efficiency of the different molecules to the surface will affect the immobilization outcome. A detailed study performed by Haddada and coworkers indicated that under similar conditions, MPTES grafts onto a silicon surface with a coverage four times lower than APTES. This correlated to a lower density of immobilized 13 nm citrate stabilized gold nanospheres onto the MPTES surface.[38] Due to a combination of the high grafting efficiency and electrostatic contributions, increased particle aggregation was initially observed on the APTES surface, but could be mitigated through particle deposition under sonication resulting in increased coverage and dispersion into smaller aggregates. Further modifying the APTES surface with 11-mercaptodecanoic acid (MUA) with a 24% grafting efficiency, a high density of monodispersed particles was obtained. The MUA provided diluted thiol terminal functions compared to amino-terminated surface, decreasing the aggregation, and the increased flexibility through the alkyl chain favored increased nanoparticle binding compared to the MPTES surface.

Control of the spacing and aggregation of gold nanoparticles through covalent interactions with the surface is limited. Therefore, several approaches to pre-condition the particles into the desired aggregation state prior to deposition has been employed. The addition of cetyltrimethylammonium

bromide (CTAB) into a solution of 13 nm citrate-stabilized gold nanospheres has been used to selectively aggregate the particles.[40] As CTAB preferentially binds to the {100} facets of the gold nanoparticles, slowly adding small amounts caused formation of dimers, chains or tetrahedron nanoparticle clusters in solution, which can retain their structure after deposition onto APTES modified glass. In another work, 55 nm gold nanospheres were capped with a 4:1 ratio of hexanethiol and dodecanethiol to achieve optimal interparticle aggregation in solution to deposit into a close-packed monolayer structure with 60% surface coverage on an MPTMS + hexanedithiol modified ITO surface (which usually cannot be achieved with such large particles).[44] This formulation consisted of a balance between poor assembly properties of nanoparticles capped with only short-chain alkanethiols and high induced aggregation using only long-chain alkanethiols to achieve desired monolayer coverage.

2.3.2 Electrostatic immobilization

As gold nanoparticles are commonly stabilized with a charged capping agent, such as citrate (negatively charged) or CTAB (positively charged), many have taken advantage of their charged nature to immobilize them onto oppositely charged solid substrates using electrostatic forces. Similar to covalent immobilization techniques, deposition is usually carried out by submerging the substrate in the colloidal gold nanoparticle solution. For electrostatic immobilization, the ionic strength of the particle solution becomes a prominent factor to modulate the particle-surface interactions as it affects both the apparent charge of the particles and the surface. In a nanoparticle system containing charged capping agents, the overall ionic strength of the solution can be controlled by both the excess capping agent concentration and the addition of salt. Studying the deposition of CTAB-stabilized gold nanorods on a negatively charged polystyrenesulfonate (PSS) modified surface, Ferhan and coworkers observed that no particle deposition occurred with the native nanoparticle solution containing a high excess of CTAB, as it shielded the charge of the surface and interparticle repulsion was too high.[48] Deposition onto the surface became favourable at moderate to high concentrations of CTAB with addition of up to 120 mM of NaCl. The added salt decreased the electrostatic repulsion of the particles through a negative double layer screening effect in accordance with the Derjaguin, Landau, Verwey and Overbeek (DLVO) theory[48–50], and the attraction to the surface was increased. Although, at higher salt concentrations a second positive shielding effect from the CTAB was proposed, inhibiting deposition.[48] Fairly high nanoparticle deposition could also be achieved at low CTAB concentrations with 20 mM salt, but increasing the salt content above 40 mM caused severe particle aggregation in solution, inhibiting deposition. An example illustrating the effects of the capping agent concentration and ionic strength on the electrostatic immobilization of gold

nanoparticles are summarized in the schematic presented in Figure 2. Depending on the charged capping agent concentration, there will be varying optimal ranges of salt concentrations in which the interactions between the gold nanoparticles and the surface are favourable. Within these ranges, the deposition density of immobilized nanoparticles can also be tuned. The modulation of the particle-surface interactions through ionic strength will be dependent on the properties of both the nanoparticles and the surface modifications chosen.

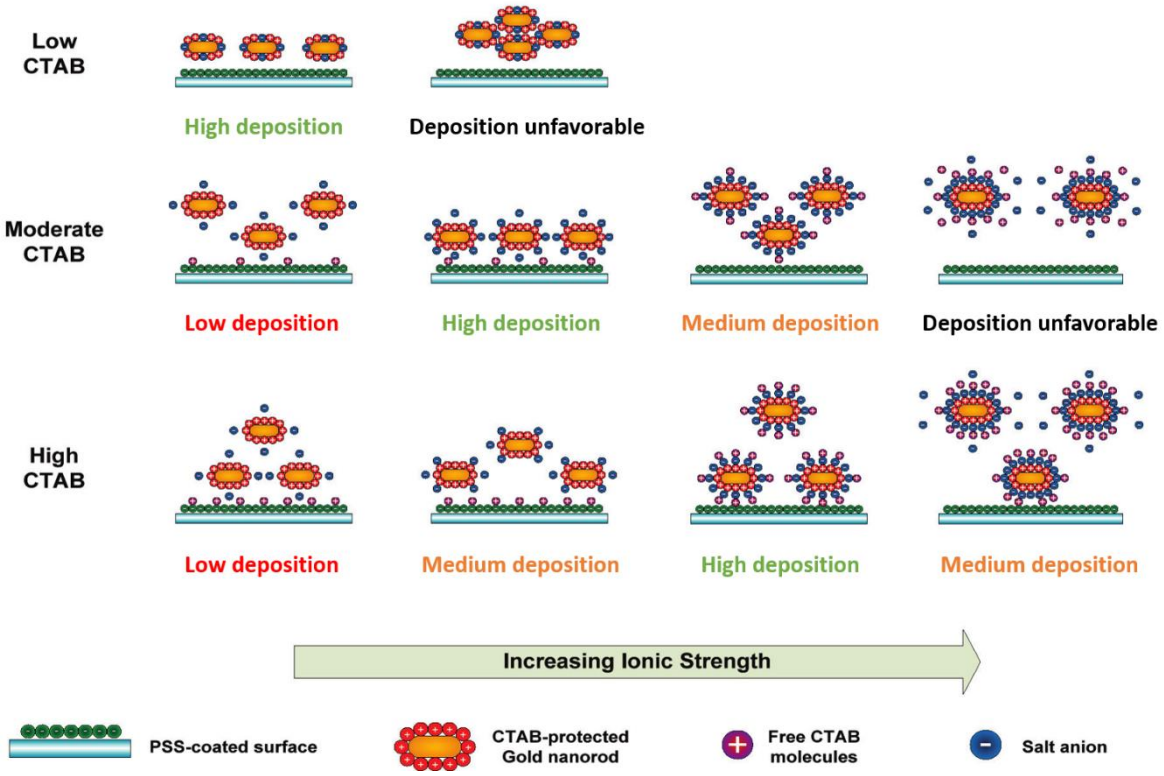

Figure 2. Schematic illustrating the effects of the gold nanoparticle solution charged capping agent concentration and ionic strength on the electrostatic immobilization onto a charged surface. Gold nanorods stabilized with a positively charged cetyltrimethylammonium bromide (CTAB) capping agent are depicted depositing onto a negatively charged surface coated with polystyrene sulfonate (PSS). Adapted from Ferhan *et al.*[48]

In addition to modulating the solution properties to control the particle-surface interactions, the ionic properties of the surface are very important and can be engineered to control the deposition of gold nanoparticles. Two-dimensional control of the nanoparticle immobilization state can be obtained using a single-layer deposition onto a charged surface, whereas three-dimensional deposition is commonly achieved through multilayer deposition.

2.3.2.1 Single layer electrostatic immobilization

The most common methods to create a charged surface to immobilize a single layer of gold nanoparticles are to modify the surface with small linker molecules capable of possessing a charge, and/or with a polyelectrolyte layer (Figure 1b). To immobilize negatively-charged gold nanoparticles, surface modifying molecules capable of possessing a positive charge such as AMPTS[51,52], APTES[49,51,53–57] and aminopropyldimethoxysilane (APDMS)[51] have been reported as well as Langmuir-Blodgett deposition of a pyrindinium bromide amphiphile film[58]. Single-layer polyelectrolyte films including poly(ethyleneimine) (PEI)[59], poly(diallyldimethylammonium chloride) (PDDA)[51,60], poly(allylamine hydrochloride) (PAH)[50], 4-vinylpyridine (VPy) copolymer[61], polydopamine[62], cationic polyacrylamide (CPAM)[63] and amino-starbust dendrimers[64] have also been successfully used to assemble negatively charged gold nanoparticles. To immobilize less commonly used positively-charged gold nanoparticles, small molecules such as 16-mercaptohexadecanoic acid (MHA)[65] and polyelectrolytes including PSS[48] have been reported.

A less common method to electrostatically bind gold nanoparticles is to use linker-free charged surfaces (Figure 1b). By treating glass slides with *aqua regia* followed by plasma cleaning, CTAB-stabilized gold nanorods (111 nm x 50 nm) were electrostatically bound to a negatively charged unmodified glass surface. Reducing the CTAB concentration to 2 μM, a monodisperse particle density of 70 particles/μm^2 was obtained on unmodified glass, mesoporous silica and titania thin film substrates. Other particle shapes including nanospheres and nanobipyramids were also immobilized using this method.[66] Using a similar method, CTAB-stabilized gold nanorods (15 nm x 18 nm) were also immobilized onto an unmodified glass/silica flow channel with the demonstrated ability to withstand extreme pH fluctuations and organic solvents.[67] Furthermore, in the flow channel the gold nanorods were able to be removed using a dilute solution of *aqua regia* or potassium iodide, with the capability of regenerating the nanoparticle surface upon subsequent treatment. To immobilize 20 nm negatively-charged citrate-stabilized nanospheres onto unmodified silicon, adjusting the nanoparticle solution to pH ~3.2 has been shown to protonate the Si-OH groups present on the surface to create a positive surface charge. Using multiple spin-coating deposition steps, a relatively high density of electrostatically immobilized particles onto linker-free silicon was reported.[68] Although electrostatic immobilization on linker-free surfaces provides a simple one-step approach, the versatility to control the surface properties is limited.

Modifying the surface with charged molecules provides the opportunity to alter the surface charge density to control gold nanoparticle immobilization. Selecting different amino-terminated alkoxysilanes, depending on their grafting properties, different surface charges on modified silicon

can be obtained. Using contact potential difference measurements, APTES modified surface was shown to have a larger surface charge compared to APDMS and APTMS, and was subsequently able to immobilize a higher density of 5 nm mercaptobenzoic acid (-COOH) stabilized gold nanospheres.[51] Creating a thin film consisting of n-dodecylacrylamide (DDA) and VPy copolymer, the surface charge density could be modulated through the VPy content of the film. From no immobilization of 30 nm citrate-stabilized gold nanospheres on films containing DDA only, the surface density of nanoparticles increased with respect to an increase in VPy content reaching a dense uniformly distributed monolayer of particles at 56 mol% VPy.[61]

In addition to controlling the surface charge density with respect to the grafting density of the charged molecule, the surface charge density can also be modulated by the ionization properties of the surface by adjusting the pH. Using a silicon surface modified with a molecular gradient of APTES, the immobilized density of 17 nm citrate stabilized gold nanoparticles was shown to directly correlate to changing APTES density and thus surface charge density. When increasing the nanoparticle solution pH above the $pK_{1/2}$ of the amino functional groups on this substrate (~7.6), the density of the particles on the surface decreased as less of the amino groups remained positively ionized. At the highest grafting density of APTES, the density of immobilized particles could be modulated from approximately 550 to 75 particles/μm^2 by increasing the deposition solution pH from 6 to 10.[54] The immobilization properties of CTAB-stabilized gold nanorods (400 nm x 25 nm) were also studied through the pH-dependent ionization of MHA functionalized onto a gold film. Contrary to expecting a higher density of particles immobilized above the $pK_{1/2}$ of MHA, a decrease in density of particles was observed on the substrate caused by high particle aggregation. Due to the low concentration of CTAB used, at pH values >10 the increasing ionic strength of the adjusted solution caused severe particle aggregation. For this system, pH 6.5 was determined as the optimal pH to obtain the highest density (14 particles/μm^2) of well-dispersed nanorods.[65] Comparing these two studies, the ability to tune nanoparticle immobilization through surface ionization is likely dependent on the size, capping agent and ionic stability of the nanoparticles.

2.3.2.2 Multilayer electrostatic immobilization

Multiple layers of gold nanoparticles can be obtained using Layer-by-Layer (LbL) assembly of the nanoparticles with oppositely charged polyelectrolytes (Figure 1c). In this strategy, alternating the self-assembly deposition of one or more permanently-charged polyelectrolytes and gold nanoparticles is used to create from 2 – 20 bilayers on the substrate to obtain the desired nanoparticle immobilization properties. Typically, LbL assembly is used to obtain a high density of three-dimensional large particle clusters or to obtain desired interparticle spacing of particles in a three-

dimensional matrix. In general, increasing the number of bilayers increases the degree of gold nanoparticle clustering on the surface.

Further insights into the interactions involved in multilayer polyelectrolyte-gold nanoparticle systems was studied using assembly of bilayers containing 12 nm citrate-stabilized gold nanospheres alternating with PAH on silicon and quartz surfaces modified with APhTMS.[69] Using x-ray photoelectron spectroscopy, it was observed that both coordination between the amine and gold particles (covalent bonding) as well electrostatic forces were present in the LbL structure. With deposition of 5 bilayers, a stepwise growth of the film was observed with each layer contributing to progressive agglomeration and growth of nanoparticle clusters. In contrast to this growth regime, another study reported that bilayers of CTAB-stabilized gold nanorods (60 nm x 20 nm) with PSS on an ITO substrate modified with PEI remained independent in their multilayer films maintaining a close-packed structure without aggregation after deposition of 7 bilayers.[70] Discrepancies in the growth of nanoparticle multilayers may be due to the different charge, size and shape of the particles or due to the different characteristics of the polyelectrolytes used, as will be discussed.

Related to the multilayer nanoparticle structure, the interpenetration ability of bilayers was studied with respect to the density of nanoparticles deposited in each layer using 11 nm citrate-stabilized gold nanospheres immobilized within quaternized chitosan layers. Controlling the density of particles deposited through deposition time modulation, lower nanoparticle coverage lead to increased bilayer interpenetration as empty spaces remained available for the adsorption of more particles into the same layer during the following bilayer deposition. The average thickness of bilayers were modulated from 3 nm to 10 nm by increasing the density of nanoparticles deposited.[71] Bilayer interpenetration is therefore an important factor to be considered to tune and predict the rate of particle clustering and stacking properties.

The selection of polyelectrolytes and substrates for LbL deposition has also been shown to influence the immobilization properties of gold nanoparticles. A silicon surface was first modified with either PAH or PEI to anchor bilayers of PSS and CTAB-stabilized gold nanorods (45 nm x 3.2 nm) onto the surface. The use of different polyelectrolytes as the base layer significantly affected the nanoparticle deposition properties; on PAH, isolated aggregates of particles were observed, whereas a much more uniform distribution of highly packed particles was observed on the PEI surface. These differences were attributed to the different polymer-polymer complexation phenomenon between PSS and PAH or PEI, affecting the surface charge availability.[72] Using the same LbL approach, a less dense distribution of gold nanorods were able to deposit onto ITO substrates compared to silicon and quartz, due to less favourable electrostatic interactions of PEI with ITO. Although a wide variety of

surface and polyelectrolytes have been used for multilayer gold nanoparticle deposition, inter-study comparisons on the immobilization properties of different polyelectrolytes and substrates could not be performed due to lack of consistency in particle type, size and deposition procedures.

Changing the charge density of the polyelectrolytes used in multilayer structures has also been used to modulate gold nanoparticle immobilization properties. Adjusting the deposition pH of PEI, a positively charged weak polyelectrolyte, onto a glass or silicon surface, the conformation as well as ionization charge density of PEI on the surface was modulated. Depositing PEI at low pH values, when it is fully ionized, a high density of dispersed 18 nm citrate-stabilized gold nanospheres was obtained and subsequently increased with multi-layer deposition. At high pH values, when PEI is less ionized, only sparse deposition of aggregated particles was observed, and with multi-layer deposition the aggregate size was shown to increase.[73] Through adjusting the number of bilayers as well as ionization of a weak polyelectrolyte, a wide range of nanoparticle deposition states can be obtained.

Another interesting method to control nanoparticle interactions within multilayered films is to adjust the inter-layer particle coupling interactions by changing the thickness and properties of the polyelectrolyte layers. Using 13 nm citrate-stabilized gold nanospheres, Au/$(PAH\text{-}PSS)_n$PAH multilayers were created, adjusting the interlayer thickness by changing n. For low particle surface coverage (5%, 15%), a change in the surface plasmon resonance of the particles through interparticle coupling between layers was observed by increasing polyelectrolyte layer thickness, however no changes were observed for surface layers with a high particle density (22%).[74] In another study, 2 to 18 layers of poly-DDA was inserted between two layers of 30 nm citrate-stabilized gold nanospheres creating a sandwich-structure to explore the effect of interlayer spacing. With only 2 layers (8 nm) of spacing, interlayer localized surface plasmon coupling was present, but at 18 layers (62.4 nm) of spacing, the localized surface plasmon resonance resembled that of a single monolayer indicating that inter-layer coupling interaction was no longer present.[75] In addition to polyelectrolyte spacing, the introduction of titania nanosheets have been shown to supress inter-layer particle coupling. In a $(PDDA/Ti_{0.91}O_2)_n$PDDA/Au multilayer structure with 3.5 nm citrate-stabilized gold nanospheres, without titania nanosheets (n=0) strong interlayer plasmon coupling was observed as the number of bilayers increased. Addition of one titania sheet layer (n=1) began to supress interlayer particle coupling, where two layers (n=2, 3.5 nm thickness) almost completely suppressed interlayer coupling.[76]

2.3.3 Polymer brush immobilization

Grafting of polymer brushes onto solid substrates is able to produce both two and three-dimensional structures of immobilized gold nanoparticles (Figure 1d). In this method, colloidal nanoparticle solutions are incubated with substrates containing polymer brushes. The gold nanoparticles are able to penetrate the hydrated polymer brushes and become entrapped through surfactant displacement, polymer chelation, and/or with attractive electrostatic or hydrogen bonding forces. Polymer brushes based on poly(ethyleneglycol) (PEG)[77–81], poly(ethylenepropylene) (PEP)[82], poly(acryl amide) (PAAm)[83,84], poly(vinyl pyridine) (PVP)[85–87] and poly((dimethylamino)ethyl methacrylate) (PDMAEMA)[84,88] have been successfully employed to immobilize gold nanoparticles. The theoretical models governing the inclusion of nanoparticles within polymer brushes has been well summarized in a previous work.[89] Herein, experimentally determined parameters to control the immobilization of gold nanoparticles within polymer brushes have been summarized.

The main parameters that have been varied to modulate the immobilization of gold nanoparticles within polymer brushes include controlling the molecular weight and grafting density of the brushes. To determine the effect of polymer brush molecular weight, and therefore length of the brushes, a molecular weight gradient of PAAm was established on silicon and glass substrates and incubated with 16 nm citrate-stabilized nanospheres. As the molecular weight of the brushes increased, the density of particles immobilized onto the surface increased. At low brush molecular weight, nanoparticles were found to adsorb only onto the surface of the brush causing two-dimensional particle assembly, whereas at higher molecular weight, the particles penetrated into the brush causing three-dimensional stacking and interparticle coupling.[83] Creating gradients of PDMAEMA and poly(N-isopropyl acryl amide) (PNIPAAm) with respect to surface grafting density, the number of immobilized 16 nm citrate-stabilized nanospheres was found to increase as the surface grafting density of the brushes increased. However for smaller 3.5 nm particles, the number of particles increased reaching a maximum at an intermediate brush grafting density, then at higher densities the number of particles immobilized began to decrease. Increased grafting density of the brushes resulted in expulsion of the smaller nanoparticles from the deeper areas, allowing them to only immobilize onto the tips of the brushes similar to the larger particles.[84]

Properties of the colloidal gold nanoparticles also play a critical role in their ability to be immobilized into polymer brushes. In general, it has been established that smaller particles are able to be incorporated into polymer brushes at higher numbers than larger particles because of their ability to access more binding sites on the brushes.[77,81,83,84] The desorption behaviour of the particles from polymer brushes is also dependent on particle size. Under thermal treatment at 85 °C, it was found

that 100 nm citrate-stabilized nanospheres desorbed faster and more completely than 50 nm and 30 nm particles immobilized in PEG-functionalized brushes, the latter being extremely difficult to desorb due to increased surface area of the particle able to interact with the polymer.[77] In addition to size, the type of stabilizing ligand also has an effect on particle-brush incorporation. It was found that while 30 nm nanospheres stabilized with citrate ions could be immobilized, the same particles stabilized with chemically-bound mercaptopropanesulfonate could not be incorporated into a PEG-functionalized brushes as the stabilizing ligand must be able to be displaced for PEG-Au chelation.[77]

Applying knowledge concerning the brush properties, to immobilize large nanoparticles a large polymer brush molecular weight and high surface grafting density should be used. Or, to overcome limitations of particle penetration into polymer brushes an 'in-stacking' strategy was proposed. This strategy uses multiple immersions of the polymer brush into the nanoparticle solution. Between immersions, the sample was dried causing the polymer chains collapse, and upon re-immersion, only the polymer chains unbound to nanoparticles re-swell allowing capture of additional particles.[78] This strategy was able to obtain dense three-dimensional assembly of 5 nm, 23 nm and 31 nm citrate-stabilized gold nanospheres into PEG-based brushes.

Design of the polymer brush properties can be used to control interparticle spacing and coupling as well as particle interaction with the surface. Incorporating 2.2 nm polystyrene-capped gold nanospheres into poly(4-vinylpyridine-b-styrene) block copolymer brushes, the nanoparticles were initially able to infiltrate into both domains of the block copolymer. However upon solvent annealing, the nanoparticles sequestered exclusively into the polystyrene domain at a controlled distance from the surface.[85] Using a weak polyelectrolyte PVP brush, the extent of 11 nm citrate-stabilized gold nanosphere penetration could be controlled with the nanoparticle deposition pH. At pH 5.5, when the PVP brush remained in a collapsed state, the particles remained on the surface of the brush, whereas decreasing the deposition pH to 2.5, particles were able to penetrate into the swollen PVP brush.[87] Furthermore, the interparticle coupling interactions could be tuned after immobilization by changing the swelling state of the polymer brush; in a swollen state, the particles became more spaced apart and less particle coupling was observed.

2.3.4 Sol-gel/polymer network immobilization

Gold nanoparticles can be immobilized onto solid substrates using three-dimensional porous sol-gel networks (Figure 1e). To take advantage of covalent thiol-gold bonding for the immobilization of colloidal gold nanoparticles, sol-gel networks based on the hydrolysis of MPTMS are most commonly used[90–94], however use of a tetra ethyl orthosilicate (TEOS) sol-gel[95] has also been

reported. The gold nanoparticles can either be incorporated into the sol-gel network in solution prior to or after deposition on the substrate. By incorporating 20 nm PVP-stabilized gold nanospheres into a TEOS sol prior to spin coating onto an ITO substrate, well distributed single or small monolayer clusters could be obtained on the surface.[95] Mixing 20 nm gold nanospheres (functionalization unspecified) into an MPTMS sol-gel solution prior to deposition resulted in relatively large aggregates of particles incorporated throughout the sol-gel network[94] in contrast to monodisperse distribution of 10 nm citrate stabilized nanospheres obtained in another report[93]. By incorporating the gold nanoparticles into the sol-gel prior to deposition on the substrate, little to no control over the particle immobilization is achieved.

Increased control of nanoparticle immobilization can be obtained by incorporating the gold nanoparticles into the sol-gel network after it has been deposited onto the surface. After creating an MPTMS sol-gel network on a gold electrode, 20 nm citrate-stabilized gold nanoparticles were able to diffuse into and distribute throughout the sol-gel to form a continuous array of particles on the surface. Increasing the nanoparticles to 41 nm and 71.5 nm in size, less incorporation into the sol-gel matrix was observed.[90] Since it is more common to synthesize and grow metal nanoparticles directly on porous material supports[96], less attention has been given to immobilize pre-formed colloidal nanoparticles on sol-gel networks.

Colloidal gold nanoparticles have also been physically incorporated into polymer matrices. Adding a solution of poly(methyl methacrylate) (PMMA) in toluene to an aqueous solution of 55 nm citrate-stabilized gold nanospheres with addition of ethanol, the nanoparticles self-assembled at the water-toluene interface. As the toluene evaporated, the PMMA was also deposited at the aqueous interface, entrapping the gold nanoparticles and creating a flexible substrate with a close-packed array of particles.[97] Increasing the amount of PMMA, more particles were incorporated into the polymer film displaying a higher degree of aggregation and interparticle interaction.

2.3.5 Other immobilization strategies

There exist a variety of other less common methods that take advantage of other weaker forces and interactions to immobilize colloidal gold nanoparticles onto solid substrates. These include attractive Van der Waals, hydrophobic/hydrophilic forces, as well as deposition by evaporation. As many of these methods have not been thoroughly studied, they will only be briefly discussed.

To immobilize gold nanoparticles through weak Van der Waals attractive forces to the surface, the particle functionality is important. Depositing gold nanorods (50 nm x 15 nm) onto a glass surface using non-specific interactions via spin coating, only films of dispersed particles could be obtained if

the particles were PEGylated as opposed to being CTAB-stabilized.[98] Another method to deposit gold nanoparticles onto the surface using weak Van der Waals forces is to destabilize the particles from solution. Destabilization of 20 nm to 100 nm citrate-stabilized gold nanospheres in solution was achieved by adding hydrofluoric acid, allowing the deposition onto an unmodified silicon surface.[99]

Using hydrophobic interactions, bovine serum albumin (BSA)-coated 13 nm gold nanospheres were immobilized onto a nitrocellulose membrane to obtain high dispersion without aggregation.[100] The favorable interactions with the hydrophobic nitrocellulose membrane was made possible by the protein coating of the nanoparticles. Exchanging the stabilizing ligand of 5 – 15 nm gold nanospheres from citrate ions to benzenethiol in a mixture of water and tetrahydrofuran, a combination of hydrophobic and surface gradient interactions were able to deposit the nanoparticles onto glass or silicon wafers submerged in the solution.[101] If the particle size is kept under 30 nm, this method is capable of producing large-area cm^2 arrays of monolayer close-packed dense nanoparticles. Similar to this technique, the Langmuir-Blodgett method has been used to transfer monolayer films of colloidal gold nanoparticles formed at the air-liquid or liquid-liquid interfaces onto substrates. Large-area close-packed monolayer arrays of 16 nm to 70 nm citrate-stabilized gold nanospheres were transferred onto an unmodified glass surface after assembly at a water/toluene interface using ethanol as an inducer.[102] Multilayer films of close-packed arrays of 26 nm citrate-stabilized nanospheres and CTAB-stabilized nanorods (74 x 31 nm) were also transferred onto glass and silicon substrates modified with PVP after assembly at water/hexane interface through the Langmuir-Blodgett method.[103]

Deposition of colloidal gold nanoparticles by evaporation or dewetting of the nanoparticle solution onto a substrate has attracted more attention in research as it is insensitive to the substrate material. However, due to non-equilibrium effects present during the evaporation process of a droplet on a surface, it is difficult to control the immobilization properties of the nanoparticles. In most cases, non-uniform clumps of particles are obtained on the surface[104] or nanocrystals are found to be concentrated on the substrate edge[105] in a coffee-stain-like manor. Controlling the evaporation rate and interparticle interactions with the solvent-air interface has shown promise to obtain desired particle immobilization. Using a rapid evaporation technique, dodecanethiol-capped 16 nm gold nanospheres were able to assemble at the air-liquid interface to create long-range monolayer compact ordering of particles upon evaporation onto the surface.[105] In contrast, slow evaporation was needed to induce the necessary capillary forces to arrange tightly-packed monolayers of CTAB-stabilized gold nanorods of various sizes.[106] Furthermore, the self-assembly of gold nanoparticle structures through evaporation deposition has been shown to be mediated by the concentration of particles[107],

surfactant concentration[108], introduction of specific ligands[109] and particle shape[110]. Increased control of nanoparticle transfer to a solid surface through evaporation was realized though a convective assembly process. In this method, a small volume of nanoparticle solution is confined in a meniscus which is dragged between two plates at a constant velocity. Decreasing the deposition speed or increasing the plate gap was able to induce monolayer to multi-layer close-packed structures of 16 nm citrate-stabilized nanospheres.[111,112]

2.4 Controlling immobilization through microfabrication techniques

Patterning of the surface through microfabrication techniques prior to the deposition of colloidal gold nanoparticles enables enhanced spatial control of nanoparticles on the surface including control of particle spacing, clustering and alignment. Microfabrication techniques create template patterns on the surface, taking advantage of most immobilization methods discussed, although usually require specialized equipment and often a clean room facility. Control of gold nanoparticle immobilization through patterned templates generated by lithography techniques, including photolithography, electron beam lithography (EBL), colloidal lithography, and atomic force microscopy (AFM) nanolithography, in addition to wet contact printing and block copolymer templates are discussed.

Lithography techniques involve patterning the surface with regions capable of immobilizing gold nanoparticles through selective removal of materials using a patterned mask. With traditional optical photolithography, exposing selective regions to light, hydrophilic and hydrophobic stripes were created on a silicon substrate. CTAB-stabilized god nanorods (495 nm x 37 nm) were selectively immobilized onto the SiO_2 stripes through hydrophilic and electrostatic interactions.[113] To gain finer control over individual particle placement, non-optical lithography techniques have also been explored. Using EBL, where patterns are produced through exposure to high energy electrons, a high density array of isolated chemical patterns of PVP polymer brushes were created in a polystyrene mat. Depending on the area of the patterned PVP spots, the number of 13 nm citrate-stabilized gold nanoparticles immobilized into each spot could be modulated from 1 to 30.[86] Patterning lines of PVP brushes instead of spots, modulation of the line pitch controlled deposition of long, continuous, single or multi-particle wide lines. In addition, creating size-controlled arrays of spots containing PEG brushes resulted in similar control of gold nanoparticle isolation.[80] Using colloidal lithography, where polystyrene nanospheres are used as the etching mask, arrays of PDMAEMA brushes could be created on the surface to selectively immobilize 4.3 nm beta-cyclodextrin capped gold nanospheres into uniform arrays.[88] Through AFM nanolithography, small areas on the surface defined through the AFM tip interactions were able to be functionalized with APTMS to electrostatically bind citrate-

stabilized gold nanospheres, controlling individual particle spacing in an array[114] or producing complex custom patterns[115].

Block copolymers, which have the ability to self-assemble into multi-domain patterns, have also been used as microfabrication techniques to direct the assembly of gold nanoparticles on solid substrates. Spin casting a poly(styrene-*b*-methyl methacrylate) (PS-*b*-PMMA) onto silicon, the diblock copolymer phase-separated to create 40 nm PMMA domains which selectively bound 10 nm and 20 nm thioctic acid stabilized gold nanoparticles achieving small dense clusters of about 2-5 particles.[116] In another work, the PMMA domains PS-b-PMMA films have been etched using acetic acid to provide trenches to capture CTAB-stabilized gold nanorods of various sizes in an end-to-end alignment.[117] Films of self-assembled PS-*b*-PMMA block copolymers phase-separated into a honeycomb pattern have also been used for molecular transfer printing of PEG brushes onto another substrate. The PEG brushes, which only assembled onto the PMMA domains, were able to transfer onto the new substrate and subsequent immobilization of 15 nm citrate-stabilized gold nanospheres into the a honeycomb pattern was possible.[81] Compared to lithography techniques, block copolymer microfabrication does not require specialized equipment, but the formation of specific patterns is limited to the phase-separation capabilities of the block copolymers.

Wet contact printing uses a patterned template to initially define the spatial patterning of nanoparticles to be transferred onto another substrate. Similar to a stamping process, the final substrate does not have to be modified in a special way to define the patterning. Using a wrinkled polydimethysiloxane (PDMS) template, 78 nm BSA-stabilized gold nanospheres were physically deposited into patterned long trenches. By contacting the PDMS stamp containing nanoparticles onto a wet quartz surface and allowing it to dry, the linear chains of nanoparticles were successfully transferred.[118] By adjusting the width of the trenches in the PDMS template, 1 – 4 particle-wide linear chains could be obtained. Although this method has not yet demonstrated the deposition of individual particle arrays, the reusability of the patterned stamp is advantageous over the other microfabrication techniques.

2.5 Colloidal solution considerations

The properties of the gold nanoparticles in solution will affect the kinetics of deposition onto the surface. Understanding the deposition kinetics as well as the parameters which affect the deposition kinetics can give a broad range of control on the surface coverage of the immobilized nanoparticles. In most immobilization approaches, the substrate is submerged in a colloidal nanoparticle solution for

a defined period of time. Initially, diffusion controlled deposition is observed with the coverage of nanoparticles on the surface (q) increasing linearly with respect to the square root of time (t):

$$q = Bt^{1/2}$$

where B is dependent on the particle size and concentration, solution viscosity and temperature, and sticking probability to the surface. Deposition in the diffusion controlled regime results in a single-layer random particle distribution on the surface. After a certain surface coverage, the deposition deviates from this trend and the final surface coverage becomes dependent on interparticle repulsion.[29,32,49] Therefore, by tuning the length of time the nanoparticle solution is exposed to the surface, the density of the deposited particles can be controlled. For example, within the diffusion-controlled regime, the surface coverage of 15 nm citrate stabilized gold nanospheres was modulated from 0.39 x 10^{11} particles/cm^2 with 5 minute incubation to 1.6 x 10^{11} particles/cm^2 with 3 h incubation with the colloid gold solution.[29] To control the final density of immobilized particles beyond the diffusion-controlled regime, the interparticle interactions can be modulated by selecting the nanoparticle stabilizing ligand, or, for charged particles, by changing the ionic strength of the nanoparticle solution. For example, 15 nm nanospheres coated with mercaptoethanol (a small, uncharged molecule) were able to deposit in a high density aggregated state on an APTMS surface, whereas only monodisperse deposition of 15 nm citrate stabilized nanospheres could be achieved.[29] When depositing CTAB-stabilized gold nanorods (36 nm x 11 nm) onto an MPTMS surface, the introduction of 10 mM NaCl into the nanoparticle solution changed the deposition from sparse, non-aggregated particles to highly aggregated particle clusters.[36]

Other factors which can be controlled to affect the kinetics of particle assembly on the surface include particle concentration in solution, particle size, and assembly temperature. Studies which have modulated the deposition time or factors affecting the particle kinetics to control the immobilization of gold nanoparticles have been summarized in Table 1. Independent of the immobilization strategy used, similar trends in the parameters are seen; increasing the deposition time, increasing the particle concentration, or increasing the temperature increases the surface density of immobilized nanoparticles, whereas increasing the particle size decreases the density. Even though most studies used similar gold nanoparticles with respect to shape, size and capping agent, the extent of modulation on the resulting density of immobilized particles for each of the given parameters however appear to be vastly different. For example, some studies required hours of incubation to obtain similar immobilized particle densities to studies which only required minutes. These discrepancies are caused by the properties of the different surfaces and immobilization strategies used. Even though the surface-particle interactions will be unique for each particle and surface, the

particle kinetics are still an important and useful tool for controlling the immobilization state of the gold nanoparticles.

Table 1. Effects of varying the deposition parameters of colloidal gold nanoparticle solutions on the resulting immobilization outcome.

Parameter	Parameter range	Immobilization outcome	Particle size	Immobilization strategy	Surface	Ref.
Time	10 mins - 120 mins	Increase ~16 to ~62 particles/μm^2	14 nm	Covalent	ITO-MPTMS	[32]
	1 hr - 3 hrs	Increase up to 25% coverage	15 nm		Au-hexanedithiol	[41]
	60 mins - 300 mins	Increase 260 to 430 particles/μm^2	10 nm[a]	Covalent/ Electrostatic	Silicon-APTES	[30]
	3 hrs - 15 hrs	Increase 50 to 140 particles/μm^2	28 nm	Electrostatic	Glass-amino starburst dendrimers	[64]
	6 hrs - 16 hrs	Increase ~50 to ~425 particles/μm^2	30 nm		Glass-p(DDA/VPy)	[75]
	2 mins - 72 hrs	Increase deposition	3.5 nm		Glass-PDDA	[76]
	10 mins - 10 hrs	Increase 150 - 2100 particles/μm^2	15 nm		Cu grid-ODEP	[58]
	15 mins - 60 mins	Increase deposition	11 nm		Au-MPTMS-chitosan	[71]
	6 mins - 60 mins	Increase ~200 to 525 particles/μm^2	15 nm		Mica-PAH	[50]
	15 s - 20 mins	Increase 10 to 50 particles/μm^2	20 nm	Physical	Silicon	[99]
Concentration	OD 0.5 - 1.0	Increase 0 to ~3000 particles/μm^2	10 nm[a]	Covalent/ Electrostatic	Silicon-APTES	[30]
	0.15 - 15 nmol/L	Increase 250 to 1800 particles/μm^2	13 nm	Electrostatic	Silicon-PEI	[74]
	5 - 50 mg/L	Increase ~50 to ~525 particles/μm^2	15 nm		Mica-PAH	[50]
Concentration & Particle size	7 x 10^{11}, 9 x 10^{10}, 5.6 x 10^9 particles/mL (20 nm, 40 nm, 100 nm)	Increase ~1 to 4 to 50 particles/μm^2	20 nm	Physical	Silicon	[99]
Particle size	4 nm, 15 nm, 87 nm	Decrease 5700 to 800 to 7.3 particles/μm^2	Various	Covalent	Glass-APTMS-lipoic acid	[119]
	28 nm, 57 nm	Decrease 140 to 20 particles/μm^2	Various	Electrostatic	Glass-amino starburst dendrimers	[64]
Temperature	4°C, RT	Increase deposition 4°C to RT	15 nm	Covalent	Au-hexanedithiol	[41]

All particles used are spherical in shape and stabilized with citrate capping agent except for: [a] oligonucleotide capping agent.
RT: room temperature

2.6 Stability of immobilized gold nanoparticles

The ability of colloidal gold nanoparticles to remain fixed in their desired immobilized state on solid substrates is an important asset for practical applications. Ideally, immobilized gold nanoparticles should be able to withstand exposure to various solvents and should be resistant to mechanical abrasion. The stability will depend on the method used to modify the surface, as well as the affinity of the gold nanoparticles to the surface modifier. Unfortunately, most studies do not report the resulting stability of their methods to immobilized colloidal gold nanoparticles, or only comment on the stability in passing. It is unclear whether the stability of the nanoparticle-modified surfaces were simply not studied in many cases, or if poor stability results were omitted from publication. The few works summarized herein provide some insight into the stability of the different immobilization methods, however more studies would be required to gain a complete understanding.

The stability of gold nanoparticles bound to thiol versus amine-terminated surfaces was evaluated to compare covalent and electrostatic immobilization approaches. Performing atomic force volume spectroscopy, an AFM tip functionalized with MPTMS was used to remove gold nanoparticles immobilized onto the surface to obtain adhesion force curves. It was found that 7 nm citrate-stabilized gold nanospheres possessed an adhesion force of approximately 30 nN on an MPTMS-modified surface compared to an adhesion force of 7 nN on an APTES-modified surface. The difference in adhesion suggests that covalently-bound gold nanoparticles are more stable than those bound electrostatically.[120] Also comparing amine versus thiol-terminated surfaces, another study performed water erosion tests on 4.5 nm dodecanethiol-stabilized gold nanospheres immobilized onto surfaces modified with MPTMS or APhTMS compared to unmodified surfaces. Similar high particle stability was observed on both MPTMS and APhTMS surfaces, withstanding forces on the order of 490 μN, whereas the majority of the nanoparticles on the non-modified surface were removed.[33] The limiting factor in stability under erosion was attributed to the stability of the organic alkoxysilane monolayers. It should be noted that the particles used in this study were not charged, therefore covalent/coordination forces were responsible for immobilization of the particles on both thiol and amino terminated surfaces, which were shown to be more stable than particles immobilized with weaker physical interactions.

Controlled electrostatic immobilization of gold nanoparticles onto a polyelectrolyte surface has also shown improved stability compared to particles immobilized through weaker physical interactions. CTAB-stabilized gold nanorods deposited by evaporation onto an unmodified glass surface showed aggregation and high removal of particles after one wash in phosphate buffered saline (PBS) solution. The same particles immobilized onto PSS-coated glass did not show signs of

aggregation and only moderate removal of particles from the surface was observed upon washing in PBS. To obtain a fully stable surface of the gold nanorods onto PSS, two washing steps in PBS were required to remove the weakly bound particles.[48]

Independent studies immobilizing gold nanoparticles through weak physical interactions have also reported poor adhesion to the surface upon scratch testing[112] and reordering of the particles on the surface over time[110]. Although indirectly measured via Raman spectroscopy, even covalently-bound gold nanoparticles have also been shown to change their immobilization state over time.[121] Evidence of particle-size dependent stability has also been reported, with smaller particles exhibiting better adhesion onto the surface.[115] Under exposure to various aqueous and organic solvents, independent works reported high stability of immobilized gold nanoparticles, but with limited details.[36,73,115] To be able to generalize the stability characteristics of the different immobilization techniques, more comprehensive studies need to be performed.

2.7 Applications

2.7.1 Surface plasmon resonance sensors

Sensors based on the surface plasmon resonance (SPR) of immobilized colloidal gold nanoparticles depend on the presence of the molecule of interest changing the refractive index of the local environment surrounding the particles. This change in refractive index around the gold nanoparticles affects their SPR properties, resulting in a shift in the absorption spectrum which can be measured using a spectrophotometer. Immobilization strategies employed for the creation of SPR sensors, and the resulting sensor performance are summarized in Table 2. Gold nanoparticles immobilized in a well-dispersed monolayer of single particles is most often desired. For SPR sensors, interparticle coupling is likely not desired as it may broaden the absorption peak as well as decrease the surface area of the particles available for binding, decreasing the sensitivity. Covalent immobilization strategies appear most capable of obtaining this immobilization state. There is no apparent trend in the surface density of immobilized particles needed for successful sensor performance, however non-spherical particles are more commonly used. With the highest SPR refractive index sensitivity being reported for gold nanostars[122], nanobipyramids are seen to also have a higher sensitivity than nanorods[56], suggesting that the particle shape plays a factor. It should be noted that the substrate material in addition to the nanoparticle stabilizing ligand/functionality has also shown to affect the SPR sensing properties.[66]

Table 2. Immobilization strategies employed for surface plasmon resonance sensors, including the resulting refractive index sensitivity and sensor properties.

Immobilization strategy	Surface	Particle: shape, size, capping agent	Immobilization state	Sensitivity (nm/RIU)	Binding Analyte	Sensor characteristics	Ref
Covalent	Glass-APTMS	Spheres, 20 nm, citrate	17% coverage, dispersed 370 particles/μm^2	--	--	Shift in absorbance peak intensity and position	39
	Glass-MPTMS	Rods, 50 x 10 nm, CTAB	Dispersed 40 particles/μm^2	366	Strepta-vidin	LOD: 25 ng/mL, LR: 0.025 - 2.0 μg/mL	31
	Glass-MPTMS	Rods, 36 x 11 nm, CTAB	Dispersed	284	IgG	LR: 33.4 - 233.4 nM, Sensitivity: 60.7 pM	36
	PDMS-APTES	Stars, --, no capping agent	Dispersed 200 particles/μm^2, small clusters	392	--	--	122
	Glass-APTES	Rods, 50 x 15 nm, PEG	Dispersed	170	IgG	K_{eq}: 2.0 x 10^9 M^{-1}	55
	Glass-APTES	Bipyramids, various, PEG	Dispersed	381	IgG	Detection at 10 nM	56
Electro-static	Glass	Rods, 50 x 18 nm, CTAB	Dispersed high density	--	NGAL	LOD: 8.5 ng/mL	67
	Glass	Rods, 111 x 50 nm, CTAB	Dispersed 70 particles/μm^2, 120 nm spacing	283	--	--	66

All particles used are immobilized in a monolayer.
NGAL: Neutrophil gelatinase-associated lipocalin, LOD: Limit of detection, LR: Linear range, K_{eq}: Equilibrium binding constant

2.7.2 Surface-enhanced Raman spectroscopy

Through the electric field produced by localized SPR properties, immobilized gold nanoparticles have the ability to enhance the Raman scattering of molecules for surface-enhanced Raman spectroscopy (SERS) sensing applications. A summary of recent strategies for immobilization of gold nanoparticles for SERS is provided in Table 3. To evaluate SERS surfaces, the average enhancement factor (EF) is generally used as the primary figure of merit, however multiple methods to approximate this value exist. In addition to these deviations, inconsistent experimental parameters such as the excitation wavelength and model analyte used can greatly influence the EF, thus caution must be used comparing the EF values reported. To obtain a high SERS EF, most strategies employ a high density coverage of gold nanoparticles on the surface with a close-packed structure or high degree of aggregation. Although Wang and coworkers demonstrated that high density close-packed gold nanoparticle layers produce the greatest SERS enhancement[102], for most particles SERS can be enhanced through a higher degree of particle aggregation[63,70,123] if a close-packed particle layer cannot be formed. These immobilization states can be achieved through covalent, electrostatic, matrix encapsulation, and physical immobilization techniques including deposition by evaporation and hydrophobic interactions. Comparing between studies, no advantage is apparent through the use of multilayer versus monolayer immobilized particles, however Oh and coworkers report an increase in SERS intensity with increasing number of particle layers, with the majority of the signal dependent on the outermost layer.[103] SERS enhancement is most affected by the degree of interparticle interactions as electric field 'hot spots' are found to be enhanced when the distance between particles is decreased[60,101,124]. The shape of the immobilized gold nanoparticles is also an important factor; nanorods have been shown to have a higher EF than spheres[103,106], whereas nanostars have demonstrated the highest EF[47] in the works surveyed. Furthermore, the aspect ratio of nanorods[106], the morphology of nanostars[47], combining nanostars with nanospheres[125], or the use of a metallic substrate[60] affect SERS properties of the immobilized particles.

Table 3. Immobilization strategies employed for surface-enhanced Raman spectroscopy (SERS) applications, including the resulting enhancement factors reported for respective analytes.

Immobilization strategy	Surface	Particle: shape, size, capping agent	Immobilization state	Analyte(s)	Enhancement Factor	Ref.
Covalent	Silicon-MPTES-MUA	Spheres, 50 nm, CTAB	Close-packed	Phenylalanine	2.6×10^4	121
	Silicon-(PS-*b*-PMMA)	Spheres, 20 nm, thioctic acid	90% small clusters	Benzenethiol	3.1×10^7	116
	Au- 6-aminohexane-1-thiol	Stars, 36 nm (+130 nm branches), no capping agent	Dispersed 110 particles/μm^2, 20% aggregates	4-mercaptobenzoic acid	4.9×10^9	47
	PDMS-APTES	Stars, various sizes (NS), no capping agent	Dispersed 200 particles/μm^2, small clusters	4-aminothiophenol, thiabendazole	--	122
Covalent/ Electrostatic	Glass-APTES	Stars, 29.2 nm (+18.1 nm branches), citrate and Spheres, 12nm, citrate	Dispersed, 11 spheres/star	4-aminothiophenol	14x over stars only	125
Electrostatic LbL	ITO-PEI-$(PSS-NP)_7$	Rods, 60 x 20 nm, CTAB	Close-packed [a]	4-aminothiophenol	--	70
Electrostatic	Polycarpolactone-(PDADMAC-PSS)	Rods, 37 x 12 nm, CTAB-PSS	Dispersed high density, small clusters	4-mercaptopyridine, Rhodamine-6G	10^5	126
	Cotton thread-CPAM	Spheres, 20 nm, citrate	Large 3D aggregates	4-aminothiophenol, ninhydrin	--	63
	Glass or Ag-PDDA	Stars, 57 nm (+11 nm branches), citrate	Dispersed 43 particles/μm^2	Benzenethiol	2.7×10^5 (glass) 4.4×10^7 (Ag)	60
	PNIPAAm-DNA	Spheres, 40 nm, citrate	Dispersed, varied spacing	Adenine	10^4 - 10^6	124
Polymer network	PDMS	Spheres, 28 nm, citrate	Close-packed	4-aminothiolphenol, methylene blue	3.5×10^7	127
	PMMA	Spheres, 55nm, citrate	Close-packed [a]	Malachite green, 4-aminothio-phenol, 4-mercaptopyridine	2.4-9.0 x 10^7	97
Physical/ Electrostatic	Silica	Rods, 27 x 10 nm, CTAB	Highly aggregated	2-aminothiophenol	6×10^5	123
Evaporation	--	Rods, 250 x 16 nm, CTAB	High density linearly aligned	Rhodamine-6G	--	106
	Silicon	Rods, 227-850 x 27-30 nm, CTAB	Close packed side-by-side	2-naphthalenethiol, Rhodamine-6G	5.3×10^5, 3.9×10^5	101
	Silicon-carbon film	Spheres, 5nm, 1-dodecanethiol	Close packed linear arrays	ammonium nitrate, cyclotrimethylene-trinitramine	7.0×10^4	107
Hydrophobic	Silicon	Spheres, 30 nm, benzenethiol	Hexagonal close packed	Benzenethiol	20.2×10^8	108
	Glass	Spheres, 16, 25, 40, 70 nm, citrate	Close packed	4-aminothiophenol	10^5 - 10^7	102
Hydrophobic	Silicon-PVP	Spheres, 26 nm, citrate and Rods, 74 x 31 nm, CTAB	[a] Close packed films	Benzenethiol	--	103

All particles used are immobilized in a monolayer unless otherwise specified: [a] multilayer
NP: nanoparticle

2.7.3 Electrochemical sensors

The ability of gold nanoparticles to conduct electrical currents allows them to enhance electrochemical sensing applications. Electrochemical sensing entails the detection of species directly or indirectly through oxidation or reduction behaviour at the electrode surface. Colloidal gold nanoparticles have been immobilized onto the sensing electrode surface using the strategies summarized in Table 4. For electrochemical sensing, it is apparent that multilayer high density coverage of gold nanoparticles is most common. This multilayer immobilization state is usually achieved through electrostatic LbL deposition or integration of the gold nanoparticles into a three dimensional sol-gel matrix. In these multilayer systems, the gold nanoparticles act as electron conduction channels to transfer the electrons obtained from the oxidative/reductive species to the electrode surface.[128] A higher density of particles has been shown to increase the charge transfer constant and conduction abilities.[71] Although the peak currents obtained are usually lower than the bare electrode surface, enhanced sensing capabilities are enabled with three-dimensional sensing surfaces containing immobilized gold nanoparticles.[72,93,94] Conversely, on two-dimensional electrochemical sensor surfaces in which only a monolayer of gold nanoparticles is present, the particles can increase the peak currents by providing a higher surface area for the redox reactions to occur on the electrode surface.[35,52,95] Typically, small gold nanospheres are used for electrochemical sensing applications for best integration into three-dimensional matrices.

Table 4. Immobilization strategies employed for electrochemical sensors, including the sensor properties for respective analytes.

Immobilization strategy	Surface	Particle size	Immobilization state	Analyte(s)/ Redox species	Sensor characteristics	Ref.
Covalent	ITO-MPTMS	40 nm [a]	Monolayer, dispersed small aggregates	H_2O_2	LOD: 0.5 μM, LR: up to 6 mM	[35]
Covalent LbL	Au-(glucose oxidase-cysteamine-GNP)6	12 nm	Multilayer, low aggregation/coupling	Glucose	LOD: 8 x 10^{-6} M, LR: 1.0 x 10^{-5} - 1.3 x 10^{-2} M	[45]
Covalent/ Electrostatic	Glassy carbon-poly(o-phenylenediamine)	--	Monolayer, close packed	Enterovirus 71	LOD: 0.04 ng/mL, LR: 0.1 - 80 ng/mL	[129]
Electrostatic	ITO-APTMS	4 nm	Monolayer, dispersed 5% coverage	H_2O_2	LOD: 10 nM, LR: 0.03-1.0 mM	[52]
Electrostatic LbL	Pyrolytic graphite-$(PAH-NP)_{10}$	5 nm [b]	Multilayer, dense aggregation	Myoglobin	Electron conduction over 100 nm	[128]
	Silicon-PEI-$(PSS-NP)_{10}$	45 x 14 nm [c]	Multilayer, high density low aggregation	$Fe(CN)_6^{3-/4}$, Cytochrome C	Reversible redox behavior possible	[72]
	Au-(quaternized chitosan - NP)$_n$	11 nm	Multilayer, high density	$Fe(CN)_6^{3-/4-}$, Ferrocene methanol	Increase in charge transfer constant as NP density increases	[71]
Sol-gel network	Au-MPTMS sol-gel	20 nm	Multilayer, high density	H_2O_2	LOD: 2.0 μM, LR: 5.0 μM - 10.0 mM	[90]
	Glassy carbon-Au island-MPTMS sol-gel	20 nm [a]	Multilayer, high density clusters around islands	Cr(VI)	LOD: 2.9 ng/L, LR: 10 - 1200 ng/L, detection in blood	[91]
	Pt-MPTMS sol-gel	15 nm	Multilayer	Acetylcholine	LOD: 1 μM, LR: 0.005 - 0.4 mM	[92]
	Carbon paste-MPTMS sol-gel	10 nm	--	Ascorbic acid, dopamine, uric acid	LOD: 0.0160 mM, LR: 0.050 - 10.0 mM (ascorbic acid), simultaneously detect all molecules	[93]
	Au-MPTMS sol-gel	20 nm [a]	Multilayer, large aggregates	E. Coli DNA	LOD: 6.3 pmol, LR: 21-400 pmol, detects complimentary vs mismatched	[94]
	ITO-TEOS sol-gel	20 nm [d]	Monolayer, dispersed single/small clusters	Catechol	LOD: 3.0 μM, LR: 1-6 μM	[95]

All particles used are spherical in shape and stabilized with citrate capping agent except for: [a] unspecified capping agent, [b] glutathione capping agent, [c] Rods + CTAB capping agent, [d] polyvinylpyrollidone capping agent
NP: nanoparticle, LOD: limit of detection, LR: linear range

2.7.4 Other applications

Immobilized gold nanoparticles have also been used for other sensor applications including fluorescent and colourimetric sensors. For fluorescent-based sensor applications, a monolayer of small monodisperse gold nanoparticles are favored. The particles are used to create a higher surface area for the binding of molecular beacon DNA, improving the efficiency and sensitivity of the sensing hydridization reaction of complimentary DNA.[30,119] Colourimetric sensors for the detection of Pb^{2+} or Cu^{2+} ions have been based on monolayer or multilayer immobilized gold nanoparticles, with sufficiently high particle densities to create a strong colour on the surface. A chemical reaction between the gold particles and the Pb^{2+} or Cu^{2+} ions cause the particles to leach from the surface, causing the surface colour to fade.[79,100,130]

Additional applications which use immobilized colloidal gold nanoparticles on solid substrates are summarized in Table 5, including details on the immobilization state of the particles used. Monolayers of gold nanoparticles have been used to decrease the adhesion energy of a surface for micro-electromechanical systems (MEMS)[33,62], to produce localized hyperthermia to eradicate biofilms[37], as well as to increase transfection efficiency[57] of cells. Their electrical properties have also been exploited to increase the current density of diode structures[68] and to enable photo-induced electron transfer[76] for photovoltaics. For applications in nanophotonics, the localized SPR properties of immobilized gold nanoparticles are also being investigated for their ability to enhance second harmonic generation (SGH) for non-linear optics. For SGH enhancement the immobilization properties of the particles are very important; linear SPR coupling between two particles must occur, so they must be immobilized in pairs without significant aggregates.[75,131] Similarly, gold nanoparticles must be immobilized in linear arrays for plasmonic waveguide applications.[117]

Table 5. Other applications employing the use of immobilized gold nanoparticles, including the immobilization state and resulting application performance.

Application	Immobilization strategy	Surface	Particle size	Immobilization state	Application performance	Reference
Fluorescence DNA sensor	Electro-static	Silicon-APTES	10 nm [a]	Dispersed 500-700 particles/μm^2	Hybridization efficiency: 104 1/Ms, LOD: 200 pM	[30]
	Covalent	Glass-APTMS-lipoic acid	4 nm, 87 nm	Dispersed 5.7 x 10^3 particles/μm^2	Hydridization efficiency: 66%, LOD: 0.1 pmol	[119]
Colourimetric Pb^{2+}/Cu^{2+} sensor	Brush	Glass-PEG brushes	4 nm	High density infiltration into brush [e]	Pb^{2+}: LOD: 8 nM, LR: 10 nM - 100 µM, visual: blue to clear	[79]
	Hydropho-bic	Nitrocellulose membrane	13 nm [b]	Dispersed	Pb^{2+}: LOD: 50 pM, LR: 100 pM - 1.5 nM Cu^{2+}: LOD: 1.0 µM, LR: 1.0 - 100 µM	[100,130]
Decrease adhesion of MEMS	Covalent	Silicon-MPTMS/APhTMS	4.5 nm [c]	53% coverage, dispersed/small aggregates	95.6 - 98.2% decrease in adhesion energy	[33]
	Electro-static	Silicon-polydopamine	16 nm	Close packed	Decrease adhesive force 20.13 to 12.69 nN	[62]
IR photothermal excitation	Covalent	Glass-MPTMS	-- [d]	Dispersed high density	Efficient cell death of S. Aureus biofilms	[37]
Laser-assisted cell transfection	Electro-static	Polystyrene-APTES	200 nm	--	Higher transfection than NPs in solution	[57]
SHG	Electro-static	Glass-p(DDA/VPy)	30 nm, 12 nm	~375 particles/μm^2, 79% isolated, 16% coupled, 5% aggregated	1-layer: 8-fold SHG light enhancement, 2 layer: 288-fold	[75,132]
Photovoltaics	Electro-static	ITO-(PDDA-titania nanosheet)	3.5 nm	Close packed with coalescence	Photoinduced electron transfer observed, control polarity of photoresponses	[76]
Schottky barrier diode	Electro-static	Protinated SiO_2	20 nm	Dispersed 1-4 particles/μm^2	Increase in diode current density	[68]

All particles used are spherical in shape and stabilized with citrate capping agent except for: [a] oligonucleotide capping agent, [b] BSA capping agent, [c] 1-dodecanethiol capping agent, [d] Stars + laurylsulfobetaine capping agent. All particle are immobilized into a monolayer except for: [e] multilayer.
LOD: limit of detection, LR: linear range

2.8 Conclusions and outlook

Immobilization of colloidal gold nanoparticles onto solid substrates has enabled a variety of sensor applications including the use of surface plasmon resonance, surface-enhanced Raman spectroscopy, and electrochemical sensors to detect biological and chemical analytes. There is a growing drive to understand ways to control the immobilization of colloidal gold nanoparticles and how the particle immobilization state affects the sensor performance. While the majority of literature has focused on modifying the parameters of the gold nanoparticle solution to tune the deposition, there is a growing body of work examining how the immobilization can be controlled from the surface properties of the substrate. Understanding of the immobilization parameters enables the modulation of gold nanoparticle deposition from monodisperse particles to large three-dimensional networks of particle clusters, which can be tailored for smart design specific to the application of interest.

To bring technologies based on immobilized gold nanoparticles to practical application, the issue concerning the unknown stability of the immobilized gold nanoparticle surface must be addressed. To understand and to be able to improve the stability of the different immobilization techniques, future studies are strongly encouraged to test the stability of the nanoparticle-modified surfaces with respect to both solution exposure and mechanical abrasion. With the versatility of modulating the properties of the gold nanoparticle surface through the immobilization state, along with the benefits of facile modification with biomolecules and increased surface area, immobilized gold nanoparticles will continue to offer powerful alternatives to conventional sensing techniques, as well as electrical and photonic applications.

Chapter 3
Controlling the immobilization of gold nanoparticles through single-layer weak polyelectrolytes

3.1 Summary

Controlling gold nanoparticle clustering on solid substrates is important for applications that depend on inter-particle localized surface plasmon coupling (LSPC). Current immobilization methods employ impractical microfabrication techniques, or multi-step nanoparticle deposition. In this Chapter, we show broad LSPC tunability through the electrostatic deposition of gold nanoparticles onto single-layer weak polyelectrolytes (PEs). By controlling the deposition pH of weak PEs, the degree of nanoparticle clustering can be modulated from disperse particles to three-dimensional clusters. Simulations of the nanoparticle clustered states using Maxwell-Garnett theory help identify the relationship between cluster size and its contribution to the LSPC shift observed. We present a simple, scalable, one-step deposition platform to control the clustering state of nanoparticles on surfaces.

3.2 Introduction

Gold nanoparticles possess unique optical and electronic properties which make them an attractive platform for investigations in optoelectronics, sensing, and therapeutic applications.[12,13,133,134] Due to their nanoscale size, gold nanoparticles exhibit localized surface plasmon resonance (LSPR), which can be tuned by the particle size, shape, interparticle interactions, as well as the surrounding dielectric environment.[12] In particular, the integration of gold nanoparticles onto solid substrates is of interest to create convenient and reliable devices, improving repeatability and costs compared to solution-based applications.[26,28] For substrate-based applications, in addition to selecting the desired particle type, the resulting immobilization state of the particles must be considered. For example, as demonstrated in Chapter 2, highly monodisperse nanoparticles are desired for visible spectroscopic surface sensing[31,39,56,66], but LSPC generated by clustered nanoparticles is utilized for surface-enhanced Raman spectroscopy (SERS)[27,135,136], second harmonic generation[131], plasmonic waveguides[137], and laser-responsive photothermal applications.[37]

Current strategies for the immobilization of colloidal gold nanoparticles include the use of covalent interactions using thiol or amine-terminated moieties, electrostatic interactions, or weaker physical interactions such as van der Waals forces.[28] The most common method to precisely control the inter-particle spacing and clustering is through nano- and microfabrication techniques[26,27,88,118,138], which are expensive, time consuming, and often limited to small area modification. Recently, electrostatic deposition has also been used to tune the self-assembly of nanoparticles onto solid substrates. Mostly, researchers have approached this method by modifying the properties of the nanoparticles[139,140] or the electrostatic properties of the nanoparticle solution.[48,66,67,140] Ferhan et al. has demonstrated the ability to control the electrostatic deposition of gold nanorods by tuning the surfactant and salt concentration of the nanorod solution[48], however the tuning ability of this and similar approaches is limited to 2-D clusters. To attain 3-D clustering of nanoparticles on surfaces and broad-spectrum LSPC tuning, electrostatic layer-by-layer stacking of strong PEs and nanoparticles has been employed.[69,70,72,74,126,141] To further control 3-D clustering properties, Yuan et al. used pH-controlled layer-by-layer assembly of polyethylenimine, a weak PE, to control the clustering of citrate-stabilized gold nanoparticles.[73] Weak PEs in layer-by-layer deposition techniques are particularly versatile, as adjusting the deposition pH controls the thickness, conformation and charge density of the PE layer.[142–144] The disadvantage of these multilayer techniques is that multiple nanoparticle deposition steps are required, introducing high potential for sample variability. The ability to obtain broad LSPC modulation and controlled nanoparticle clustering on solid substrates through simple and cost-effective techniques still remains challenging.

In this Chapter, we demonstrate broad-spectrum LSPC tuning of assembled gold nanoparticles on single layers of weak PEs. First, the plasmonic properties of the immobilized nanoparticles were compared to those in solution. Next, varying the deposition pH of both strong and weak PE layers, the effect of the nanoparticle clustering and LSPC modulation was studied. In addition, we explored the immobilization dependence on nanoparticle size and shape. Simulations of the different nanoparticle cluster states obtained from the experimental data provided correlation between cluster size and the resulting LSPC optical properties.

3.3 Materials and Methods

3.3.1 Materials

Gold (III) chloride hydrate, silver nitrate, cetyltrimethylammonium bromide (CTAB), sodium borohydride, silver nitrate, L-ascorbic acid, sodium hydroxide (NaOH), hydrochloric acid (HCl), (3-aminopropyl)triethoxysilane (APTES), acetic acid, poly(sodium 4-styrenesulfonate) (PSS) (~70,000 g/mol), polyacrylic acid (PAA) (~100,000 g/mol) and sodium carboxymethyl cellulose (CMC) (~90,000 g/mol) were purchased from Sigma-Aldrich (Oakville, ON, Canada). Trisodium citrate dehydrate and glass coverslips were purchased from Thermo Fisher Scientific (Burlington, ON, Canada). All procured chemicals were used without further purification.

3.3.2 Synthesis of gold nanoparticles

Gold nanoparticles stabilized with CTAB, a cationic surfactant, were chosen for this study to impart a positive charge onto the nanoparticles needed for electrostatic immobilization.

3.3.2.1 Synthesis of gold nanospheres and nanostars

Spherical and star-shaped gold nanoparticles were synthesized using a previously published protocol employing a CTAB-mediated growth from a gold nanoseed precursor.[14] To synthesize the gold nanoseed precursor, 60 µL of 0.1 M freshly prepared ice-cold sodium borohydride was added to 20 mL of a solution containing 2.4 x 10^{-4} M gold (III) chloride hydrate and 10^{-4} M trisodium citrate dihydrate under vigorous stirring. The nanoseed solution was incubated overnight in dark ambient conditions and filtered (0.2 µm) prior to use. A 210 mL solution of 1.46 mM CTAB and 7.33 mM CTAB was prepared to synthesize the nanospheres and nanostars respectively. Under moderate stirring, 8.97 mL of 11 mM gold (III) chloride hydrate was added to each CTAB solution, followed by the addition of 10 mM silver nitrate (0.67 mL for nanospheres, 1.34 mL for nanostars). Then, 1.44 mL of 100 mM l-ascorbic acid was added dropwise to each solution. Immediately after the solutions turned clear, the appropriate volume of gold nanoseed (5.60 mL for nanospheres and 2.24 mL for nanostars) was added.

3.3.2.2 Synthesis of gold nanocubes

Gold nanocubes were synthesized using another previously described method using CTAB-mediated growth[16,145]. First, gold nanoseeds were synthesized by adding 2.5 mL of a 10 mM aqueous gold (III)

chloride solution to 7.5 mL of a 100 mM CTAB solution at approximately 30 °C. Under vigorous stirring, 0.8 mL of 10 mM sodium borohydride was added to the gold solution to form the nanoseeds. The seed solution was then left at 30 °C for at least 3 hrs, diluted 1:10 in Millipore water and filtered (0.2 μm) prior to use. A solution containing 48 mL of 300 mM CTAB and 6 mL of gold (III) chloride in 240 mL Millipore water was prepared for nanocube growth. Next, 28.5 mL of 600 mM ascorbic acid was added to the growth solution and was mixed by inversion. After the solution turned colourless, 150 μL of the diluted, filtered gold nanoseed was added. The solution was mixed by inversion and left undisturbed for 15 minutes.

All three types of nanoparticles were purified by centrifugation at 10,000 rpm for 15 mins and resuspended in 1 mM CTAB solution. The gold nanocubes were resuspended to only half of the original volume to increase the concentration of the nanoparticles to approximately those of the nanospheres and nanostars. To characterize the particles, samples were prepared by adding 5 μL droplets onto a copper grid, allowing them to dry overnight prior to imaging using a Phillips (Eindhoven, Netherlands) CM10 transmission electron microscope (TEM).

3.3.3 Immobilization of gold nanoparticles

Glass coverslips were washed by sonicating in ethanol for 20 minutes followed by thorough rinsing in Millipore water (>12 MΩcm). Then, the coverslips were submerged in a 2M solution of NaOH for 20 minutes, rinsed thoroughly in Millipore water and dried under a stream of nitrogen. Immediately before use, a 10% v/v solution of APTES was prepared in reagent grade ethanol. The coverslips were submerged in the APTES solution for one hour on a Stovall Life Science Inc. (Peosta, IA, USA) Belly Dancer orbital shaker in ambient conditions for the silanization reaction to occur. Then, the coverslips were rinsed three times in ethanol, rinsed in Millipore water, and dried with nitrogen. Solutions of PSS, PAA, and CMC were prepared at a concentration of 20 mg/mL in Millipore water. The pH of the polyelectrolyte solutions were adjusted to the appropriate value using HCl or NaOH. Next, the coverslips were submerged in the polyelectrolyte solutions, and incubated on the orbital shaker for one hour. The coverslips were rinsed three times in Millipore water and dried with nitrogen. Immediately before use, the gold nanoparticle solution was centrifuged at 12,000 rpm for 10 minutes and the CTAB concentration in solution was decreased to 20 μM by replacing the appropriate amount of supernatant with Millipore water. Next, a droplet of the gold nanoparticle solution was placed onto the coverslip to cover the entire surface and was left covered and

undisturbed overnight in ambient conditions (~16hrs). Finally, the samples were rinsed five times with Millipore water to remove the unbound nanoparticles and were dried under nitrogen flow.

3.3.4 Characterization of optical properties

To characterize the visual properties of the immobilized nanoparticles, the samples were photographed using a Canon EOS Rebel T3 DSLR camera under controlled lighting conditions. The sample images presented in each figure were obtained in the same photograph. The brightness and contrast of each photograph was adjusted for best representation.

The spectrophotometric properties of the particles were analyzed using a BioTek (Winooski, VT, USA) Epoch microplate spectrophotometer. Triplicate absorbance spectra from 350 nm to 999 nm were obtained from different areas on the sample surface. The absorbance intensities at each wavelength were normalized prior to averaging. To compare nanoparticles in solution to those immobilized, the spectra were normalized to baselines of 900 nm and 950 nm respectively using the following equation:

$$Baseline\ normalized\ absorbance = Measured\ absorbance - Absorbance\ at\ baseline$$

To compare the shape of the spectra for the different immobilization conditions, the spectra were normalized to the absorbance at the primary peak wavelength:

$$Peak\ normalized\ absorbance = \frac{Measured\ absorbance}{Absorbance\ at\ 1^0\ peak\ wavelength}$$

Analysis of peak positions and corresponding intensity was performed using OriginPro (Originlab, Northampton, MA, USA) software.

3.3.5 Atomic force microscopy

The immobilized nanoparticles were imaged using a Bruker (Santa Barbara, CA, USA) Dimension Icon Atomic Force Microscope (AFM). Samples were allowed to dry in ambient conditions for at least 24 hours prior to imaging. A silicon nitride probe (f_0: 70 kHz, k: 0.4 N/m) was used to image the samples using the PeakForce Tapping™ mode. Image processing and particle count analysis was performed using Nanoscope Analysis software (Bruker).

3.3.6 Modeling of immobilized gold nanoparticle aggregation

The optical characteristics of the different immobilization states of the gold nanoparticles were modeled using Maxwell Garnett (MG) medium theory.[146] Spherical gold nanoparticles with a radius of 9 nm were classified as non-aggregated particles or into six types of clusters for the simulation. The clusters were assumed to be in a hexagonal close packed structure with sizes smaller than the wavelength of light. Air was used as the medium surrounding the particles, while the interspace inside of each cluster was filled with water. The effective permittivity (ε_{eff}) of the different cluster states was calculated using the MG equation:

$$\frac{\varepsilon_{eff} - \varepsilon_s}{\varepsilon_{eff} + 2\varepsilon_s} = V_a \times \frac{\varepsilon_a - \varepsilon_s}{\varepsilon_a + 2\varepsilon_s}$$

where ε_a is the complex permittivity of gold, ε_s is the permittivity of water, and V_a is the volume fraction of the gold/water ratio in the clusters.[147] The absorption coefficient (α_{abs}) for the different cluster states were then calculated from the complex ε_{eff} in the MG equation[148]:

$$\alpha_{abs} = \frac{4\pi}{\lambda}\kappa = \frac{4\pi}{\lambda}\sqrt{\frac{\sqrt{\varepsilon_1^2 + \varepsilon_2^2} - \varepsilon_1}{2}}$$

where κ is the imaginary part of the effective refractive index of the clusters, λ is the wavelength of light, ε_1 and ε_2 are the real and imaginary parts of the ε_{eff} respectively.

To predict the absorbance spectrum of the immobilized nanoparticles, the occupied area of the clusters on the surface was determined from AFM image analysis. The volume fraction of the non-aggregated particles was assumed to be 0.125 for the absorption coefficient calculation. Finally, the absorption spectra of the immobilized nanoparticles were recombined with Beer-Lambert Law[149,150]:

$$A = -\log\left(\frac{I}{I_0}\right) = -\log(e^{-\alpha z}) = -\log(e^{-\alpha_1 z_1 - \alpha_2 z_2 - \alpha_3 z_3 \cdots})$$

where A is the absorbance, I_0 and I are the incident and transmitted light intensity respectively, α is the absorption coefficient of the six different clusters states and non-aggregated particles, and z is the optical length. The optical length for different cluster types was determined from the height of the cluster weighted by the percent surface coverage. The resulting absorbance spectra were normalized to the absorbance intensity at the peak wavelength condition, similar to the experimental results. It should be noted that MG theory is suitable for well-separated (isolated) particles, in which interaction

between particles is ignored.[151] The model uses one material as the host and considers the volume fraction of the other material. Hence, MG theory is usually used in the case of low volume fraction.

3.4 Results

In this study, the electrostatic immobilization of gold nanoparticles coated with CTAB, a positively charged surfactant, was explored on surfaces modified with negatively charged PEs. The immobilization scheme is depicted in Figure 3a. First, the glass surface treated with NaOH is modified with an APTES monolayer to impart a positive charge onto the surface. This positively charged base layer allows the self-assembly of negatively charged PEs onto the surface, reversing the charge of the surface to deposit the gold nanoparticles. In recent published works, only strong, PEs such as polystyrene sulfonate (PSS) have been used to deposit positively charged nanoparticles.[48,72,126] In this report, we not only used PSS, but studied the effects of using weak PEs including polyacrylic acid (PAA) and carboxymethyl cellulose (CMC), whose structures are given in Figure 3b. Furthermore, we looked at how changing the particle size and shape affected the electrostatic-induced particle deposition using small nanospheres and larger nanostars and nanocubes (Figure 3c). The synthesized particles used in this study were measured to be 17.3 ± 0.9 nm, 46.7 ± 3.9 nm, and 48.0 ± 1.9 nm in size (mean ± s.d., n = 15) for nanospheres, nanostars, and nanocubes respectively, as determined by TEM (Figure 4).

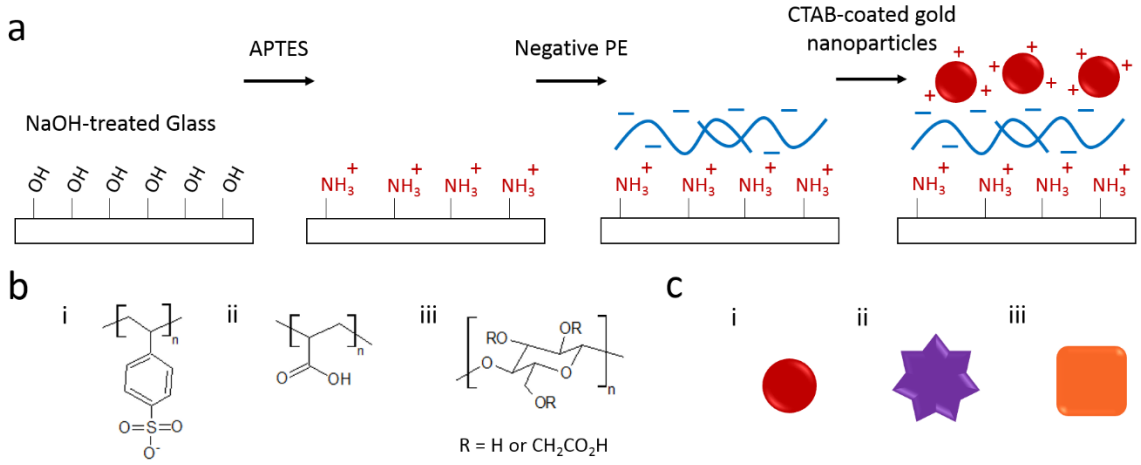

Figure 3. Schematic representation of the strategy to study the immobilization of gold nanoparticles on PEs: a) Surface modification steps for immobilization of gold nanoparticles. b) Structure of PEs used in surface modification: (i) PSS, (ii) PAA, (iii) and CMC. c) Different

shapes and sizes of gold nanoparticles explored: (i) small nanospheres, and (ii) larger nanostars and (iii) nanocubes.

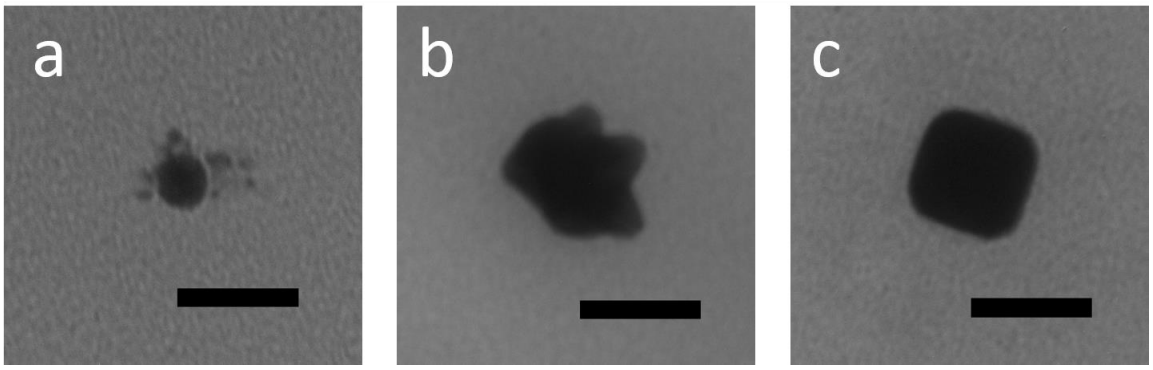

Figure 4. Transmission electron micrographs of gold nanospheres (a), nanostars (b), and nanocubes (c) (scale bars = 50 nm).

3.4.1 Immobilization of nanoparticles on a permanent polyelectrolyte at neutral pH

The LSPR properties of our immobilized nanoparticles were initially characterized on a substrate modified with PSS, a strong permanent PE. First, using the nanospheres as model particles, the effect of CTAB concentration in solution was explored since many recent published works recommend lowering the CTAB concentration prior to deposition.[65,66,72] We found that no deposition occurred in the native CTAB solution (1 mM), and that the CTAB concentration had to be reduced to 20 μM to obtain a strong absorbance signal on the surface (Figure 5). The CTAB concentration is known to affect the solution ionic strength, which plays an important role in the electrostatic deposition of nanoparticles.[48] Thus, a CTAB concentration of 20 μM was used herein for the deposition of gold nanoparticles.

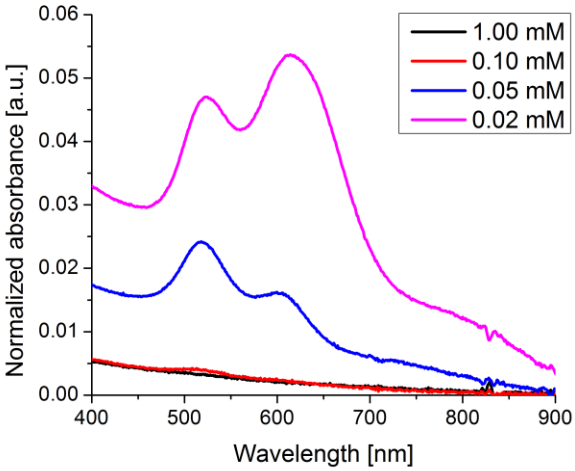

Figure 5. Baseline normalized UV-Vis absorbance spectra of the immobilized nanospheres deposited with decreasing concentrations of CTAB in solution.

All three nanoparticle types were immobilized onto glass surfaces containing PSS deposited at an unadjusted neutral pH. As seen in the photographs presented in Figure 6a, the visual properties of the immobilized nanoparticles differ from those in solution. The most prominent difference is seen with the nanospheres; they appear red in solution yet blue on the surface. The ultraviolet-visible (UV-Vis) absorption spectrum of the immobilized nanospheres shows the creation of a secondary peak around 610 nm caused by inter-particle LSPC[74], compared to the single peak observed when they are in solution (Figure 6b). Both nanostars and nanocubes show no indication of LSPC when immobilized, but a blue-shift in the absorbance peak position of approximately 15 nm is observed (Table 6). A decrease in the absorption intensity by an order of magnitude is observed for all three particle types.

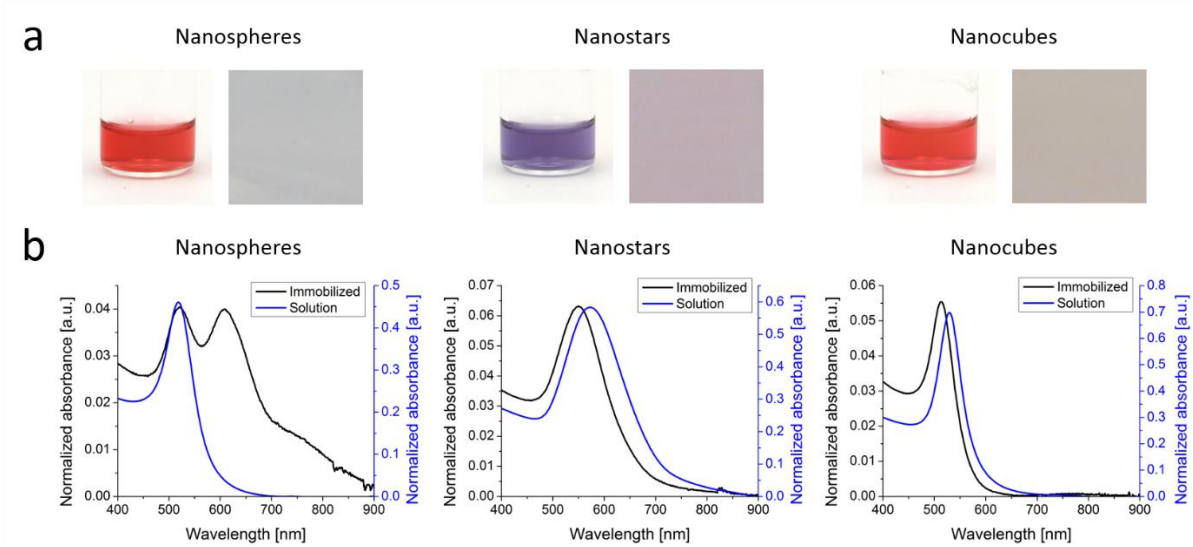

Figure 6. Comparison of gold nanoparticles in solution to those immobilized onto PSS: a) Photographs comparing the visual difference, where left images show the solution in a vial and right images represent a coverslip with immobilized gold nanoparticles. b) Baseline normalized UV-Vis absorption spectra.

Table 6. Absorption peak positions of gold nanoparticles in solution and immobilized onto glass.

Particle Type	Peak position [nm]	
	Solution	Immobilized
Nanospheres	518	520, 608
Nanostars	572	550
Nanocubes	529	513

3.4.2 Effect of polyelectrolyte deposition pH on nanoparticle immobilization

Prior to deposition, solutions of PSS, PAA, and CMC were adjusted to pH values ranging from 2 – 8. Nanospheres were initially used as model particles to be immobilized onto different PE modified surfaces. Visually, (Figure 7a) of the immobilized nanospheres undergo a change of colour from light orange to dark blue as the PE deposition pH is decreased, with varying degrees of modulation with

the different PEs. The UV-Vis spectra (Figure 7b) of each surface show that the secondary LSPC peak, indicative of nanoparticle clustering, increases in intensity with respect to the primary peak and red-shifts as the PE deposition pH is decreased. Similar to the visual appearance, these characteristics are modulated differently for each PE. For PSS, a change in the LSPC peak position (Figure 7c) and intensity ratio (Figure 7d) is only observed when the deposition pH is changed from 8 to 6, then remains constant at lower pH. Immobilization on PAA demonstrates the broadest range of control of the longitudinal peak position (from 591 to 704 nm), and peak intensity ratio (0.78 to 1.52) within the selected pH conditions. The modulation of peak position (from 590 to 690 nm) and intensity ratio (0.73 to 1.41) of CMC does not have as broad of a range compared to PAA.

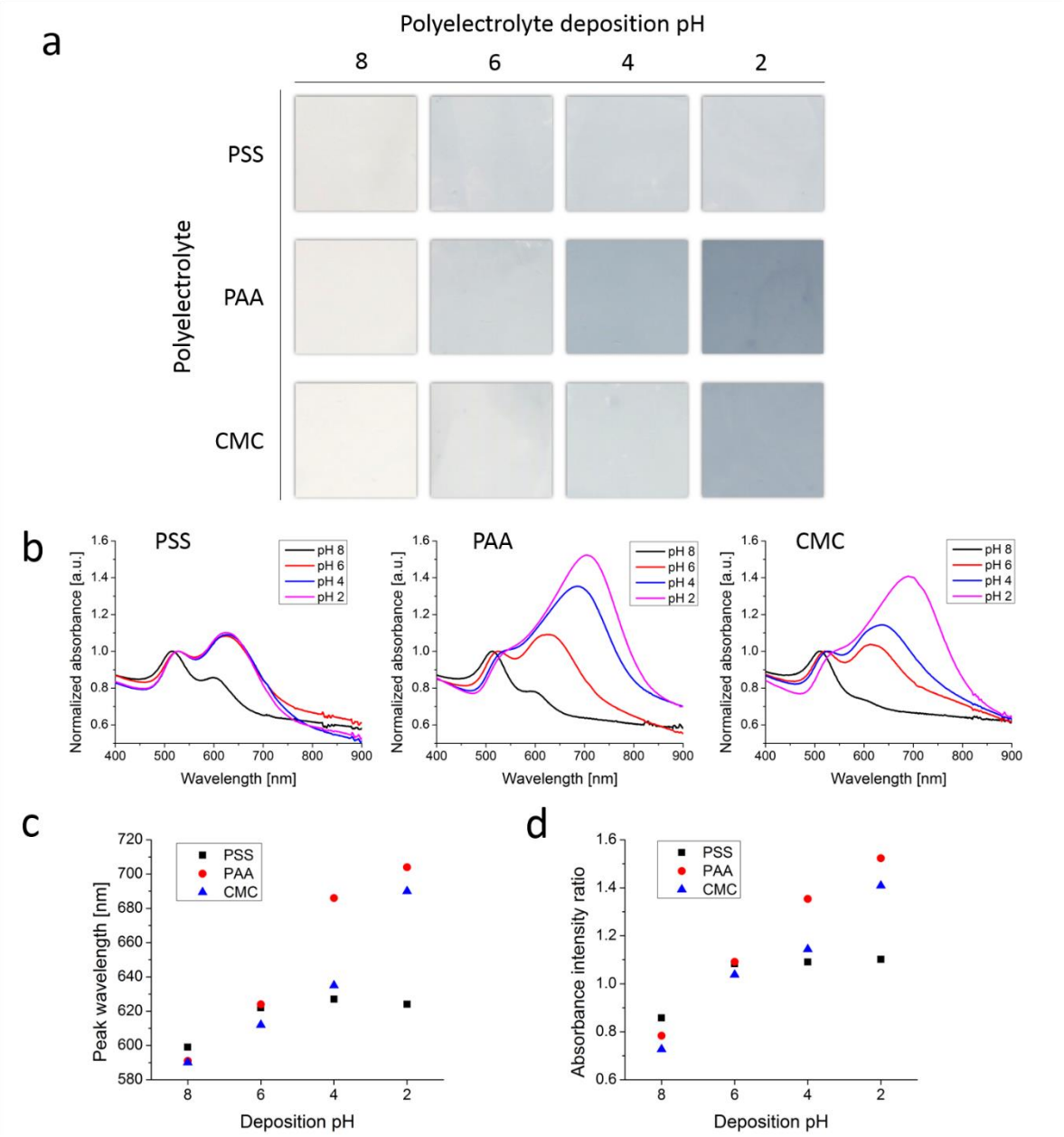

Figure 7. Immobilization of gold nanospheres (17 nm) onto PSS, PAA and CMC deposited at varying pH: a) Photographs of the resulting immobilized nanoparticles on glass coverslips. b) Peak normalized UV-Vis absorption spectra of immobilized nanoparticles. c) Analysis of the secondary plasmon peak positions. d) Analysis of the intensity ratio of the secondary/primary plasmon peaks.

We studied the effect of particle size and shape by immobilizing nanostars and nanocubes onto PAA deposited at varying pH. Both nanocubes and nanostars are similar in size and larger than the nanospheres. Visually, we observed less modulation of nanostar and nanocube deposition (Figure 8a) compared to nanospheres (Figure 7a) when changing the PAA deposition pH. For both nanostars and nanocubes, the deposition at pH 2 and 4 appear similar to each other, as well as the deposition at pH 6 and 8. Looking at UV-Vis spectra (Figure 8b), a red-shifted LSPC peak is observed at deposition pH of 4 and 2, but the intensity is only less than or approximately equal to that of the primary peak. As both particles displayed similar deposition properties, only nanostars were selected for further studies.

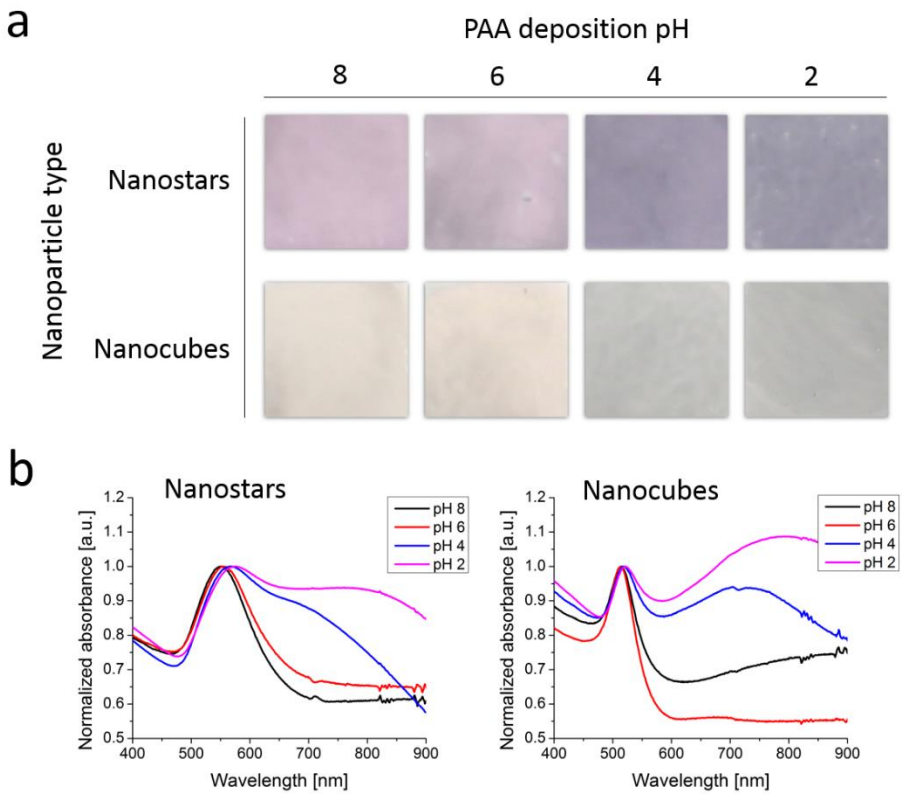

Figure 8. Immobilization of gold nanostars and nanocubes (~48 nm) onto PAA deposited at varying pH: a) Photographs of the resulting immobilized nanoparticles. b) Peak normalized UV-Vis absorption spectra of immobilized nanoparticles.

3.4.3 Atomic force microscopy of nanoparticle clusters

In Figure 9a and 9b, AFM topographic images of nanospheres immobilized onto PSS and PAA are presented respectively. When PSS is deposited at pH 8, a uniformly distributed monolayer of nanospheres is formed. At pH 6, small clusters of particles are observed in addition to the single particles. The immobilization state of nanospheres on PSS then remains the same as deposition pH is further reduced, in accordance with the UV-Vis results previously presented. For PAA deposited at pH 8 and 6 the particle clustering resembles that of PSS; however, when the deposition pH is further reduced much larger networks of clusters are observed, including some 2-particle and 3-particle high stacking for pH 4 and 2 respectively. For all pH conditions, the density of nanospheres on the surface is higher for PAA (Table 7). When immobilizing larger nanostars onto PAA (Figure 9c), the drastic change in clustering is not apparent. For PAA deposition at pH 8 and 6, the nanostars are monodisperse, and at pH 4 and 2 only small, mostly monolayer clusters formed. However, the total particle density of the clustered nanostars still nearly doubled compared to that of the monodispersed ones, a trend similar to nanospheres (Table 7).

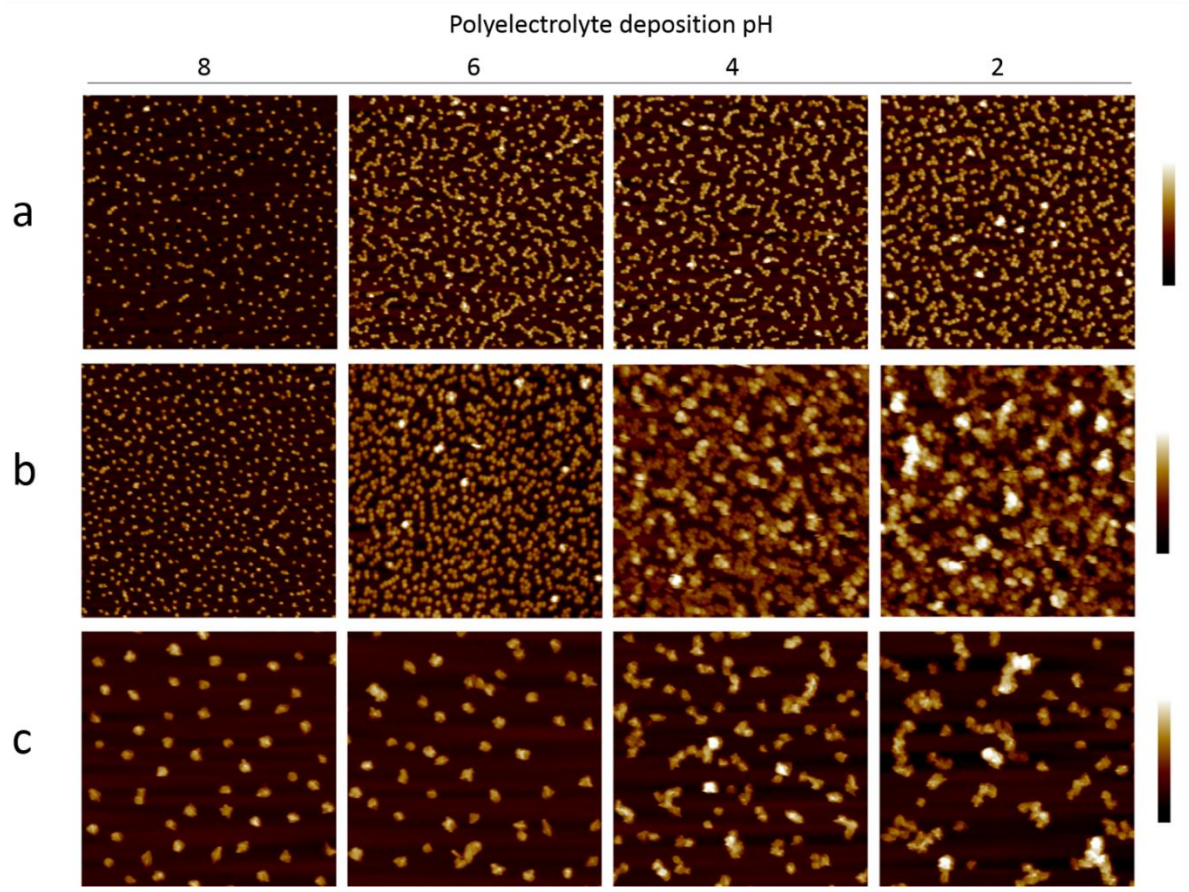

Figure 9. AFM topographic images of immobilized gold nanoparticles on PEs deposited at varying pH: a) Nanospheres immobilized onto PSS (scale bar height: 0-35 nm). b) Nanospheres immobilized onto PAA (scale bar height: 0-35 nm for pH 8-6, 0-60 nm for pH 4-2). c) Nanostars immobilized onto PAA (scale bar height: 0-90 nm). All images in are 1.2 x 1.2 µm in size.

Table 7. Density of particles immobilized onto PSS and PAA deposited at varying pH, determined from atomic force microscopy image analysis.

		Total particle density [/μm^2]			
Particle type	**Polymer**	**pH 8**	**pH 6**	**pH 4**	**pH 2**
Nanospheres	PSS	270.0	583.3	583.4	572.5
Nanospheres	PAA	403	631.5	871.9	787.1
Nanostars	PAA	36.9	35.2	78	63.5

Analyzing the AFM images, the average distribution of the resulting 2-D nanoparticle cluster sizes is presented in Figure 6. For nanospheres immobilized onto PSS (Figure 10a) and PAA (Figure 10b), a drop of ~50 % in the distribution of single particles is observed when the PE deposition pH is decreased from 8 to 6, and is compensated by clusters containing 3 – 6 particles. Further decreasing the deposition pH of PAA introduces much larger 2-D clusters ranging in size from 7 – 50 particles. Note that this analysis does not include 2-particle and 3-particle high stacking observed in Figure 9b. In Figure 10c, the differences between the immobilization distributions of the larger nanostars on PAA compared to the nanospheres becomes apparent. For nanostars, over 90% of the surface population is of single particles for depositions at pH 8 and 6, and predominately smaller clusters of 2 – 4 particles are formed upon decreasing the pH.

The morphological changes of the modified surface prior to nanoparticle immobilization were also examined using AFM (Figure 11). Glass coverslips modified with NaOH etching and APTES immobilization were very smooth and uniform with measured root-mean-square (RMS) surface roughness of 0.271 nm and 0.311 nm respectively. Depositing PAA onto the APTES layer resulted in RMS surface roughness of 0.350 nm, 0.368 nm, 0.503 nm, and 0.607 nm when the pH is decreased from 8 to 2 respectively, without drastic changes in the surface morphology.

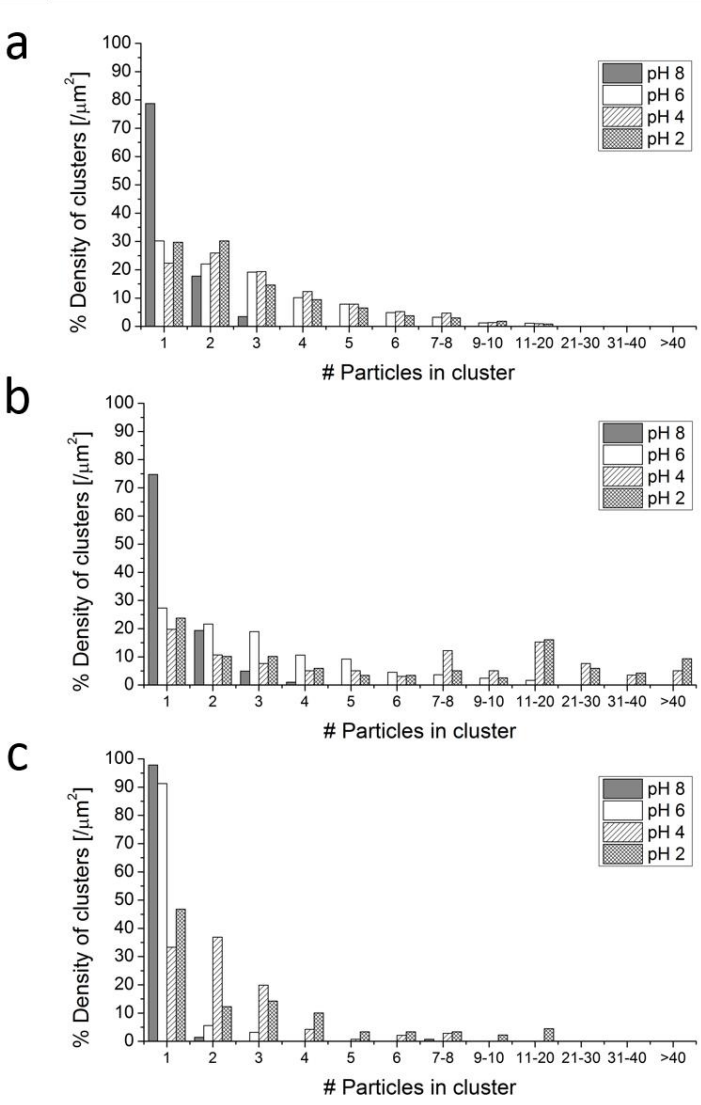

Figure 10. Cluster size distribution of immobilized gold nanoparticles on PEs deposited at varying pH. a) Nanospheres deposited onto PSS. b) Nanospheres deposited onto PAA. c) Nanostars deposited onto PAA.

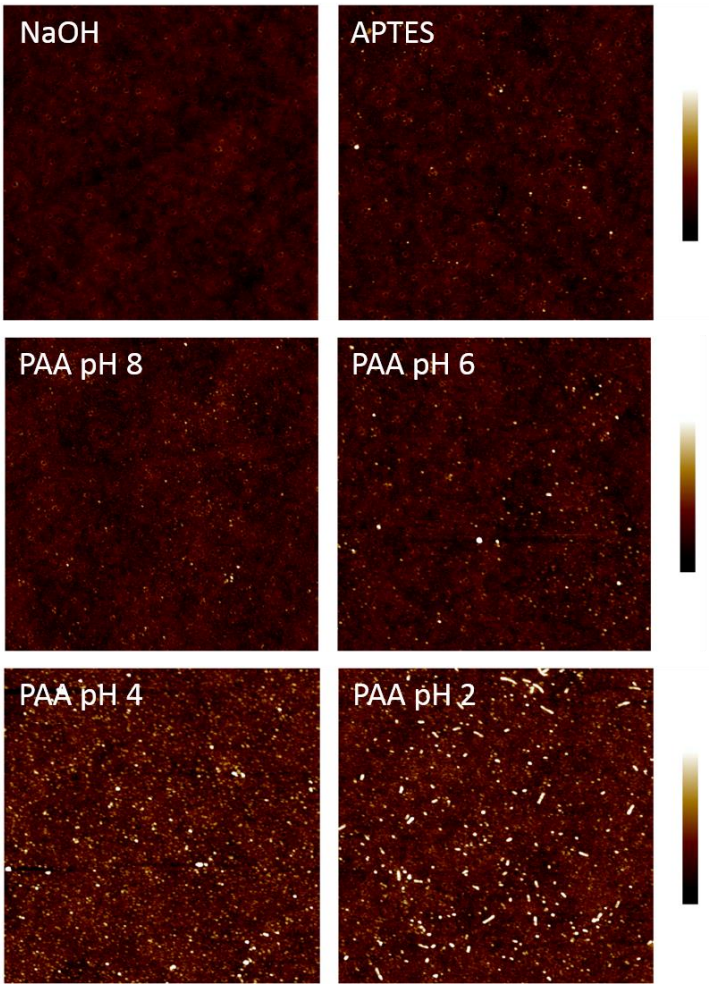

Figure 11. AFM topographic images of glass coverslips with modular surface modifications including NaOH treatment, APTES monolayer formation, and PAA deposited from pH 8 – 2. All images are 2.0 x 2.0 µm in size with height scale from 0 – 4.4 nm.

3.4.4 Modelling gold nanoparticle immobilization states

From the AFM images (Figure 9b), six different aggregation types of nanoparticles were identified (Figure 12a) and used in the model with the corresponding calculated volume fractions listed in Table 8. Although the immobilized nanoparticles on the surface are exposed to air when dried, the space within the particle clusters was assumed to be filled with water, as the peaks corresponding to the clustered nanoparticles did not show a blue-shift with a change in refractive index when transitioning from water to air. The simulated results of the absorbance coefficient over the optical light spectrum

corresponding to the identified clusters are shown in Figure 12b. LSPC between a pair of particles is shown to produce a peak at 578 nm, whereas increasing the monolayer cluster size produces peaks that red-shift to 600 – 640 nm (Figure 12c). Absorbance around 700 nm and above is only observed when 3-D 2-particle and 3-particle high clusters are formed. The relative amount of surface area occupied by each nanoparticle cluster type (Table 8) was calculated based on the cluster distributions determined from AFM analysis (Figure 10) to model the absorbance properties of nanospheres immobilized onto PAA. The resulting shape of the obtained absorption spectra shown in Figure 13 closely resembles those of the experimental results (Figure 7b).

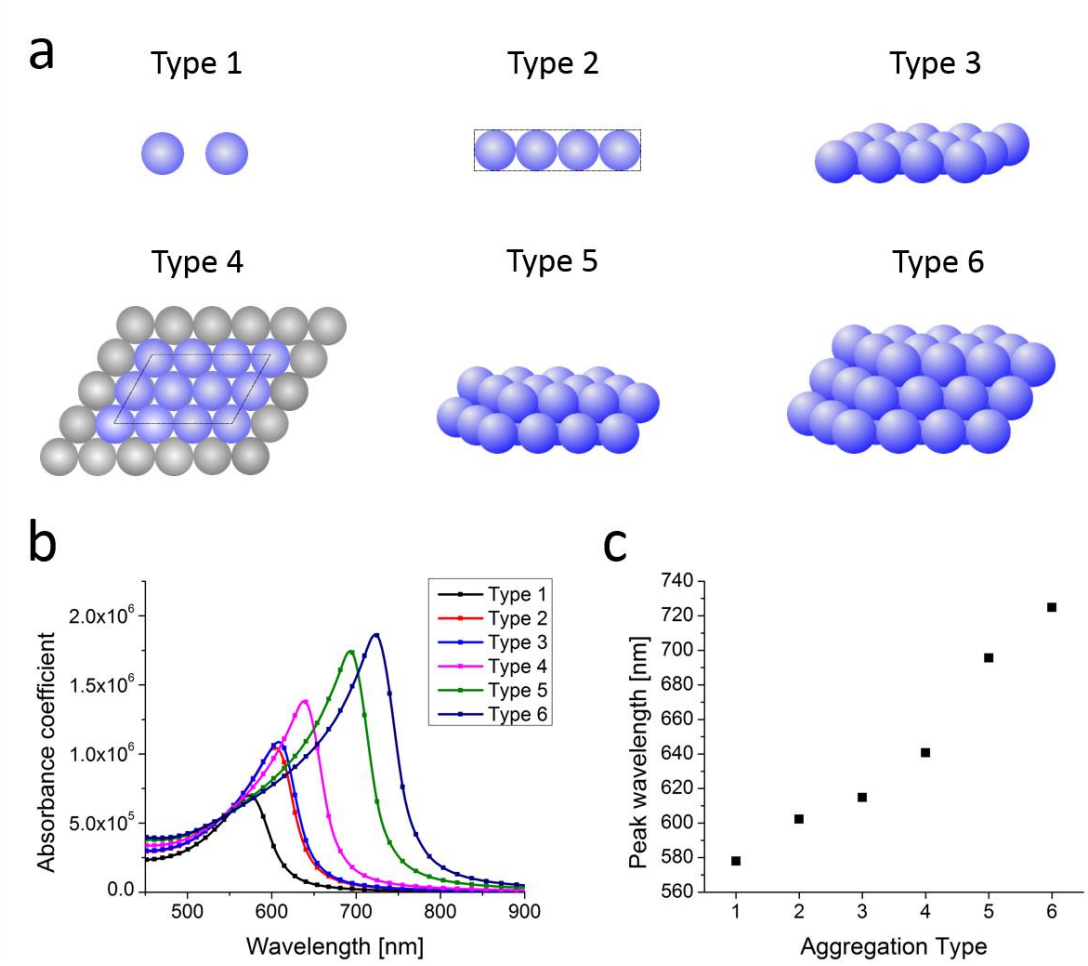

Figure 12. a) Aggregation types used in the MG medium theory model. b) Simulated result of the absorbance coefficient over the visible spectra for each aggregation type. c) Analysis of the peak wavelength of the absorbance coefficient for each aggregation type.

Table 8. Parameters used for modelling of immobilized nanoparticles.

Aggregation type	Volume fraction (V_a)	Number of particles in cluster	Percentage of surface covered by clusters			
			PAA pH 8	PAA pH 6	PAA pH 4	PAA pH 2
Type 1	0.4289	2	2.95290%	2.13960%	0.26276%	0.15015%
Type 2	0.5236	3-4	1.42640%	4.91732%	0.53177%	0.40039%
Type 3	0.5337	5-8	0.00000%	4.99553%	1.66413%	0.55680%
Type 4	0.6046	≥ 9 Single layer	0.00000%	1.48583%	5.72124%	2.81213%
Type 5	0.6910	Two layer	0.00000%	0.45670%	4.69523%	4.77969%
Type 6	0.7255	Three layer	0.00000%	0.00000%	2.00196%	3.02171%
Non-aggregated	0.1250	1	95.62070%	86.00502%	85.12290%	88.27913%

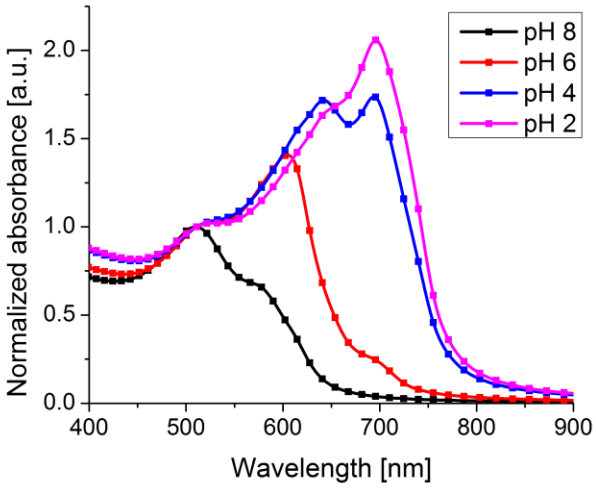

Figure 13. Simulated result of the peak normalized absorbance spectra for gold nanospheres immobilized onto PAA deposited at varying pH using the combination of aggregation types detailed in Table 8.

3.5 Discussion

To obtain specific properties of nanoparticles on a substrate, it is important to understand how the LSPR properties of the immobilized particles may differ from those in solution. For the nanoparticles used in this work, both the position and intensity of the absorbance peaks changed with deposition, affecting the visual properties of the particles (Figure 6). The presence of the secondary absorbance peak for the immobilized nanospheres (Figure 6b) indicates that a population of aggregated nanospheres is present on the surface and would account for the blue colour. Since no secondary peaks are observed for nanostars or nanocubes, there is likely no aggregation present on the surface. The blue-shift in primary peak position from solution to surface for both nanostars and nanocubes (Figure 6b) is caused by the decrease in refractive index in the surrounding medium from water to air.[66] The peak corresponding to the singly-dispersed immobilized nanospheres does not show this blue-shift compared to solution, likely due to the overlapping contribution of the aggregation peak. The order of magnitude difference in absorption intensity between nanoparticles in solution and those immobilized is a result of the difference in sample path length.

The changes in the immobilization properties of the nanoparticles can be attributed to varying the PE charge density and conformation on the surface with deposition pH. In the case of PSS, which is a strong PE that does not change its ionization state with pH, the change in the resulting immobilization properties between deposition pH of 8 and 6 (Figure 7 and Figure 9a) is not obvious. To explain this phenomenon, one must consider the APTES layer used to assemble the PSS. A surface-immobilized monolayer of APTES has a reported apparent pK_b of 7.6 [152], at which half of the amino groups are ionized. Therefore, when the PSS is being deposited at pH 8, the APTES layer is less protonated than at lower pH values, resulting in a lower positive charge density of the base layer. This decreases the amount of PSS that will self-assemble onto the surface for charge neutralization, producing a lower net negative charge on the surface. Thus, a lower density of particles is deposited onto PSS at pH 8 compared to lower pH values (Table 7) with less particle clustering (Figure 10a).

For PAA and CMC, the variable ionization of the polymer chain is the main contributor to changes in the surface properties. When depositing a weak polyelectrolyte onto an oppositely charged surface, the resulting thickness of the weak polyelectrolyte layer is dependent on the deposition pH.[142,143,153,154] In solution, PAA has a pK_a of approximately 6.5.[153] Therefore, when PAA is deposited at pH 8, it has a very high degree of ionization and will assemble as a thin layer with flat chain conformation to

match the charge of the APTES layer, which possesses a lower charge density at this pH. As the deposition pH is decreased, PAA becomes less ionized, adapts a more open loop-rich coiled conformation, and requires a thicker layer to be deposited to match the charge of the fully protonated APTES layer. The surface roughness measurements of the PAA films used in this study obtained from AFM images (Figure 11) agree with previously published works which elucidate the mechanism of this theory.[143] In an aqueous environment it can be expected that the PAA layer extends even further from the surface at lower ionization due to polymer swelling effects[155], which in conjunction with the resulting surface charge will affect nanoparticle immobilization.

When depositing the nanoparticles, the PE-modified surfaces were subjected to the nanoparticle solutions at a neutral pH of approximately 6.5-7. For PAA layers deposited onto surface through electrostatic interactions, the apparent pK_a of the immobilized layer is known to decrease to approximately 3 or 4 depending on the pH at deposition due to the influence of the underlying layers to the electrostatic environment.[156] With a reduced apparent pK_a, all of the PAA surfaces in this study would become ionized with similar charge densities in the nanoparticle solution, creating varying amounts of charge overcompensation proportional to the deposited PAA layer thickness.[157] As the deposition pH of the PAA is decreased, the resulting increased surface charge in addition to the extended conformations of the PE[73] induces increased nanoparticle deposition (Table 7). For nanospheres immobilized onto PAA deposited at pH 4 and 2, these properties are extreme enough to induce large clusters of particles (Figure 10b) with multilayer stacking (Figure 9b).

Nanosphere deposition onto CMC produces different immobilization properties to that of PAA (Figure 7). Assembly of CMC on a charged layer demonstrates similar phenomenon to that discussed with PAA[158], however CMC has a lower reported pK_a of 2 – 4 in solution.[159] At deposition pH of 2 and 4, CMC would have a higher surface charge density compared to PAA, and would deposit in a thinner and more compact layer on the surface. This in turn creates a lower overall surface charge for nanoparticle deposition, resulting in less deposition and particle clustering compared to PAA as inferred by the visual properties (Figure 6a) and secondary peak position and intensity in the UV-Vis spectra (Figure 6b). Furthermore, the structural and acid group separation distance difference between the two polymers is also likely to contribute to variation in nanoparticle immobilization. This demonstrates that the immobilization properties and LSPC tuning is specific to the type of weak PE used.

When depositing the larger nanostars and nanocubes onto PAA at varying pH, a lower range of LSPC modulation is observed (Figure 9). This indicates that less nanoparticle clustering is being induced compared to the immobilization of the smaller nanospheres. Since both nanostars and nanocubes exhibited similar immobilization characteristics, the deposition properties are therefore not dependent on particle shape. Analyzing the AFM images of the immobilized nanostars (Figure 9c), the decrease in particle clustering is confirmed (Figure 10c) and a lower deposition density (Table 7) was observed compared to immobilization of the smaller nanospheres. When the same surfaces are used to immobilize the larger nanostars, less clustering is observed because the larger particles possess a greater overall charge, and would be less susceptible to the surface PE conformations. The ability to attain large clusters of particles through weak polyelectrolyte electrostatic deposition is thus greatly hindered by increasing the particle size. To induce multilayer clustering of larger nanoparticles, it is predicted that a much higher surface charge would be needed. A summary of the process for controlling the deposition and clustering of the nanoparticles with respect to weak PE deposition and different sized particles is represented in Figure 14.

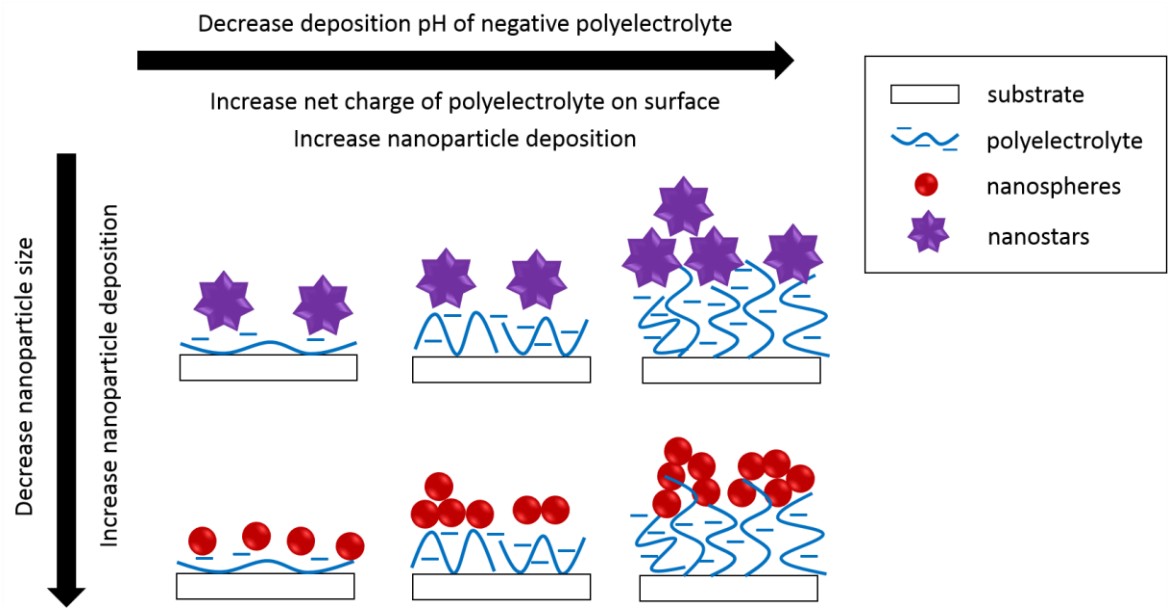

Figure 14. Schematic describing the relationship between the nanoparticle size and the deposition pH of weak PEs on the surface on the resulting immobilized nanoparticle characteristics.

An alternative method to adjust the PE layer thickness and conformation would be to modulate the salt content of the PE solution upon deposition. Upon increasing the amount of salt, the effective charge of the PEs would decrease in accordance with DVLO theory, and thicker layers would deposit onto the surface. If the salt ions could then be removed, varying degrees of charge overcompensation on the surface could be obtained. This specific method was not selected as the presence of salt can disrupt the colloidal stability of the gold nanoparticles.

For applications where a specific LSPR of the immobilized nanoparticles is desired, it is important to understand the relationship between the nanoparticle clustering and their resulting optical properties. The LSPC effect on the surface plasmon resonance of gold nanospheres immobilized onto PAA at varying pH was modeled using MG theory (Figure 13). The MG effective medium theory had been used in estimating optical characteristic of thin film and particle clusters[146], for example, the absorption spectra of nickel particle clusters[160] and silica-coated gold nanoparticles.[139] In this work, it has been effectively used to model the immobilization of gold nanoparticles present in multiple cluster states on the surface. This enabled the direct connection between different cluster types observed (Figure 12a), their respective surface coverage (Figure 10b) and the resulting LSPC properties (Figure 13). Knowing the absorbance coefficients of different cluster types (Figure 12b-c), MG theory can be a useful tool to determine the type of nanoparticle clustering required to obtain a desired absorbance spectrum. With this knowledge, the properties of the surface can be engineered accordingly to obtain the desired clustering using pH controlled PE deposition.

The resulting ability to tune the LSPC properties in this work is equal to or better than other studies that employ layer-by-layer assembly of gold nanoparticles with PEs[69,73,74], with the advantage of only using a single deposition step. Furthermore, to the best of our knowledge this is the first report using pH-controlled negatively charged weak PE deposition to modulate the deposition of positively-charged gold nanoparticles. The ability to control the clustering and LSPC outcome of nanoparticles on solid substrates is important for all applications. For example, as demonstrated in Chapter 2, SERS typically requires nanoparticle clusters as the Raman signal is most strongly enhanced by electromagnetic fields produced by inter-particle interactions. For LSPR sensing of changes in refractive index or biomolecule binding, mono-disperse nanoparticles are used, or unique combinations of mono-disperse and small particle clusters can be used for colourimetric sensing as described in Chapter 4.

3.6 Conclusions

We demonstrated the ability to tune the clustering properties of gold nanoparticles on single-layer PE films. Strong PEs have limited ability to affect the nanoparticle deposition, whereas by using weak PEs, a broad range of particle clustering and thus optical properties can be obtained. By adjusting the assembly pH of the weak PEs, the overall charge on the surface, dependent on PE layer thickness and conformation, can be controlled to affect the electrostatic assembly of the nanoparticles. The use of different weak PEs results in varied modulation of the clustering properties. Furthermore, the resulting particle density and clustering is dependent on the size of the nanoparticles; increased deposition and clustering can be obtained when smaller particles are used. Modelling of the resulting nanoparticle clusters using MG effective medium theory provided understanding of the optical contributions of different cluster types. This can be used as a tool to predict the clustering distribution needed for desired optical properties for various applications. This work provides an easy method to engineer the surface properties to control the clustering of gold nanoparticles in a single deposition, and can be used as a versatile platform for other nanoparticle systems.

Chapter 4
Colourimetric detection of biofilms using immobilized gold nanoparticles

4.1 Summary

Biofilms in contact lens cases amplify the risk of microbial and infiltrative keratitis. A simple, consumer-friendly biosensor for the detection of biofilms is needed to alert users of contact lens case contamination and prevent eye infections. In this Chapter, we report a novel colourimetric detection system based on immobilized gold nanoparticles. The gold nanoparticles exhibit single and clustered populations on the surface to produce a visible colour change from blue to red when the refractive index of the medium is increased. The sensor surface is able to detect the presence of *S. aureus* and *A. xylosoxidans* biofilms though a visual colour change on surfaces of glass, polypropylene, and acrylonitrile-butadiene-styrene contact lens case. The biofilms and their interactions with the sensor surface is characterized using optical and electron microscopy. We present a simple colourimetric biosensor that can be integrated onto a variety of surfaces for the detection of biofilms.

4.2 Introduction

Microbial contamination is prevalent in over 50% of contact lens cases used by reusable contact lens wearers.[1–3] While many of these users may be asymptomatic, contact lens and contact lens case contamination of pathogenic organisms is known to greatly increase the risk of and cause microbial keratitis and infiltrative keratitis.[3–5] Non-compliance with lens care practices[161] in addition to microbial resistance to disinfectant strategies[162,163] leave users vulnerable to these infections. Furthermore, the prevalence of biofilms inside contact lens cases has been widely demonstrated.[4,6] Biofilms pose an even greater risk to wearers because they are known to increase the resistance of bacteria to disinfectant solutions[7–9] and render antimicrobial cases less effective.[10]

Conventional methods to detect the presence of biofilm include the tissue culture plate method, tube method using crystal violet staining, Congo red agar method, and imaging techniques.[11] These techniques require *ex situ* evaluation in a laboratory environment using specialized equipment or reagents. A simple point-of-care system for the detection of biofilm is needed to alert users of contact lens case contamination, so they can discontinue use of the case to prevent related eye infections.

Simple colourimetric strategies for the detection of pathogenic bacteria have been developed using gold nanoparticles.[13] In particular, Verma et al. developed a colourimetric biosensor based on unmodified gold nanostars for the detection and identification of emerging ocular pathogens.[14–16] In this "chemical nose" detection method, the electrostatic-induced aggregation of the gold nanostars around bacteria cells produces a unique colour change for various cell types. This biosensor however is limited to planktonic bacteria present in solution, and cannot be implemented for contact lens users for risk of nanomaterial exposure to the eye. To eliminate exposure of the sensor components to the eye, a surface-based biosensor is preferable. However, current surface-based gold nanoparticle biosensors are limited in that they are modified with specific biomolecules such as antibodies and aptamers to only detect one bacterial species, and they require specialized equipment to read the detection signal.[164,165] A simple surface-based biosensor to non-specifically detect the presence of biofilm is desired.

In this Chapter, we present a novel colourimetric detection system employing immobilized gold nanoparticles. Based on the immobilization state of the nanoparticles, this detection system is capable of producing change in colour from blue to red when the refractive index on the surface is increased. To evaluate the biosensor for detection of biofilms, we chose Gram-positive *Staphylococcus aureus* and Gram-negative *Achromobacter xylosoxidans* as model ocular pathogens found in biofilms in contact lens cases.[4,6] We demonstrate the detection of biofilm of both bacterial strains through a visual colourimetric change on glass and plastic surfaces, including a commercial contact lens case.

4.3 Materials and Methods

4.3.1 Materials

All the chemicals and containers used in this study were purchased from the same sources as those mentioned in Chapter 3 unless otherwise stated. In addition, acetic acid, glutaraldehyde solution (Grade I), and poly(diallyldimethylammonium chloride) (PDADMAC) (100,000-200,000 g/mol) were purchased from Sigma-Aldrich (Oakville, ON, Canada). BuPH phosphate buffered saline packs were purchased from Thermo Fisher Scientific (Burlington, ON, Canada). Transparent, sterile 24-well microplates, BD trypticase soy agar (TSA) culture plates, calcium alginate swabs, BD prepared nutrient broth, Nalgene sterilization filter units (0.2 µm pore size), sodium chloride (ACS grade) and crystal violet were purchased from VWR International (Mississauga, ON, Canada). *Staphylococcus*

aureus (ATCC 6538) and *Achromobacter xylosoxidans* (ATCC 27961) were purchased from Cedarlane Labs (Burlington, ON, Canada). A diced silicon wafer was purchased from Canemco & Marivac for scanning electron microscopy (SEM) imaging (Lakefield, QC, Canada). An opaque white polypropylene plastic sheet was purchased from McMaster-Carr (Aurora, OH, USA). Acrylonitrile-butadiene-styrene (ABS) contact lens cases were obtained from Abbott Medical Optics (Santa Ana, CA, USA). All procured chemicals were used without further purification.

4.3.2 Synthesis of gold nanoparticles

Spherical gold nanoparticles were synthesized from the procedure using CTAB-mediated growth from a gold nanoseed precursor described in Chapter 3.[14] Briefly, to synthesize the gold nanoseed precursor, 60 µL of 0.1 M freshly prepared ice-cold sodium borohydride was added to 20 mL of a solution containing 2.4 x 10^{-4} M gold (III) chloride hydrate and 10^{-4} M trisodium citrate dihydrate under vigorous stirring. The nanoseed solution was incubated overnight in dark ambient conditions and filtered (0.2 µm) prior to use. Next, a 210 mL solution of 1.46 mM CTAB was prepared to synthesize spherical gold nanoparticles. Under moderate stirring, 8.97 mL of 11 mM gold (III) chloride hydrate was added to the CTAB solution, followed by 0.67 mL of 10 mM silver nitrate. Then, 1.44 mL of 100 mM l-ascorbic acid was added dropwise. Immediately after the solution turned clear, 5.60 mL of the gold nanoseed solution was added. The nanoparticles were purified by centrifugation at 10,000 rpm for 15 mins, resuspended in 1 mM CTAB solution, and stored in dark ambient conditions until further use.

4.3.3 Immobilization of gold nanoparticles

4.3.3.1 Immobilization onto glass substrate

Gold nanoparticles were electrostatically immobilized onto glass surfaces using the protocol developed in Chapter 3 using a polyacrylic acid (PAA) layer deposited at pH 6. In brief, glass coverslips were washed by sonicating in ethanol for 20 minutes followed by thorough rinsing in Millipore water (>12MΩcm). Then, the coverslips were submerged in a 2M solution of NaOH for 20 minutes, rinsed thoroughly in Millipore water and dried under a stream of nitrogen. Immediately before use, a 10% v/v solution of (3-aminopropyl)triethoxysilane (APTES) was prepared in reagent grade ethanol. The coverslips were submerged in the APTES solution for one hour on a Stovall Life Science Inc. (Peosta, IA, USA) Belly Dancer orbital shaker in ambient conditions. Then, the

coverslips were rinsed three times in ethanol, rinsed in Millipore water, and dried with nitrogen. A 20 mg/mL solution of PAA was prepared in Millipore water and adjusted to pH 6 using sodium hydroxide. Next, the coverslips were submerged in the PAA solution, and incubated on the orbital shaker for one hour. The coverslips were rinsed three times in Millipore water and dried with nitrogen. Immediately before use, the gold nanoparticle solution was centrifuged at 12,000 rpm for 10 minutes and the CTAB concentration in solution was decreased to 20 μM by replacing the appropriate amount of supernatant with Millipore water. Next, a droplet of the gold nanoparticle solution was placed onto the coverslip to cover the entire surface and was left covered and undisturbed overnight in ambient conditions (~16hrs). Then, the samples were rinsed five times with Millipore water to remove the unbound nanoparticles and were dried under nitrogen flow. The surface of the glass coverslips now appeared blue in colour, indicating the immobilization of the nanoparticles.

The immobilized nanoparticles were characterized by atomic force microscopy using a Bruker (Santa Barbara, CA, USA) Dimension Icon Atomic Force Microscope. Samples were allowed to dry in air for at least 24 hours prior to imaging. A silicon nitride probe (f_0: 70 kHz, k: 0.4 N/m) was used to image the samples in air using the PeakForce Tapping™ mode. Image processing and particle count analysis was performed using Nanoscope Analysis software (Bruker).

4.3.3.2 Immobilization onto plastic

A polypropylene sheet was cut into 1 cm x 1 cm squares. First, the squares were washed with soap and water to remove any visual residue, sonicated in ethanol for 20 minutes followed by rinsing in Millipore water. Then the surface of polypropylene and ABS (contact lens case) plastics were treated with ultraviolet ozone (UV-ozone) radiation for 15 minutes at room temperature using a Novascan (Ames, IA, USA) PSD UV-ozone system to functionalize the surface for further modification. Surface modification of the plastics was confirmed by a decrease in contact angle, and the presence of hydroxyl groups on the surface after modification was confirmed using X-ray photoelectron spectroscopy (Figure A1 and A2). Further surface modification of the plastics with APTES, PAA, and the deposition of gold nanoparticles was performed according to the procedure outlined for glass coverslips.

4.3.4 Multilayer polymer film assembly

Solutions of PAA and PDADMAC were prepared at a concentration of 20 mg/mL. The solution of PAA was adjusted to pH 6 using sodium hydroxide. Layer-by-layer self-assembly of the polyelectrolytes was achieved by submerging a pretreated nanoparticle-immobilized glass sample into the PAA solution followed by the PDADMAC solution for 15 minutes each. Between treatments in each polymer solution, the sample was washed three times in Millipore water and allowed to dry. This was repeated until 6 bilayers of PAA/PDADMAC on the surface was reached. Before each treatment in PAA solution, the sample was photographed using a Canon EOS Rebel T3 camera and an ultraviolet-visible (UV-Vis) spectrum of the sample was obtained.

4.3.5 Bacterial culture.

S. aureus and *A. xylosoxidans* were inoculated on TSA plates and incubated at 37°C for at least 24 hours. Each bacteria culture was harvested using calcium alginate swabs into 5 mL of sterile saline solution (0.85% saline with ~0.006% nutrient broth) and placed into 15 mL centrifuge tubes. The bacteria were washed six times with saline solution by centrifugation at 4000 rpm for 10 minutes. Each bacterial strain was then diluted to obtain on optical density at 660 nm (OD_{660}) of 0.1 ± 0.005, corresponding to a concentration of ~10^8 CFU/mL.[15]

4.3.6 Detection of biofilm

4.3.6.1 Detection on glass substrates

The glass coverslips containing immobilized gold nanoparticles were pretreated by submerging in 0.85% saline solution overnight (~16hrs), washed three times in Millipore water and allowed to air dry. The glass coverslips were then cut into four pieces to obtain samples approximately 1 cm x 1 cm in size. Prior to performing the detection assay, each sample was photographed under controlled lighting conditions. Then, the samples were placed into a transparent 24-well microplate and triplicate UV-Vis absorption spectra were taken, along with area scans at the two peak positions and 950 nm. Next, 1 mL of the bacteria or saline control was added to triplicate samples in the microplate wells. In parallel, bacteria and saline control were also added to wells containing unmodified glass samples. All samples were left to incubate undisturbed overnight for 16 hrs in ambient conditions. After incubation, the samples were washed three times in Millipore water to remove planktonic bacteria, and left to air dry. Once completely dry, pictures of the samples were taken again followed by UV-

Vis spectral scans and area scans. Area scans at the peak positions were used to analyze peak intensity as this gave a better representation of variation across the sample surface.

4.3.6.2 Detection on plastic substrates

The plastic samples containing immobilized gold nanoparticles were pretreated by submerging in 0.85% saline solution overnight (~16hrs), washing three times in Millipore water and allowing them to air dry. Each sample was photographed before the detection assay under controlled lighting conditions. For the polypropylene squares, a 150 μL droplet of the bacteria or saline control was added to each surface, while 1 mL of the bacteria or saline control was added into the contact lens case wells. All samples were left to incubate undisturbed overnight for 16 hrs in ambient conditions. After incubation, the samples were washed three times in Millipore water to remove planktonic bacteria, and left to air dry. Once completely dry, pictures of the samples were taken.

4.3.7 Ultraviolet-visible spectroscopy

Absorption spectra from 350 nm – 999 nm with 1 nm increments were obtained using a BioTek (Winooski, VT, USA) Epoch microplate spectrophotometer. Area scans at wavelengths of interest were taken using a 9 x 9 matrix. All absorption intensities were normalized to a baseline value by subtracting the intensity at 900 nm for particles in solution, or 950 nm for immobilized particles.

To determine the spectral response of the immobilized nanoparticles with a biofilm on the surface, the absorbance contribution from the nanoparticles was isolated from that of the biofilm. All absorbance scans were first normalized by subtracting the absorbance at 950 nm, and readings from each sample were averaged. Then, the absorbance contribution was determined using the following equation:

$$Nanoparticle\ absorbance\ contribution = Biofilm\ on\ sensor\ surface - Biofilm\ on\ unmodified\ glass$$

4.3.8 Colourimetric analysis

The colour of the samples was analyzed from the unaltered digital photographs using Mathworks® MATLAB®. A representative area of 60 x 60 pixels from each sample was analyzed using the hue-saturation-value (HSV) colour scale with values ranging from 0 to 1. To compare the hue of a sample between multiple images (i.e. before and after), the values were normalized to those of the white

background in each image to account for any changes in lighting conditions over time. The images presented in this manuscript were each normalized to the white background and modified uniformly for each sample being compared using GIMP image editing software for best representation.

4.3.9 Microscopy for biofilm characterization

The biofilm characteristics on the sensor surfaces was analyzed using a Zeiss (Oberkochen, Germany) LEO 1550 field emission scanning electron beam microscope. Scanning electron microscopy (SEM) was performed on samples prepared and tested in parallel on silicon substrates. After the planktonic cells were removed from the silicon substrates, the adherent cells were fixed using 2.5% glutaraldehyde solution in PBS for 2 hrs in ambient conditions. Then, the samples were washed twice with PBS first followed by deionized water, then allowed to dry overnight prior to imaging.

The surface coverage of the biofilm on glass samples was analyzed using a Zeiss (Oberkochen, Germany) Axioskop optical microscope. Image analysis of the optical micrographs was performed using National Institutes of Health Image-J software.

4.3.10 Crystal Violet assay for biofilm analysis

One milliliter of CV solution (0.1% w/v) was added to the wells containing glass or polypropylene samples in a 24-well plate, or two millilitres of CV solution was added to the wells of contact lens cases. The samples were incubated statically for 15 minutes in ambient conditions followed by rinsing five times with DI water to remove any unbound CV. After allowing the samples to air dry overnight, photographs of the samples were taken (Figure A3). To dissolve the CV staining, the equivalent amount of a 30% acetic acid solution was added to the sample wells, which were placed on a Belly Dancer orbital shaker at moderate speed for 15 minutes. Then, 300 μL of the solubilized CV solution was extracted and placed into a 96-well plate where the absorbance was measured at 590 nm to quantify the amount of biofilm present on the surface.[166]

4.4 Results and Discussion

4.4.1 Characterization of immobilized nanoparticles

The synthesized gold nanoparticles were spherical with a diameter of 17.1 ± 1.1 nm (mean ± s.d.) measured with a transmission electron microscope, similar as those used in Chapter 3 (Figure 4a). The particles are positively charged due to CTAB as stabilizing surfactant, allowing them to assemble onto the negatively charged PAA polymer layer on the glass surface. Although the nanoparticles appear red in solution, the resulting immobilized nanoparticles appeared blue on the surface (Figure 15a), the change in colour being a typical indication of gold nanoparticle aggregation or clustering.[167] The UV-Vis absorption spectra of the immobilized nanoparticles show two main absorption peaks in the visible range around 520 nm (1^0 peak) and 610 nm (2^0 peak), while the spectra of the nanoparticles in solution show only a single peak around 520 nm (Figure 15b). The presence of two peaks suggests that there are two population states of nanoparticles on the surface. In this case, the absorbance of the broad 2^0 peak in the red region of the spectrum is dominant over the 1^0 peak, causing the surface to appear blue in colour. We assigned the two different population states suggested by the two peaks to single particles (1^0 peak) and small monolayer clusters (2^0 peak) by analyzing topographic images acquired by AFM (Figure 15c). Further analysis revealed that 27% of the total population are of single nanoparticles and 73% of the particle groups are clusters containing 2-20 nanoparticles. As previously explained in Chapter 3, The red shift in peak position of the single particles in solution to those on the surface (1^0 peak) can be attributed to the overlapping contribution of the 2^0 peak, whereas the absorbance intensity is higher in solution due to a higher particle concentration and longer pathlength.[12]

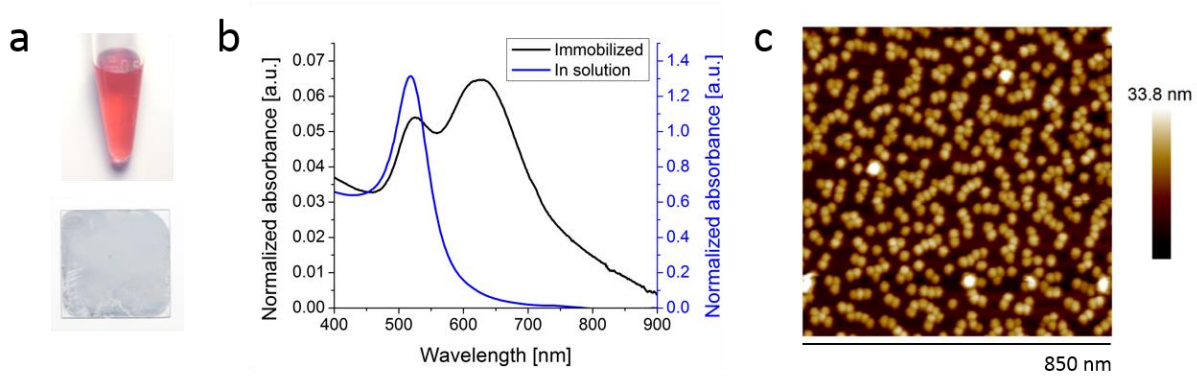

Figure 15. a) Photographs of gold nanoparticles in solution (top) and immobilized onto a glass surface (bottom). b) Absorption spectra of the immobilized gold nanoparticles and those in solution. c) AFM height sensor image of immobilized gold nanoparticles.

4.4.2 Sensor response to multilayer film formation

To characterize the sensor response of the immobilized gold nanoparticles to a change in refractive index, we deposited thin polymer films on top of the immobilized particles. Layer-by-layer self-assembly of oppositely charged polyelectrolytes was chosen as the polymer deposition method as it is known to produce thin, uniform films with controlled thickness.[144] Specifically, we used the assembly of PDADMAC and PAA (deposited at pH 6) bilayers which have been shown to have a thickness of approximately 14 Å.[153] Similar multilayer films including the use of PAA have a refractive index of approximately 1.5, which is much higher than that of air.[168] In coating the surface with polymer bilayers, the refractive index of the medium surrounding the immobilized nanoparticles increased, leading to a change in the surface plasmon resonance properties of the particles and a sensor response.[12] The visual change in the surface sensor was characterized by obtaining a photograph of the dried sensor surface after deposition of each polymer bilayer (Figure 16a). In these photographs, we demonstrate that the colour of the surface visually shifts from blue to red after the buildup of the polymer bilayers. To quantify the colour change objectively, simple image analysis was performed using the hue-saturation-value colour space. The difference in hue after each polymer bilayer deposition from the initial state is plotted in Figure 16b. A drastic change in hue is observed at the 2nd bilayer deposition, and subsequent deposition of bilayers does not continue to produce further distinguishable changes. This indicates that the sensor optical properties change when a threshold is

reached; a drastic colour change is produced when the effective refractive index of the medium surrounding the particles on the surface reaches a certain value.

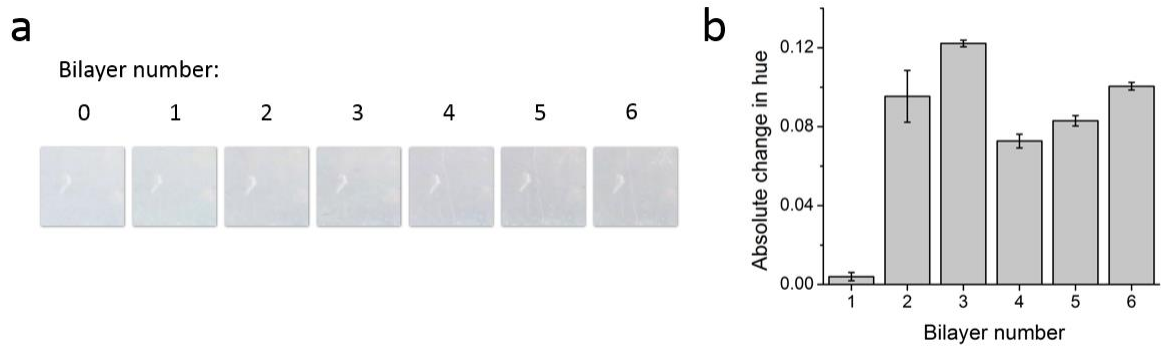

Figure 16. Colourimetric analysis of multilayer film deposition on the sensor surface: a) Photographs of the dried surface after each PDADMAC/PAA bilayer deposition. b) Difference in hue values after each bilayer deposition compared to the original sensor surface (mean ± s.e.m., 400 pixels).

The surface plasmon resonance response of the nanoparticles was characterized by obtaining UV-Vis absorption spectra after each bilayer deposition (Figure 17a). Increasing the number of polymer layers on the sensor surface results in an increase in the absorbance peak intensity and a red shift in absorbance peak position. Both of these phenomenon have been thoroughly studied and documented for monodisperse gold nanoparticles immobilized onto a surface.[39] However, this detection system is unique in that there are two populations of particle states on the surface, resulting in two distinct absorbance peaks. Looking at the initial absorption spectrum (layer 0), the 1^0 peak has a lower absorbance intensity than the 2^0 peak. As the number of deposited bilayers increases, the 1^0 peak intensity becomes higher than the 2^0 peak. The peak intensities and their ratio after each bilayer deposition are plotted in Figure 17b. Here we see that the $1^0/2^0$ peak intensity ratio, which initially starts below 1.00, increases to 1.32 at the second bilayer deposition and remains fairly constant thereafter as both peak intensities continue to increase at the same rate. The discrepancy between the intensity changes of the two peaks seen at low polymer deposition suggests that the particles immobilized in a single state are more sensitive to local changes in refractive index than the particles immobilized in clustered states. Analysis of the peak wavelength position also supports this theory as

the 1^0 peak shows a general red shift in position, whereas the 2^0 peak position stays relatively stagnant (Figure 17c).

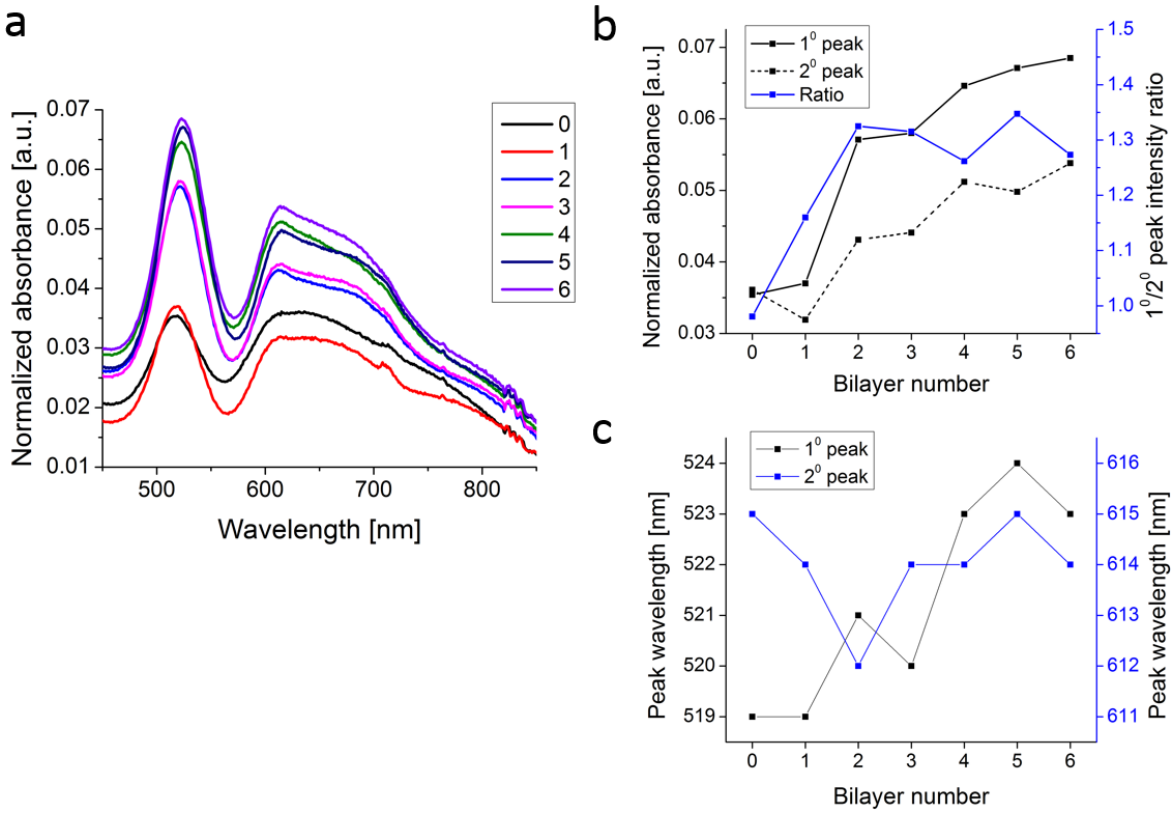

Figure 17. Spectrophotometric response of multilayer film deposition on the sensor surface: a) UV-Vis absorption spectra of the surface after each PDADMAC/PAA bilayer deposition. b) Absorbance intensity analysis at the peak positions after each bilayer deposition. The ratio of the $1^0/2^0$ peak intensities is plotted on the secondary y-axis. c) Analysis of peak wavelength for both 1^0 and 2^0 absorbance peaks. The intensity values reported were normalized by subtracting the intensity at 950 nm for each scan.

The absorption spectra of the particles suggest that the colour change can be attributed to the two particle populations on the surface. The small shift in the 1^0 peak position (1-5 nm) is unlikely to contribute to a change in visual colour. The drastic increase in the peak intensity ratio, however, directly correlates with the quantitative change in colour observed at the 2nd bilayer deposition. If the

peaks are considered separately, the broad 2^0 absorption peak ranging from 600 – 700 nm would result in a blue colour, and the 1^0 peak around 520 nm would result in a red colour. It is therefore predicted that the change in the peak dominance dictated by the relative peak intensities, from the 2^0 peak to the 1^0 peak, is responsible for the observed colour change from blue to red. Furthermore, the threshold effect of the colour change upon increasing polymer layers is accounted for within this theory as the peak intensity ratio becomes constant after the 2nd bilayer. Although the visual change in colour appears to function only on a threshold level, the spectrophotometric data suggests that the incremental changes in refractive index and therefore film thickness on the surface can also be quantified by this sensor technique.

4.4.3 Detection of biofilm on glass substrates

In forming a biofilm, bacteria adhere to the surface and colonize the substrate while producing a matrix of extracellular polymeric substance (EPS), which is thought to protect the bacterial cells from harsh environments.[169] We hypothesize that the adhesion of the cells and the production of EPS on the surface will increase the refractive index of the surface thus producing a drastic colour change. To mimic practical applications of the sensor with realistic biofilms, the bacteria were in standard saline solution without the use of excess nutrients and were incubated on the sensor surface at room temperature. Triplicate sensor surfaces were used for each bacterial strain as well as saline controls. To characterize the visual change of the sensor surface, photographs of the surface were taken before and after treatment with bacterial solutions (Figure 18a). Treatment with both *S. aureus* and *A. xylosoxidans* produced a change in colour from blue to red, while the saline controls did not produce a change in colour. The colour changes were also characterized quantitatively using image analysis and UV-Vis. Hue analysis showed a significant difference in the presence of bacteria (Figure 18b), coinciding with an increase in the $1^0/2^0$ absorption peak intensity ratio (Figure 18c). The change in peak intensity ratio seen with *S. aureus* appears less significant only because there was a wider spread in the peak intensities between the triplicate samples. However, each sample underwent a similar magnitude of peak intensity change and produced visible colour changes. In both analysis techniques, due to the non-specific detection mechanism of the sensor, we observed no significant difference between the two bacterial strains. This indicates that the sensor surface is capable of non-specifically detecting the presence of any biofilm.

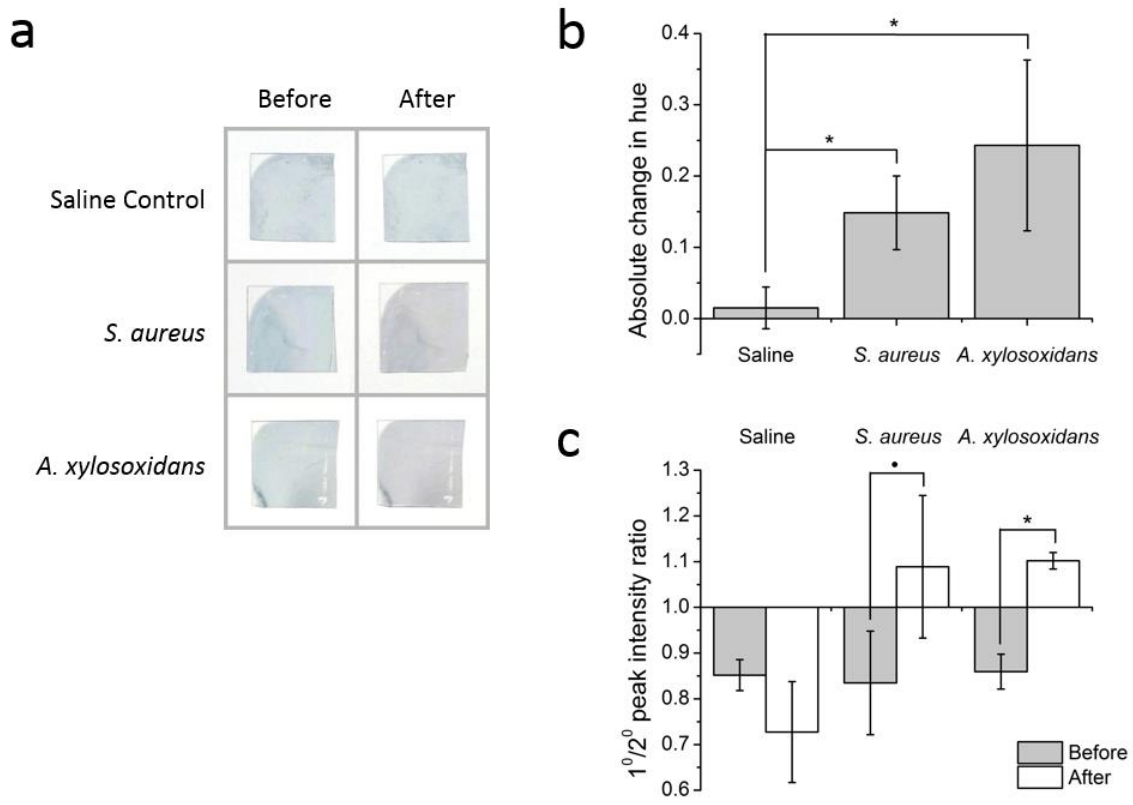

Figure 18. Response of the sensor surface to biofilms of S. aureus, A. xylosoxidans and saline control: a) Photographs of representative samples before and after bacterial exposure. b) Change in mean hue values observed from the initial sensor colour (mean ± s.d., n=3, $p < 0.05$). c) Absorption analysis of the $1^0/2^0$ peak intensity ratio before and after bacterial exposure (mean ± s.d., n=3, * $p < 0.05$, • $p < 0.10$).

The presence of bacterial cells and biofilm formation was confirmed using CV staining. As CV is a dye known to bind to polysaccharides and negatively charged molecules on the cells and EPS[166], it was suspected that it may also bind to the negatively charged PAA used to modify the surface. In Figure 19a, we see that the CV stains the PAA component of the surface (as seen in the control without the nanoparticles), however this background staining is low compared with the biofilm staining response of both *S. aureus* and *A. xylosoxidans* biofilms. The characteristics of bacteria on the surface and the formation of biofilm were further studied using optical microscopy (Figure 19c) and scanning electron microscopy (Figure 19d). In the optical micrographs, connecting networks of

cells are seen on the sensor surfaces treated with *S. aureus* and *A. xylosoxidans* and are absent on the saline control. Note that the immobilized nanoparticles on the surface cannot be seen at this scale. The presence of each cell type as well as the secretion of EPS on the sensor surfaces is confirmed visually in the scanning electron micrographs. The saline control images confirm that nothing from the medium is being deposited on the surfaces. In these images, the bright white specs seen distributed over the surface are the gold nanoparticles, as seen more clearly in the higher magnification image of the saline control. We see that the particles are strongly adhered to the surface and are not disturbed by the biofilm formation, but are simply covered by it. This confirms our hypothesis that the coverage of biofilm on the surface is capable of producing a colour change of the sensor surface likely by refractive index effects. Area analysis of the surface coverage from the optical micrographs of each triplicate sample was performed to quantify the presence of bacteria and biofilm (Figure 19b). Both *S. aureus* and *A. xylosoxidans* cover on average 44 - 47% of the surface under the experimental conditions used. Although the surface coverage is very similar, the difference between the amount of CV staining for *S. aureus* and *A. xylosoxidans* can be attributed to the different characteristics of EPS formation observed on the samples. Additionally, the sensor surface is not cytotoxic, as confirmed by a cell viability assay using the culture plate method (Figure 20).

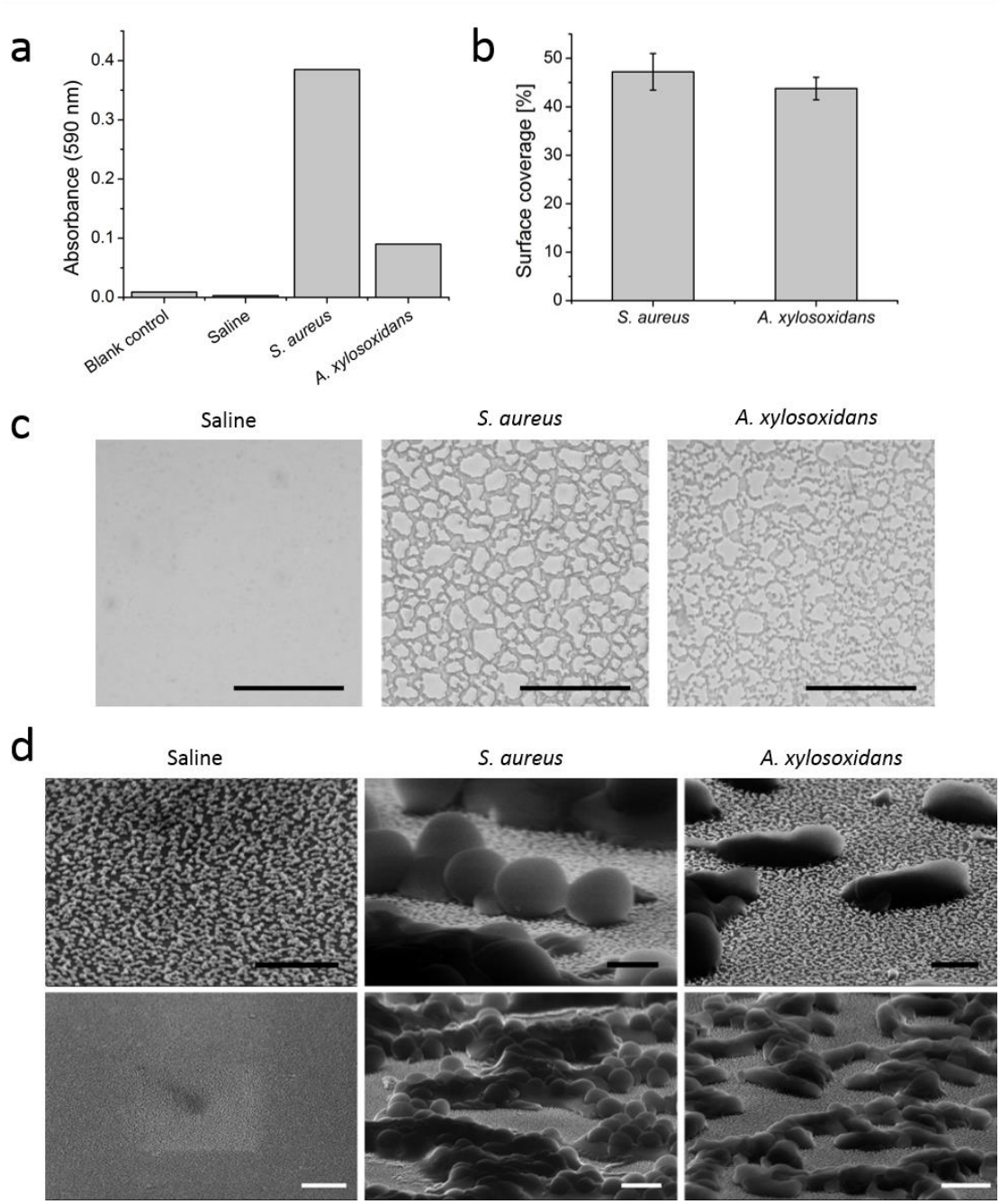

Figure 19. Interaction of bacteria on the sensor surface: a) CV staining of total biofilm on representative samples and on a blank control containing no nanoparticles. b) Analysis of the surface coverage of biofilm from optical micrographs of the triplicate samples (mean ± s.d., no significance detected). c) Optical micrographs of the sensor surfaces exposed to saline, *S. aureus*

and *A. xylosoxidans* (scale bars = 50 µm). c) Scanning electron microscopy (SEM) images of the sensor surfaces exposed to saline, *S. aureus* and *A. xylosoxidans* (scale bars: black = 400 nm, white = 1 µm).

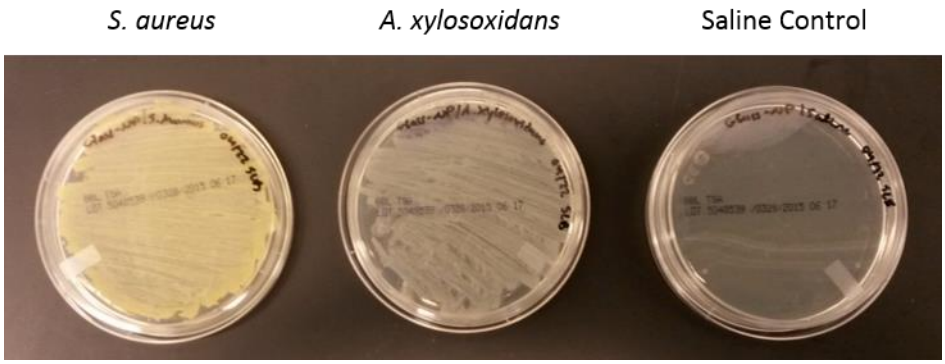

Figure 20. Culture plate images confirming growth and cell viability of S. aureus and A. xylosoxidans from the sensor surface compared with negative saline control.

4.4.4 Detection of biofilm on plastic substrates

An end-user of this surface-based biofilm sensor would likely be interested in detecting the presence of biofilm not on glass but on materials that we more commonly interact with. For this reason, the surface modification technique for sensor integration was designed such that it could be transferable to a variety of materials including plastics. Gold nanoparticles were successfully immobilized onto the surface of polypropylene plastic with similar visual properties to that of a glass substrate. The response of the polypropylene sensor surface to the presence of biofilm was then tested under the same conditions. Photographs taken of the sensor surfaces before and after bacterial treatment demonstrate a visual colour change from blue towards red for both *S. aureus* and *A. xylosoxidans* (Figure 21a). The change in colour from the photographs presented may be subtle to certain users, but a drastic change in hue from performing image analysis is still present (Figure 21b). Due to the opaque nature of the plastic substrate, spectrographic analysis of the nanoparticle response could not be performed. The presence of both *S. aureus* and *A. xylosoxidans* biofilm formation was confirmed using the CV assay (Figure 21c). The similar change in colour to what was observed using glass

substrates provides strong evidence that the nanoparticles are immobilized and are sensing the presence of biofilm on the surface in a similar fashion.

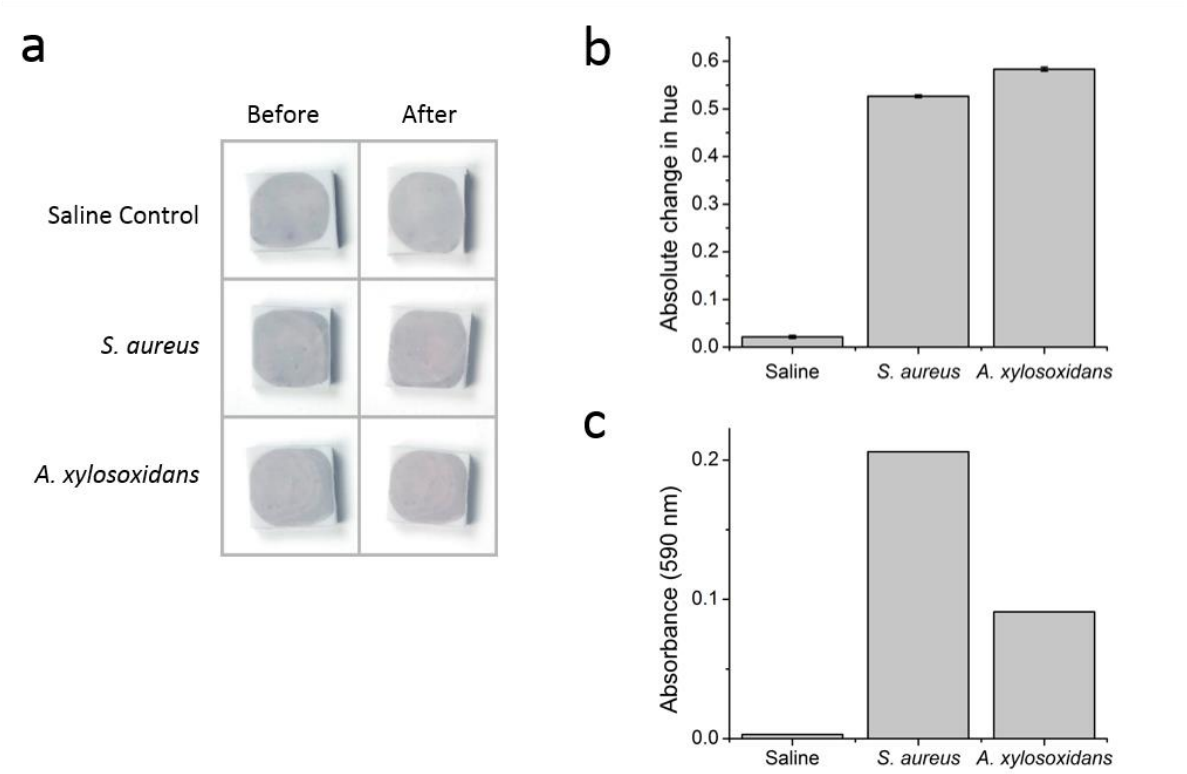

Figure 21. Colour change of the sensor on polypropylene surface in response to biofilm and saline control: a) Photographs before and after bacterial exposure to the surface. b) Change in mean hue values observed from image analysis of photographs (absolute change ± s.e.m., 3600 pixels). c) CV staining of total biofilm on the surfaces.

To further demonstrate the versatility and practical application of this sensor platform, the gold nanoparticles were immobilized onto the surface of the wells of a commercial ABS contact lens case. The sensor response was tested against *S. aureus*, *A. xylosoxidans*, and saline control, similar to all previous tests, in addition to also testing the response to Biotrue multipurpose solution (Bausch + Lomb, Rochester, NY, USA) used for contact lens cleaning and disinfecting. Photographs taken of the contact lens case wells before and after treatment demonstrate a colour change from blue to red for both *S. aureus* and *A. xylosoxidans*, while the saline control and Biotrue multipurpose solution

show no colour change (Figure 22a). Again, simple image analysis of the photographs demonstrates a drastic change in hue only in the presence of both bacterial strains (Figure 22b). The presence of biofilm on the sensor surfaces was again confirmed using CV assay (Figure 22c). Testing a multipurpose solution control was important as these solutions often contain wetting agents, buffering agents and biocides including quaternary ammonium polymers[10] which may have an affinity to non-specifically bind to the sensor surface. The negative response of the sensor to the multipurpose solution indicates that there is no modification of the refractive index of the surface due to solution components. The positive response to both gram-positive and gram-negative bacterial biofilms of relevant ocular pathogens demonstrates that a promising application of this sensor surface is to detect biofilms in contact lens cases.

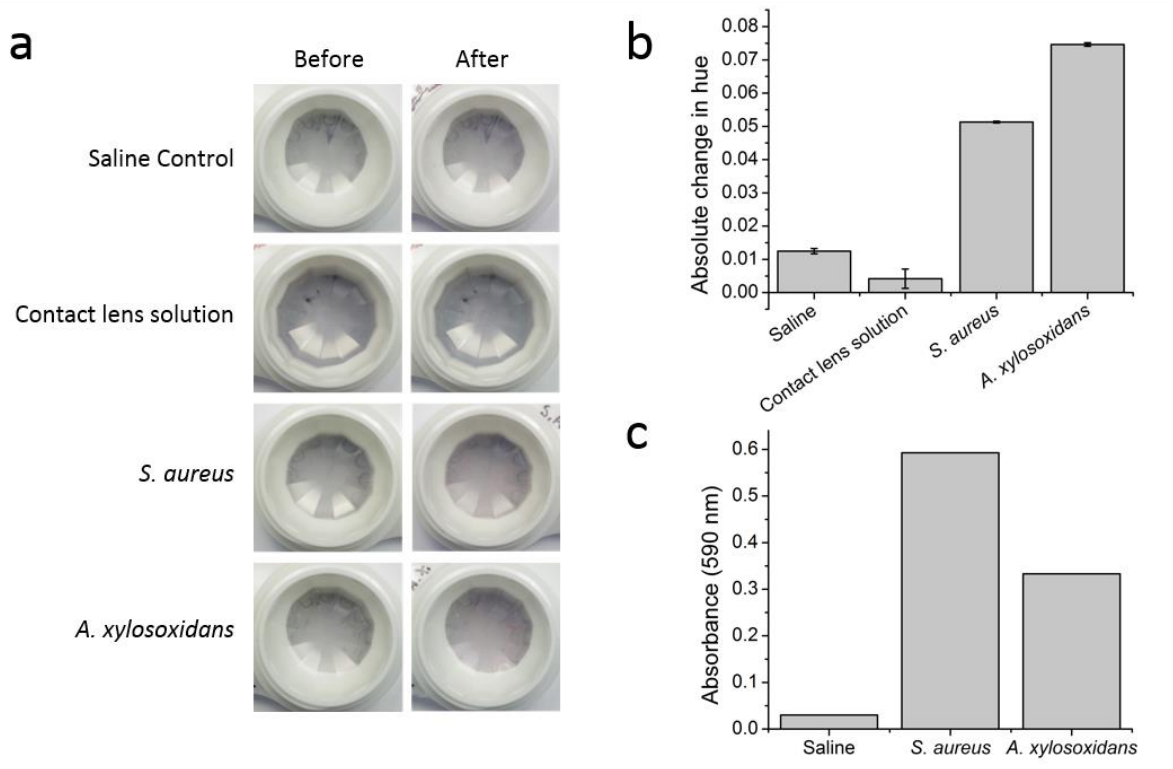

Figure 22. Colour change of the sensor on a commercial contact lens case in response to biofilm and saline control: a) Photographs before and after bacterial exposure to the surface. b) Change in mean hue value observed from image analysis of photographs (absolute change ± s.e.m., 3600 pixels). c) CV staining of total biofilm on the surfaces.

4.5 Conclusions

A novel surface-based colourimetric sensor using gold nanoparticles was demonstrated to detect multilayer polymer film formation on the surface to reflect changes in refractive index. To the best of our knowledge, this is the first time gold nanoparticles have been intentionally immobilized with both populations of single and clustered particles to create a drastic colour change with an increase in refractive index on the surface. This sensor is capable of providing a visual colourimetric response, from blue to red, to a threshold refractive index on the surface. We demonstrated that this sensor is capable of producing a visual colour change to detect the presence of gram-positive and gram-negative bacteria biofilms on the surface. This change in colour is also detectable through simple image analysis techniques. The colourimetric sensor was successfully integrated onto glass and plastic substrates, including a commercial contact lens case. The simplicity of this detection system requires no technical expertise or training for easy user adaptation. For those who have difficulties identifying colours, a smartphone application can easily be developed to analyze the colour in images taken with a cell phone. Therefore, contact lens wearers would be able to easily identify the presence of biofilm inside their contact lens case and be able to discontinue use, avoiding the risk of contracting microbial keratitis or infiltrative keratitis. In addition, the versatility of the substrate to which the sensor can be applied allows this platform to be used for detection of biofilms in healthcare, sanitation, food services, and water treatment industries.

Chapter 5
Conclusions and Future Work

5.1 Summary

This thesis presents new findings in the fields of nanotechnology, materials science and chemical engineering. Beginning with a literature review on methods to immobilize gold nanoparticles, the current strategies to control the immobilization state of the gold nanoparticles and the relation to different applications were established. With this knowledge, a novel method to control and tune the immobilization state of gold nanoparticles was developed using a surface modified with a single weak polyelectrolyte layer to electrostatically bind the nanoparticles. Using this method, an optimal immobilization state of the gold nanoparticles was used to develop a colourimetric biosensor for the detection of biofilms. The detection mechanism was based on the intrinsic interactions of the gold nanoparticles with changes in refractive index on the surface. The biosensor was then successfully integrated onto and able to detect biofilms on a plastic surface and contact lens case. Thus, this thesis provides promising results for an immobilized nanoparticle biosensor platform for the visual colourimetric detection of biofilms on surfaces to warn users of biofilm contamination.

5.2 Conclusions

The immobilization state of charged gold nanoparticles can be tuned using single-layer weak polyelectrolyte (PE) films. The surface properties of the substrate can be modulated by adjusting the assembly pH of the weak PEs, affecting the electrostatic assembly of the gold nanoparticles through the PE layer thickness, conformation, and overall surface charge. Using polyacrylic acid as the PE layer, the degree of nanoparticle clustering can be modulated from single dispersed particles to large three-dimensional clusters, resulting in a wide range of optical properties. Different weak PEs produce varied modulation of the clustering properties. Increasing the size of the nanoparticle decreases the immobilized particle density and limits the degree of clustering, limiting the range of optical properties attainable.

Using a unique immobilization state containing populations of single and small clusters of gold nanoparticles, a drastic colour change of the surface can be produced with an increase in refractive index. The mechanism of detection involves the different sensitivities of the two gold nanoparticle

populations, producing a significant change in the ratio of absorption peak intensities associated with the two population states. This causes a colour change to be produced, from blue to red, when a threshold refractive index on the surface is reached. This sensor platform is capable of being used as a biosensor, producing a visual colour change to detect the presence of Gram-positive *Staphylococcus aureus* and Gram-negative *Achromobacter xylosoxidans* biofilms on the surface. Covering 44-47% of the biosensor surface, the extracellular polymeric substance of the biofilms produces sufficient increase in refractive index for detection. The colour change is also detectable through absorbance spectroscopy and simple image analysis techniques. Furthermore, the sensor response is non-specific between the two different types of biofilms. The colourimetric biosensor was successfully integrated onto and capable of detecting the presence of biofilm on glass and plastic substrates, including a commercial contact lens case.

Overall, this novel detection mechanism based on immobilized gold nanoparticles is an excellent biosensor platform to detect the presence of biofilms on surfaces. The simplicity of the detection readout, and the non-specific nature towards different types of biofilms makes this technology ideal for detection in contact lens cases to warn everyday users of contamination, to prevent related infections. In addition, the versatility of this biosensor to be integrated onto a variety of surfaces provides great potential for expansion into many additional applications.

5.3 Recommendations for future work

Based on the results of this research, the following avenues are recommended for future work:

1. Test and improve the durability of the immobilized gold nanoparticles to create a more robust sensor surface. In general, the stability of electrostatically immobilized gold nanoparticles is not well understood. It is recommended to test the stability of the sensor surface under mechanical abrasion and exposure to different environmental conditions including high temperature and solvent exposure. Methods to improve the stability of the sensor surface can include a covalent immobilization approach, or use of a thin polymeric overlayer to secure the nanoparticles.
2. Expand the characterization of the biosensor surface for contact lens case applications. This would include testing the detection capabilities of the biosensor for an expanded library of relevant ocular pathogens know to produce biofilms including *Pseudomonas*,

Stenotrophomonas, and *Delftia*. It is recommended to test potential non-specific interactions of the biosensor to additional relevant conditions that may occur in contact lens applications including incubation with proteins and other formulations of cleaning solutions.

3. Investigate the potential affects the biosensor surface has on cell growth and biofilm production. Some nanoparticles are known to induce cell death, or alter the properties of cells. This can be tested by comparing cell adhesion, growth and viability to similar surfaces that do not contain the biosensor.
4. Explore other applications where this biosensor platform can be applied. This includes the detection of relevant biofilm formation on surfaces used in healthcare and food services industries. To facilitate integration onto existing surfaces, integrating the biosensor onto a sticker surface is recommended. The sensor platform can also be applied for the detection of fouling on pipes in the water treatment industry.
5. Develop a smart phone application to analyze the colourimetric response of the biosensor surface. This will improve the accessibility of the biosensor platform to those who are colour blind, and potentially increase user compliance.

Appendix A

Supplementary Experimental Data

Characterization of plastic surface modification

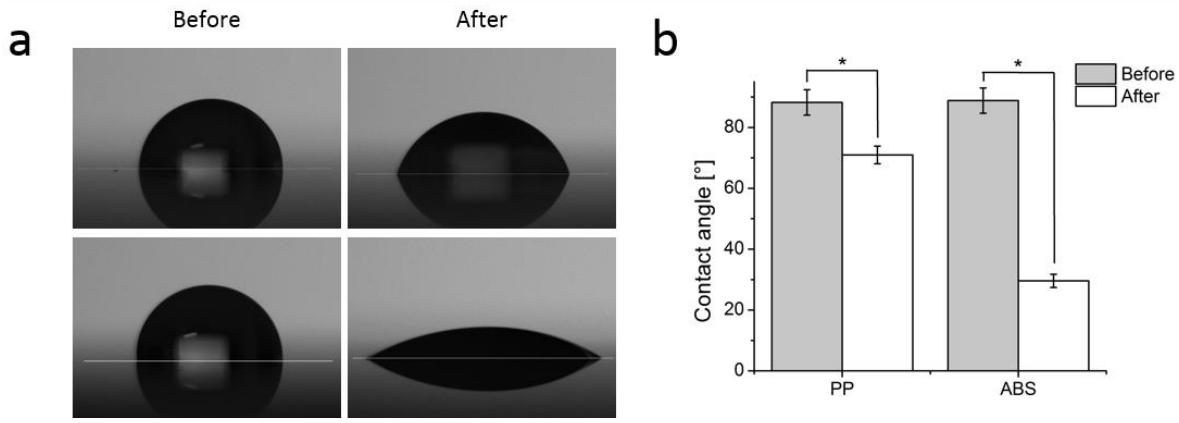

Figure A1. Contact angle measurements of a 3 μL droplet of Millipore water on plastic surfaces before and after UV-ozone treatment: a) Representative images of polypropylene (PP) (top) and acrylonitrile-butadiene-styrene (ABS) (bottom) surfaces before and after treatment. b) Change in contact angle observed after treatment for triplicate surfaces (mean ± s.d., n = 6). The increased hydrophilicity observed indicates the incorporation of oxygen functionality into the surface from the UV-ozone treatment.

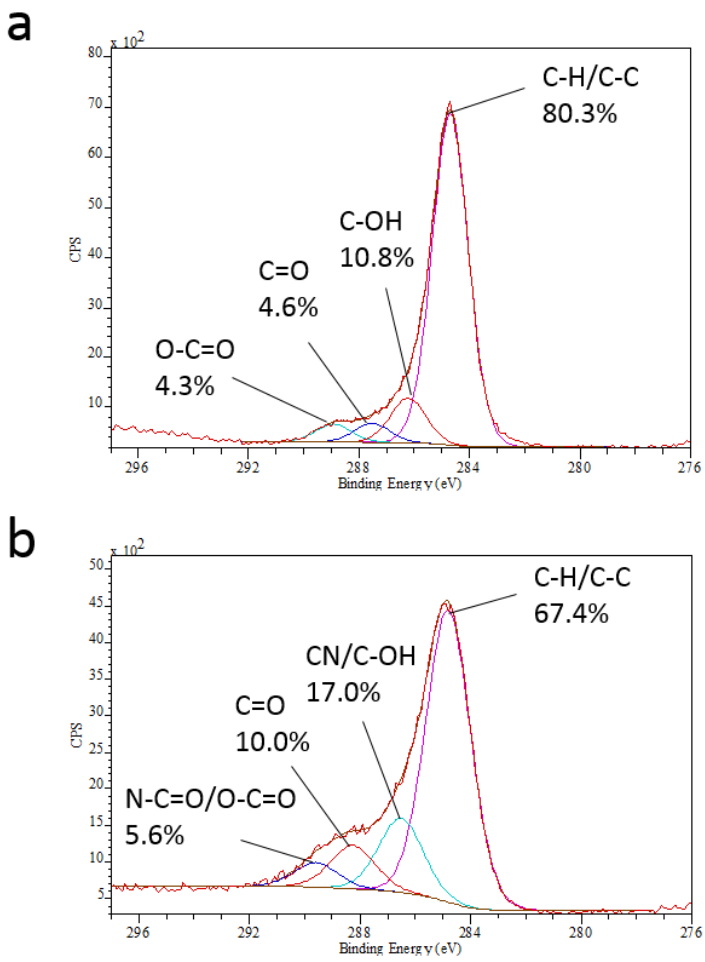

Figure A2. X-ray photoelectron spectroscopy high resolution Carbon 1s bonding analysis of polypropylene (a) and ABS (b) surfaces after UV-Ozone treatment. Data was acquired using a Thermo Scientific ESCALab 250 imaging XPS system and curve fitting analysis was performed using CasaXPS software. The presence of hydroxyl functionality is confirmed on the surface of both materials.

Crystal Violet staining visual characterization

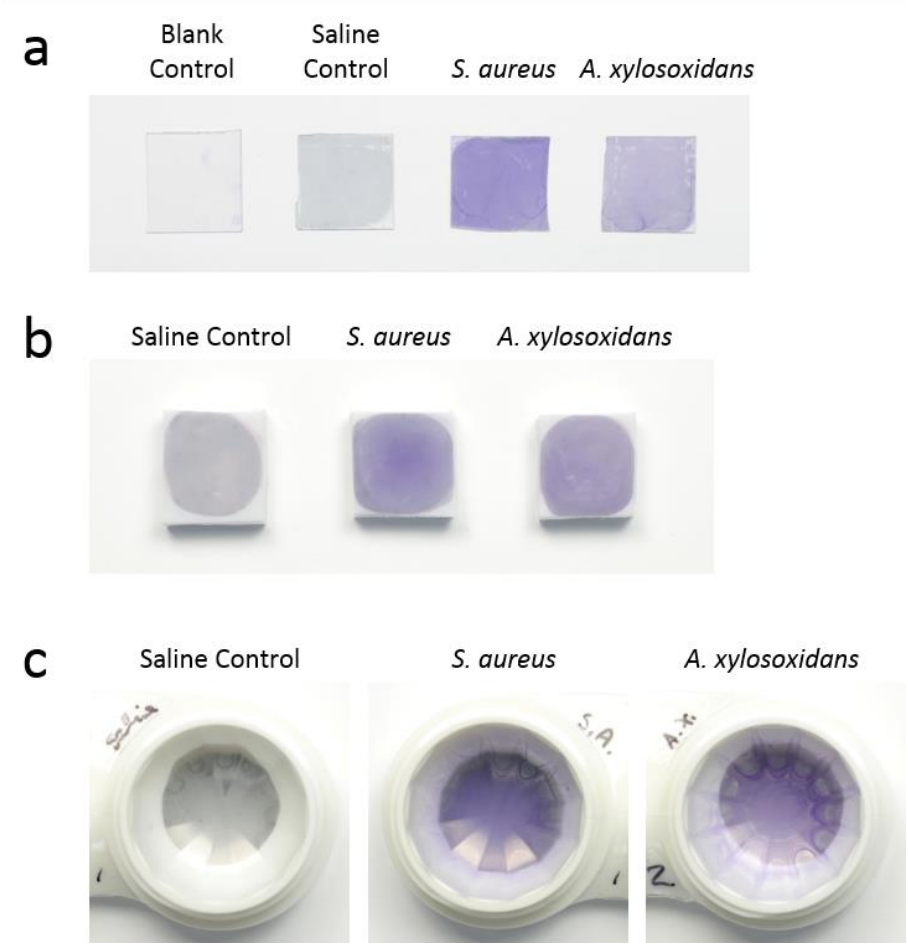

Figure A3. Photographs of CV biofilm staining on glass (a), polypropylene (b) and ABS contact lens case (c) sensor surfaces.

Bibliography

(1) Wu, Y. T.; Zhu, H.; Harmis, N. Y.; Iskandar, S. Y.; Willcox, M.; Stapleton, F. Profile and Frequency of Microbial Contamination of Contact Lens Cases. *Optom. Vis. Sci.* **2010**, *87* (3), E152–E158.

(2) Willcox, M. D. P.; Carnt, N.; Diec, J.; Naduvilath, T.; Evans, V.; Stapleton, F.; Iskandar, S.; Harmis, N.; de la Jara, P. L.; Holden, B. a. Contact Lens Case Contamination during Daily Wear of Silicone Hydrogels. *Optom. Vis. Sci.* **2010**, *87* (7), 456–464.

(3) Szczotka-Flynn, L. B.; Pearlman, E.; Ghannoum, M. Microbial Contamination of Contact Lenses, Lens Care Solutions, and Their Accessories: A Literature Review. *Eye Contact Lens* **2010**, *36* (2), 116–129.

(4) McLaughlin-Borlace, L.; Stapleton, F.; Matheson, M.; Dart, J. K. Bacterial Biofilm on Contact Lenses and Lens Storage Cases in Wearers with Microbial Keratitis. *J. Appl. Microbiol.* **1998**, *84* (5), 827–838.

(5) Martins, E. N.; Farah, M. E.; Alvarenga, L. S.; Yu, M. C. Z.; Höflin-Lima, A. L. Infectious Keratitis: Correlation between Corneal and Contact Lens Cultures. *CLAO J.* **2002**, *28* (3), 146–148.

(6) Wiley, L.; Bridge, D. R.; Wiley, L. a.; Odom, J. V.; Elliott, T.; Olson, J. C. Bacterial Biofilm Diversity in Contact Lens-Related Disease: Emerging Role of Achromobacter, Stenotrophomonas, and Delftia. *Investig. Ophthalmol. Vis. Sci.* **2012**, *53* (7), 3896–3905.

(7) Szczotka-Flynn, L. B.; Imamura, Y.; Chandra, J.; Yu, C.; Mukherjee, P. K.; Pearlman, E.; Ghannoum, M. a. Increased Resistance of Contact Lens-Related Bacterial Biofilms to Antimicrobial Activity of Soft Contact Lens Care Solutions. *Cornea* **2009**, *28* (8), 918–926.

(8) Vijay, A. K.; Willcox, M.; Hua, Z.; Stapleton, F. Contact Lens Storage Case Hygiene Practice and Storage Case Contamination. *Eye Contact Lens* **2015**, *41* (2), 91–97.

(9) Chang, J. M.; McCanna, D. J.; Subbaraman, L. N.; Jones, L. W. Efficacy of Antimicrobials against Biofilms of Achromobacter and Pseudomonas. *Optom. Vis. Sci.* **2015**, *92* (4), 506–513.

(10) Vermeltfoort, P. B. J.; Hooymans, J. M. M.; Busscher, H. J.; van der Mei, H. C. Bacterial Transmission from Lens Storage Cases to Contact Lenses-Effects of Lens Care Solutions and Silver Impregnation of Cases. *J. Biomed. Mater. Res. B. Appl. Biomater.* **2008**, *87* (1), 237–243.

(11) Mathur, T.; Singhal, S.; Khan, S.; Upadhyay, D. J.; Fatma, T.; Rattan, A. Detection of Biofilm Formation among the Clinical Isolates of Staphylococci: An Evaluation of Three Different Screening Methods. *Indian J. Med. Microbiol.* **2006**, *24* (1), 25–29.

(12) Willets, K. A.; Van Duyne, R. P. Localized Surface Plasmon Resonance Spectroscopy and Sensing. *Annu. Rev. Phys. Chem.* **2007**, *58*, 267–297.

(13) Verma, M. S.; Rogowski, J. L.; Jones, L.; Gu, F. X. Colourimetric Biosensing of Pathogens Using Gold Nanoparticles. *Biotechnol. Adv.* **2015**.

(14) Verma, M. S.; Chen, P. Z.; Jones, L.; Gu, F. X. Branching and Size of CTAB-Coated Gold Nanostars Control the Colourimetric Detection of Bacteria. *RSC Adv.* **2014**, *4* (21), 10660.

(15) Verma, M. S.; Chen, P. Z.; Jones, L.; Gu, F. X. "Chemical Nose" for the Visual Identification of Emerging Ocular Pathogens Using Gold Nanostars. *Biosens. Bioelectron.* **2014**, *61*, 386–390.

(16) Verma, M. S.; Chen, P. Z.; Jones, L.; Gu, F. X. Controlling "chemical Nose" Biosensor Characteristics by Modulating Gold Nanoparticle Shape and Concentration. *Sens. Bio-Sensing Res.* **2015**, 1–5.

(17) Daniel, M.; Astruc, D. Gold Nanoparticles : Assembly, Supramolecular Chemistry, Quantum-Size-Related Properties, and Applications toward Biology, Catalysis, and Nanotechnology. *Chem. Rev.* **2004**, *104* (1), 293–346.

(18) Hadano, S.; Handa, H.; Nagai, K.; Iyoda, T.; Li, J.; Watanabe, S. Surface-Enhanced Raman Scattering (SERS) Effect of Hexagonally Arranged Gold Nanoparticle Array with 29-Nm Particles and 23-Nm Gaps Using Liquid-Crystalline Block-Copolymer Template. *Chem. Lett.* **2013**, *42* (1), 71–73.

(19) De Rosa, C.; Auriemma, F.; Diletto, C.; Di Girolamo, R.; Malafronte, a.; Morvillo, P.; Zito, G.; Rusciano, G.; Pesce, G.; Sasso, a. Toward Hyperuniform Disordered Plasmonic Nanostructures for Reproducible Surface-Enhanced Raman Spectroscopy. *Phys. Chem. Chem. Phys.* **2015**, *17* (12), 8061–8069.

(20) Park, B.-W.; Kim, D.-S.; Yoon, D.-Y. Surface Modification of Gold Electrode with Gold Nanoparticles and Mixed Self-Assembled Monolayers for Enzyme Biosensors. *Korean J. Chem. Eng.* **2010**, *28* (1), 64–70.

(21) Kahl, M.; Voges, E.; Kostrewa, S.; Viets, C.; Hill, W. Periodically Structured Metallic Substrates for SERS. *Sensors Actuators B Chem.* **1998**, *51* (1-3), 285–291.

(22) Kimling, J.; Maier, M.; Okenve, V.; Kotaidis, V.; Ballot, H.; Plech, a; Okenve, B. Turkevitch Method for Gold Nanoparticle Synthesis Revisited. *J. Phys. Chem. B* **2006**, *110* (95 mL), 15700–15707.

(23) Grzelczak, M.; Pérez-Juste, J.; Mulvaney, P.; Liz-Marzán, L. M. Shape Control in Gold Nanoparticle Synthesis. *Chem. Soc. Rev.* **2008**, *37* (9), 1783–1791.

(24) Cao, J.; Sun, T.; Grattan, K. T. V. Gold Nanorod-Based Localized Surface Plasmon Resonance Biosensors: A Review. *Sensors Actuators, B Chem.* **2014**, *195*, 332–351.

(25) Putzbach, W.; Ronkainen, N. J. Immobilization Techniques in the Fabrication of Nanomaterial-Based Electrochemical Biosensors: A Review. *Sensors (Basel).* **2013**, *13* (4), 4811–4840.

(26) Fan, M.; Andrade, G. F. S.; Brolo, A. G. A Review on the Fabrication of Substrates for Surface Enhanced Raman Spectroscopy and Their Applications in Analytical Chemistry. *Anal. Chim. Acta* **2011**, *693* (1-2), 7–25.

(27) Shiohara, A.; Wang, Y.; Liz-Marzán, L. M. Recent Approaches toward Creation of Hot Spots for SERS Detection. *J. Photochem. Photobiol. C Photochem. Rev.* **2014**, *21*, 2–25.

(28) Pena-Pereira, F.; Duarte, R. M. B. O.; Duarte, A. C. Immobilization Strategies and Analytical Applications for Metallic and Metal-Oxide Nanomaterials on Surfaces. *TrAC Trends Anal. Chem.* **2012**, *40*, 90–105.

(29) Grabar, K. C.; Smith, P. C.; Musick, M. D.; Davis, J. a.; Walter, D. G.; Jackson, M. a.; Guthrie, A. P.; Natan, M. J. Kinetic Control of Interparticle Spacing in Au Colloid-Based Surfaces: Rational Nanometer-Scale Architecture. *J. Am. Chem. Soc.* **1996**, *118* (5), 1148–1153.

(30) Minard-Basquin, C.; Kügler, R.; Matsuzawa, N. N.; Yasuda, a. Gold-Nanoparticle-Assisted Oligonucleotide Immobilisation for Improved DNA Detection. *IEE Proc. Nanobiotechnol.* **2005**, *152* (2), 97–103.

(31) Chen, C.-D.; Cheng, S.-F.; Chau, L.-K.; Wang, C. R. C. Sensing Capability of the Localized Surface Plasmon Resonance of Gold Nanorods. *Biosens. Bioelectron.* **2007**, *22* (6), 926–932.

(32) Ballarin, B.; Cassani, M. C.; Scavetta, E.; Tonelli, D. Self-Assembled Gold Nanoparticles Modified ITO Electrodes: The Monolayer Binder Molecule Effect. *Electrochim. Acta* **2008**, *53* (27), 8034–8044.

(33) Hurst, K. M.; Ansari, N.; Roberts, C. B.; Ashurst, W. R. Self-Assembled Monolayer-Immobilized Gold Nanoparticles as Durable, Anti-Stiction Coatings for MEMS. *J. Microelectromechanical Syst.* **2011**, *20* (2), 424–435.

(34) Ori, G.; Gentili, D.; Cavallini, M.; Franchini, M. C.; Zapparoli, M.; Montorsi, M.; Siligardi, C. Immobilization of Monolayer Protected Lipophilic Gold Nanorods on a Glass Surface. *Nanotechnology* **2012**, *23* (5), 055605.

(35) Yagati, A. K.; Lee, T.; Min, J.; Choi, J.-W. Electrochemical Performance of Gold Nanoparticle-Cytochrome c Hybrid Interface for H2O2 Detection. *Colloids Surf. B. Biointerfaces* **2012**, *92*, 161–167.

(36) Wang, Y.; Tang, L. Chemisorption Assembly of Au Nanorods on Mercaptosilanized Glass Substrate for Label-Free Nanoplasmon Biochip. *Anal. Chim. Acta* **2013**, *796*, 122–129.

(37) Pallavicini, P.; Donà, A.; Taglietti, A.; Minzioni, P.; Patrini, M.; Dacarro, G.; Chirico, G.; Sironi, L.; Bloise, N.; Visai, L.; Scarabelli, L. Self-Assembled Monolayers of Gold Nanostars: A Convenient Tool for near-IR Photothermal Biofilm Eradication. *Chem. Commun. (Camb).* **2014**, *50* (16), 1969–1971.

(38) Ben Haddada, M.; Blanchard, J.; Casale, S.; Krafft, J.-M.; Vallée, A.; Méthivier, C.; Boujday, S. Optimizing the Immobilization of Gold Nanoparticles on Functionalized Silicon Surfaces: Amine- vs Thiol-Terminated Silane. *Gold Bull.* **2013**, *46* (4), 335–341.

(39) Okamoto, T.; Yamaguchi, I.; Kobayashi, T. Local Plasmon Sensor with Gold Colloid Monolayers Deposited upon Glass Substrates. *Opt. Lett.* **2000**, *25* (6), 372–374.

(40) Yang, Y.; Matsubara, S.; Nogami, M.; Shi, J.; Huang, W. One-Dimensional Self-Assembly of Gold Nanoparticles for Tunable Surface Plasmon Resonance Properties. *Nanotechnology* **2006**, *17*, 2821–2827.

(41) Morel, A.-L.; Volmant, R.-M.; Méthivier, C.; Krafft, J.-M.; Boujday, S.; Pradier, C.-M. Optimized Immobilization of Gold Nanoparticles on Planar Surfaces through Alkyldithiols and Their Use to Build 3D Biosensors. *Colloids Surf. B. Biointerfaces* **2010**, *81* (1), 304–312.

(42) Svorčík, V.; Kolská, Z.; Kvítek, O.; Siegel, J.; Rezníčková, A.; Rezanka, P.; Záruba, K. "Soft and Rigid" Dithiols and Au Nanoparticles Grafting on Plasma-Treated Polyethyleneterephthalate. *Nanoscale Res. Lett.* **2011**, *6* (1), 607.

(43) Řezníčková, A.; Kolská, Z.; Sajdl, P.; Švorčík, V. Grafting of Plasma Activated Polyethyleneterephthalate with Gold Nanorods. *Mater. Lett.* **2013**, *91*, 341–344.

(44) Ochiai, T.; Isozaki, K.; Nishiyama, S.; Miki, K. Enhancement of Self-Assembly of Large (>10 Nm) Gold Nanoparticles on an ITO Substrate. *Appl. Phys. Express* **2014**, *7* (6), 065001.

(45) Yang, W.; Wang, J.; Zhao, S.; Sun, Y.; Sun, C. Multilayered Construction of Glucose Oxidase and Gold Nanoparticles on Au Electrodes Based on Layer-by-Layer Covalent Attachment. *Electrochem. commun.* **2006**, *8* (4), 665–672.

(46) Lee, J. U.; Lee, W.; Yoon, S. S.; Kim, J.; Byun, J. H. Site-Selective Immobilization of Gold Nanoparticles on Graphene Sheets and Its Electrochemical Properties. *Appl. Surf. Sci.* **2014**, *315*, 73–80.

(47) Indrasekara, A. S. D. S.; Meyers, S.; Shubeita, S.; Feldman, L. C.; Gustafsson, T.; Fabris, L. Gold Nanostar Substrates for SERS-Based Chemical Sensing in the Femtomolar Regime. *Nanoscale* **2014**, *6* (15), 8891–8899.

(48) Ferhan, A. R.; Guo, L.; Kim, D.-H. Influence of Ionic Strength and Surfactant Concentration on Electrostatic Surfacial Assembly of Cetyltrimethylammonium Bromide-Capped Gold Nanorods on Fully Immersed Glass. *Langmuir* **2010**, *26* (14), 12433–12442.

(49) Brouwer, E. a M.; Kooij, E. S.; Wormeester, H.; Poelsema, B. Ionic Strength Dependent Kinetics of Nanocolloidal Gold Deposition. *Langmuir* **2003**, *19* (19), 8102–8108.

(50) Bubniene, U.; Oćwieja, M.; Bugelyte, B.; Adamczyk, Z.; Nattich-Rak, M.; Voronovic, J.; Ramanaviciene, a.; Ramanavicius, a. Deposition of Gold Nanoparticles on Mica Modified by Poly(allylamine Hydrochloride) Monolayers. *Colloids Surfaces A Physicochem. Eng. Asp.* **2014**, *441*, 204–210.

(51) Cant, N. E.; Critchley, K.; Zhang, H.-L.; Evans, S. D. Surface Functionalisation for the Self-Assembly of Nanoparticle/polymer Multilayer Films. *Thin Solid Films* **2003**, *426* (1-2), 31–39.

(52) Xiong, W.; Qu, Q.; Liu, S. Self-Assembly of Ultra-Small Gold Nanoparticles on an Indium Tin Oxide Electrode for the Enzyme-Free Detection of Hydrogen Peroxide. *Microchim. Acta* **2014**, *181* (9-10), 983–989.

(53) Liu, F. K.; Chang, Y. C.; Ko, F. H.; Chu, T. C.; Dai, B. T. Rapid Fabrication of High Quality Self-Assembled Nanometer Gold Particles by Spin Coating Method. In *Microelectronic Engineering*; 2003; Vol. 67-68, pp 702–709.

(54) Bhat, R. R.; Genzer, J. Tuning the Number Density of Nanoparticles by Multivariant Tailoring of Attachment Points on Flat Substrates. *Nanotechnology*. 2006, p 025301.

(55) Mayer, K.; Lee, S.; Liao, H.; Rostro, B. A Label-Free Immunoassay Based upon Localized Surface Plasmon Resonance of Gold Nanorods. *ACS Nano* **2008**, *2* (4), 687–692.

(56) Lee, S.; Mayer, K.; Hafner, J. Improved Localized Surface Plasmon Resonance Immunoassay with Gold Bipyramid Substrates. *Anal. Chem.* **2009**, *81* (11), 4450–4455.

(57) Kalies, S.; Heinemann, D.; Schomaker, M.; Gentemann, L.; Meyer, H.; Ripken, T. Immobilization of Gold Nanoparticles on Cell Culture Surfaces for Safe and Enhanced Gold Nanoparticle-Mediated Laser Transfection. *J. Biomed. Opt.* **2014**, *19* (7), 70505.

(58) Rajesh, K.; Sreedhar, B.; Radhakrishnan, T. P. Assembly of Gold Nanoparticles on a Molecular Ultrathin Film: Tuning the Surface Plasmon Resonance. *Chemphyschem* **2010**, *11* (8), 1780–1786.

(59) Nagel, J.; Chunsod, P.; Zimmerer, C.; Simon, F.; Janke, A.; Heinrich, G. Immobilization of Gold Nanoparticles on a Polycarbonate Surface Layer during Molding. *Mater. Chem. Phys.* **2011**, *129* (1-2), 599–604.

(60) Lee, J.; Hua, B.; Park, S.; Ha, M.; Lee, Y.; Fan, Z.; Ko, H. Tailoring Surface Plasmons of High-Density Gold Nanostar Assemblies on Metal Films for Surface-Enhanced Raman Spectroscopy. *Nanoscale* **2014**, *6* (1), 616–623.

(61) Tanaka, H.; Mitsuishi, M.; Miyashita, T. Tailored-Control of Gold Nanoparticle Adsorption onto Polymer Nanosheets. *Langmuir* **2003**, *19* (8), 3103–3105.

(62) E, S.; Shi, L.; Guo, Z. Tribological Properties of Self-Assembled Gold Nanoparticles on Silicon with Polydopamine as the Adhesion Layer. *Appl. Surf. Sci.* **2014**, *292*, 750–755.

(63) Ballerini, D.; Ngo, Y.; Garnier, G. Gold Nanoparticle-Functionalized Thread as a Substrate for SERS Study of Analytes Both Bound and Unbound to Gold. *AIChE …* **2014**, *60* (5).

(64) Bar, G.; Rubin, S.; Cutts, R. W.; Taylor, T. N.; Zawodzinski, T. a. Dendrimer-Modified Silicon Oxide Surfaces as Platforms for the Deposition of Gold and Silver Colloid Monolayers: Preparation Method, Characterization, and Correlation between Microstructure and Optical Properties. *Langmuir* **1996**, *12* (5), 1172–1179.

(65) Gole, A.; Orendorff, C.; Murphy, C. Immobilization of Gold Nanorods onto Acid-Terminated Self-Assembled Monolayers via Electrostatic Interactions. *Langmuir* **2004**, *20* (17), 7117–7122.

(66) Shao, L.; Ruan, Q.; Jiang, R.; Wang, J. Macroscale Colloidal Noble Metal Nanocrystal Arrays and Their Refractive Index-Based Sensing Characteristics. *Small* **2014**, *10* (4), 802–811.

(67) Guo, L.; Huang, Y.; Kikutani, Y.; Tanaka, Y.; Kitamori, T.; Kim, D.-H. In Situ Assembly, Regeneration and Plasmonic Immunosensing of a Au Nanorod Monolayer in a Closed-Surface Flow Channel. *Lab Chip* **2011**, *11* (19), 3299–3304.

(68) Gorji, M. S.; Razak, K. A.; Cheong, K. Y. Gold Nanoparticles Deposited on Linker-Free Silicon Substrate and Embedded in Aluminum Schottky Contact. *J. Colloid Interface Sci.* **2013**, *408*, 220–228.

(69) Zhang, F.; Srinivasan, M. P. Layer-by-Layer Assembled Gold Nanoparticle Films on Amine-Terminated Substrates. *J. Colloid Interface Sci.* **2008**, *319* (2), 450–456.

(70) Hu, X.; Cheng, W.; Wang, T.; Wang, Y.; Wang, E.; Dong, S. Fabrication, Characterization, and Application in SERS of Self-Assembled Polyelectrolyte-Gold Nanorod Multilayered Films. *J. Phys. Chem. B* **2005**, *109* (41), 19385–19389.

(71) Bracamonte, M. V.; Pérez, O. E. L.; Teijelo, M. L.; Rivas, G. a.; Ferreyra, N. F. Quaternized Chitosan Mediated Assembly of Gold Nanoparticles Multilayers. *Electrochim. Acta* **2014**, *146*, 178–185.

(72) Placido, T.; Fanizza, E.; Cosma, P.; Striccoli, M.; Curri, M. L.; Comparelli, R.; Agostiano, A. Electroactive Layer-by-Layer Plasmonic Architectures Based on Au Nanorods. *Langmuir* **2014**, *30* (10), 2608–2618.

(73) Yuan, W.; Li, C. M. Direct Modulation of Localized Surface Plasmon Coupling of Au Nanoparticles on Solid Substrates via Weak Polyelectrolyte-Mediated Layer-by-Layer Self Assembly. *Langmuir* **2009**, *25* (13), 7578–7585.

(74) Jiang, C.; Markutsya, S.; Tsukruk, V. V. Collective and Individual Plasmon Resonances in Nanoparticle Films Obtained by Spin-Assisted Layer-by-Layer Assembly. *Langmuir* **2004**, *20* (3), 882–890.

(75) Ishifuji, M.; Mitsuishi, M.; Miyashita, T. Bottom-up Design of Hybrid Polymer Nanoassemblies Elucidates Plasmon- Enhanced Second Harmonic Generation from Nonlinear Optical Dyes Bottom-up Design of Hybrid Polymer Nanoassemblies Elucidates Plasmon-Enhanced Second Harmonic Generation from Nonlinear O. *J.Am.Chem.Soc* **2009**, No. 12, 4418–4424.

(76) Sakai, N.; Sasaki, T.; Matsubara, K.; Tatsuma, T. Layer-by-Layer Assembly of Gold Nanoparticles with Titania Nanosheets: Control of Plasmon Resonance and Photovoltaic Properties. *J. Mater. Chem.* **2010**, *20* (21), 4371.

(77) Diamanti, S.; Arifuzzaman, S.; Genzer, J.; Vaia, R. Tuning Gold Nanoparticle− Poly (2-Hydroxyethyl Methacrylate) Brush Interactions: From Reversible Swelling to Capture and Release. *ACS Nano* **2009**, *3* (4), 807–818.

(78) Ferhan, A. R.; Kim, D.-H. In-Stacking: A Strategy for 3D Nanoparticle Assembly in Densely-Grafted Polymer Brushes. *J. Mater. Chem.* **2012**, *22* (4), 1274.

(79) Ferhan, A. R.; Guo, L.; Zhou, X.; Chen, P.; Hong, S.; Kim, D.-H. Solid-Phase Colourimetric Sensor Based on Gold Nanoparticle-Loaded Polymer Brushes: Lead Detection as a Case Study. *Anal. Chem.* **2013**, *85* (8), 4094–4099.

(80) Onses, M. S.; Nealey, P. F. Tunable Assembly of Gold Nanoparticles on Nanopatterned Poly(ethylene Glycol) Brushes. *Small* **2013**, *9* (24), 4168–4174.

(81) Onses, M. S. Fabrication of Nanopatterned Poly(ethylene Glycol) Brushes by Molecular Transfer Printing from Poly(styrene- Block -Methyl Methacrylate) Films to Generate Arrays of Au Nanoparticles. *Langmuir* **2015**, *31* (3), 1225–1230.

(82) Liu, Z.; Pappacena, K.; Cerise, J.; Kim, J.; Durning, C. J.; O'Shaughnessy, B.; Levicky, R. Organization of Nanoparticles on Soft Polymer Surfaces. *Nano Lett.* **2002**, *2* (3), 219–224.

(83) Bhat, R. R.; Genzer, J.; Chaney, B. N.; Sugg, H. W.; Liebmann-Vinson, A. Controlling the Assembly of Nanoparticles Using Surface Grafted Molecular and Macromolecular Gradients. *Nanotechnology* **2003**, *14* (10), 1145–1152.

(84) Bhat, R. R.; Genzer, J. Combinatorial Study of Nanoparticle Dispersion in Surface-Grafted Macromolecular Gradients. *Appl. Surf. Sci.* **2006**, *252* (7), 2549–2554.

(85) Oren, R.; Liang, Z.; Barnard, J. S.; Warren, S. C.; Wiesner, U.; Huck, W. T. S. Organization of Nanoparticles in Polymer Brushes. *J. Am. Chem. Soc.* **2009**, *131* (5), 1670–1671.

(86) Onses, M. S.; Liu, C.-C.; Thode, C. J.; Nealey, P. F. Highly Selective Immobilization of Au Nanoparticles onto Isolated and Dense Nanopatterns of poly(2-Vinyl Pyridine) Brushes down to Single-Particle Resolution. *Langmuir* **2012**, *28* (18), 7299–7307.

(87) Roiter, Y.; Minko, I.; Nykypanchuk, D.; Tokarev, I.; Minko, S. Mechanism of Nanoparticle Actuation by Responsive Polymer Brushes: From Reconfigurable Composite Surfaces to Plasmonic Effects. *Nanoscale* **2012**, *4* (1), 284–292.

(88) Fang, L.; Li, Y.; Chen, Z.; Liu, W.; Zhang, J.; Xiang, S.; Shen, H.; Li, Z.; Yang, B. Tunable Polymer Brush/Au NPs Hybrid Plasmonic Arrays Based on Host–guest Interaction. *ACS Appl. Mater. Interfaces* **2014**, *6* (22), 19951–19957.

(89) Kim, J. U.; O'Shaughnessy, B. Nanoinclusions in Dry Polymer Brushes. *Macromolecules* **2006**, *39* (1), 413–425.

(90) Jia, J.; Wang, B.; Wu, A.; Cheng, G.; Li, Z.; Dong, S. A Method to Construct a Third-Generation Horseradish Peroxidase Biosensor: Self-Assembling Gold Nanoparticles to Three-Dimensional Sol-Gel Network. *Anal. Chem.* **2002**, *74* (9), 2217–2223.

(91) Ouyang, R.; Bragg, S. a; Chambers, J. Q.; Xue, Z.-L. Flower-like Self-Assembly of Gold Nanoparticles for Highly Sensitive Electrochemical Detection of chromium(VI). *Anal. Chim. Acta* **2012**, *722*, 1–7.

(92) Hou, S.; Ou, Z.; Chen, Q.; Wu, B. Amperometric Acetylcholine Biosensor Based on Self-Assembly of Gold Nanoparticles and Acetylcholinesterase on the Sol-Gel/multi-Walled Carbon Nanotubes/choline Oxidase Composite-Modified Platinum Electrode. *Biosens. Bioelectron.* **2012**, *33* (1), 44–49.

(93) De Morais, A.; Silveira, G.; Villis, P. C. M.; Maroneze, C. M.; Gushikem, Y.; Pissetti, F. L.; Lucho, A. M. S. Gold Nanoparticles on a Thiol-Functionalized Silica Network for Ascorbic Acid Electrochemical Detection in Presence of Dopamine and Uric Acid. *J. Solid State Electrochem.* **2012**, *16* (9), 2957–2966.

(94) Redondo-Marugan, J.; Petit-Dominguez, M. D.; Casero, E.; Vázquez, L.; García, T.; Parra-Alfambra, a. M.; Lorenzo, E. Sol–gel Derived Gold Nanoparticles Biosensing Platform for Escherichia Coli Detection. *Sensors Actuators B Chem.* **2013**, *182*, 307–314.

(95) Singh, S.; Jain, D. V. S.; Singla, M. L. Sol–gel Based Composite of Gold Nanoparticles as Matix for Tyrosinase for Amperometric Catechol Biosensor. *Sensors Actuators B Chem.* **2013**, *182*, 161–169.

(96) White, R. J.; Luque, R.; Budarin, V. L.; Clark, J. H.; Macquarrie, D. J. Supported Metal Nanoparticles on Porous Materials. Methods and Applications. *Chem. Soc. Rev.* **2009**, *38* (2), 481–494.

(97) Zhong, L.-B.; Yin, J.; Zheng, Y.-M.; Liu, Q.; Cheng, X.-X.; Luo, F.-H. Self-Assembly of Au Nanoparticles on PMMA Template as Flexible, Transparent, and Highly Active SERS Substrates. *Anal. Chem.* **2014**, *86* (13), 6262–6267.

(98) Liao, H.; Hafner, J. H. Gold Nanorod Bioconjugates. *Chem. Mater.* **2005**, *17* (18), 4636–4641.

(99) O'Reilly, A. J.; Francis, C.; Quitoriano, N. J. Gold Nanoparticle Deposition on Si by Destabilising Gold Colloid with HF. *J. Colloid Interface Sci.* **2012**, *370* (1), 46–50.

(100) Lee, Y.-F.; Huang, C.-C. Colourimetric Assay of Lead Ions in Biological Samples Using a Nanogold-Based Membrane. *ACS Appl. Mater. Interfaces* **2011**, *3* (7), 2747–2754.

(101) Fontana, J.; Livenere, J.; Bezares, F. J.; Caldwell, J. D.; Rendell, R.; Ratna, B. R. Large Surface-Enhanced Raman Scattering from Self-Assembled Gold Nanosphere Monolayers. *Appl. Phys. Lett.* **2013**, *102* (20), 201606.

(102) Wang, Y.; Chen, H.; Wang, E. Facile Fabrication of Gold Nanoparticle Arrays for Efficient Surface-Enhanced Raman Scattering. *Nanotechnology* **2008**, *19* (10), 105604.

(103) Oh, M. K.; Yun, S.; Kim, S. K.; Park, S. Effect of Layer Structures of Gold Nanoparticle Films on Surface Enhanced Raman Scattering. *Anal. Chim. Acta* **2009**, *649* (1), 111–116.

(104) Rabani, E.; Reichman, D. R.; Geissler, P. L.; Brus, L. E. Drying-Mediated Self-Assembly of Nanoparticles. *Nature* **2003**, *426* (6964), 271–274.

(105) Bigioni, T. P.; Lin, X.-M.; Nguyen, T. T.; Corwin, E. I.; Witten, T. a; Jaeger, H. M. Kinetically Driven Self Assembly of Highly Ordered Nanoparticle Monolayers. *Nat. Mater.* **2006**, *5* (4), 265–270.

(106) Shi, X.-Z.; Shen, C.-M.; Wang, D.-K.; Li, C.; Tian, Y.; Xu, Z.-C.; Wang, C.-M.; Gao, H.-J. Surface-Enhanced Raman Scattering Properties of Highly Ordered Self-Assemblies of Gold Nanorods with Different Aspect Ratios. *Chinese Phys. B* **2011**, *20* (7), 076103.

(107) Chen, T. F.; Lu, S. H.; Wang, a. J.; Zheng, D.; Wu, Z. L.; Wang, Y. S. Detection of Explosives by Surface Enhanced Raman Scattering Using Substrate with a Monolayer of Ordered Au Nanoparticles. *Appl. Surf. Sci.* **2014**, *317* (3), 940–945.

(108) Kawamura, G.; Yang, Y.; Nogami, M. Facile Assembling of Gold Nanorods with Large Aspect Ratio and Their Surface-Enhanced Raman Scattering Properties. *Appl. Phys. Lett.* **2007**, *90* (26), 98–101.

(109) Xie, Y.; Guo, S.; Ji, Y.; Guo, C.; Liu, X.; Chen, Z.; Wu, X.; Liu, Q. Self-Assembly of Gold Nanorods into Symmetric Superlattices Directed by OH-Terminated Hexa(ethylene Glycol) Alkanethiol. *Langmuir* **2011**, *27* (18), 11394–11400.

(110) Xu, Z. C.; Shen, C. M.; Xiao, C. W.; Yang, T. Z.; Chen, S. T.; Li, H. L.; Gao, H. J. Fabrication of Gold Nanorod Self-Assemblies from Rod and Sphere Mixtures via Shape Self-Selective Behavior. *Chem. Phys. Lett.* **2006**, *432* (1-3), 222–225.

(111) Prevo, B. G.; Velev, O. D. Controlled, Rapid Deposition of Structured Coatings from Micro- and Nanoparticle Suspensions. *Langmuir* **2004**, *20* (6), 2099–2107.

(112) Prevo, B. G.; Fuller, J. C.; Velev, O. D. Rapid Deposition of Gold Nanoparticle Films with Controlled Thickness and Structure by Convective Assembly. *Chem. Mater.* **2005**, *17* (1), 28–35.

(113) Ahmed, W.; Glass, C.; Stefan Kooij, E.; van Ruitenbeek, J. M. Tuning the Oriented Deposition of Gold Nanorods on Patterned Substrates. *Nanotechnology* **2014**, *25* (3), 035301.

(114) Li, Q.; Zheng, J.; Liu, Z. Site-Selective Assemblies of Gold Nanoparticles on an AFM Tip-Defined Silicon Template. *Langmuir* **2003**, *19* (1), 166–171.

(115) Liu, S.; Maoz, R.; Sagiv, J. Planned Nanostructures of Colloidal Gold via Self-Assembly on Hierarchically Assembled Organic Bilayer Template Patterns with in-Situ Generated Terminal Amino Functionality. *Nano Lett.* **2004**, *4* (5), 845–851.

(116) Adams, S. M.; Campione, S.; Caldwell, J. D.; Bezares, F. J.; Culbertson, J. C.; Capolino, F.; Ragan, R. Non-Lithographic SERS Substrates: Tailoring Surface Chemistry for Au Nanoparticle Cluster Assembly. *Small* **2012**, *8* (14), 2239–2249.

(117) Tong, Q.; Malachosky, E. W.; Raybin, J.; Guyot-Sionnest, P.; Sibener, S. J. End-to-End Alignment of Gold Nanorods on Topographically Enhanced, Cylinder Forming Diblock Copolymer Templates and Their Surface Enhanced Raman Scattering Properties. *J. Phys. Chem. C* **2014**, *118* (33), 19259–19265.

(118) Hanske, C.; Tebbe, M.; Kuttner, C.; Bieber, V.; Tsukruk, V. V; Chanana, M.; König, T. A. F.; Fery, A. Strongly Coupled Plasmonic Modes on Macroscopic Areas via Template-Assisted Colloidal Self-Assembly. *Nano Lett.* **2014**, *14* (12), 6863–6871.

(119) Uddayasankar, U.; Krull, U. J. Analytical Performance of Molecular Beacons on Surface Immobilized Gold Nanoparticles of Varying Size and Density. *Anal. Chim. Acta* **2013**, *803*, 113–122.

(120) Flavel, B. S.; Nussio, M. R.; Quinton, J. S.; Shapter, J. G. Adhesion of Chemically and Electrostatically Bound Gold Nanoparticles to a Self-Assembled Silane Monolayer

Investigated by Atomic Force Volume Spectroscopy. *J. Nanoparticle Res.* **2009**, *11* (8), 2013–2022.

(121) Kaminska, A.; Inya-Agha, O.; Forster, R. J.; Keyes, T. E. Chemically Bound Gold Nanoparticle Arrays on Silicon: Assembly, Properties and SERS Study of Protein Interactions. *Phys. Chem. Chem. Phys.* **2008**, *10* (28), 4172–4180.

(122) Shiohara, A.; Langer, J.; Polavarapu, L.; Liz-Marzán, L. M. Solution Processed Polydimethylsiloxane/gold Nanostar Flexible Substrates for Plasmonic Sensing. *Nanoscale* **2014**, *6* (16), 9817–9823.

(123) Nikoobakht, B.; El-Sayed, M. a. Surface-Enhanced Raman Scattering Studies on Aggregated Gold Nanorods. *J. Phys. Chem. A* **2003**, *107* (18), 3372–3378.

(124) Manikas, A. C.; Romeo, G.; Papa, A.; Netti, P. a. Highly Efficient Surface-Enhanced Raman Scattering Substrate Formulation by Self-Assembled Gold Nanoparticles Physisorbed on poly(N -Isopropylacrylamide) Thermoresponsive Hydrogels. *Langmuir* **2014**, *30* (13), 3869–3875.

(125) Shiohara, A.; Novikov, S. M.; Solís, D. M.; Taboada, J. M.; Obelleiro, F.; Liz-Marzán, L. M. Plasmon Modes and Hot Spots in Gold Nanostar–Satellite Clusters. *J. Phys. Chem. C* **2014**.

(126) Tang, W.; Chase, D. B.; Rabolt, J. F. Immobilization of Gold Nanorods onto Electrospun Polycaprolactone Fibers via Polyelectrolyte Decoration--a 3D SERS Substrate. *Anal. Chem.* **2013**, *85* (22), 10702–10709.

(127) Lu, G.; Li, H.; Zhang, H. Gold-Nanoparticle-Embedded Polydimethylsiloxane Elastomers for Highly Sensitive Raman Detection. *Small* **2012**, *8* (9), 1336–1340.

(128) Chai, H.; Liu, H.; Guo, X.; Zheng, D.; Kutes, Y.; Huey, B. D.; Rusling, J. F.; Hu, N. Long Distance Electron Transfer Across >100 Nm Thick Au Nanoparticle/Polyion Films to a Surface Redox Protein. *Electroanalysis* **2012**, *24* (5), 1129–1140.

(129) Kong, Y.; Li, J.; Wu, S.; Cheng, W.; Rana, R. K.; Zhu, J.-J. Functionalization of Poly(o-Phenylenediamine) with Gold Nanoparticles as a Label-Free Immunoassay Platform for the Detection of Human Enterovirus 71. *Sensors Actuators B Chem.* **2013**, *183*, 187–193.

(130) Lee, Y.-F.; Deng, T.-W.; Chiu, W.-J.; Wei, T.-Y.; Roy, P.; Huang, C.-C. Visual Detection of copper(II) Ions in Blood Samples by Controlling the Leaching of Protein-Capped Gold Nanoparticles. *Analyst* **2012**, *137* (8), 1800–1806.

(131) Ishifuji, M.; Mitsuishi, M.; Miyashita, T. Enhanced Optical Second Harmonic Generation in Hybrid Polymer Nanoassemblies Based on Coupled Surface Plasmon Resonance of a Gold Nanoparticle Array. *Appl. Phys. Lett.* **2006**, *89* (1), 011903.

(132) Mitsuishi, M.; Ishifuji, M.; Endo, H.; Tanaka, H.; Miyashita, T. Hybrid Polymer Nanoassemblies: Polymer Nanosheets Organized with Metal Nanoparticle Arrays for Surface Plasmon Photonics. *Polym. J.* **2007**, *39* (5), 411–422.

(133) Huang, X.; Jain, P. K.; El-Sayed, I. H.; El-Sayed, M. a. Plasmonic Photothermal Therapy (PPTT) Using Gold Nanoparticles. *Lasers Med. Sci.* **2008**, *23* (3), 217–228.

(134) Maier, S. A.; Brongersma, M. L.; Kik, P. G.; Meltzer, S.; Requicha, A. A. G.; Atwater, H. A. Plasmonics - A Route to Nanoscale Optical Devices. *Adv. Mater.* **2001**, *13* (19), 1501–1505.

(135) Fasolato, C.; Domenici, F.; Sennato, S.; Mura, F.; De Angelis, L.; Luongo, F.; Costantini, F.; Bordi, F.; Postorino, P. Dimensional Scale Effects on Surface Enhanced Raman Scattering Efficiency of Self-Assembled Silver Nanoparticle Clusters. *Appl. Phys. Lett.* **2014**, *105* (7), 073105.

(136) Lee, J.; Hua, B.; Park, S.; Ha, M.; Lee, Y.; Fan, Z.; Ko, H. Tailoring Surface Plasmons of High-Density Gold Nanostar Assemblies on Metal Films for Surface-Enhanced Raman Spectroscopy. *Nanoscale* **2014**, *6* (1), 616–623.

(137) Maier, S. A.; Kik, P. G.; Atwater, H. A.; Meltzer, S.; Harel, E.; Koel, B. E.; Requicha, A. A. G. Local Detection of Electromagnetic Energy Transport below the Diffraction Limit in Metal Nanoparticle Plasmon Waveguides. *Nat. Mater.* **2003**, *2* (4), 229–232.

(138) Kim, D. S.; Honglawan, A.; Kim, K.; Kim, M. H.; Jeong, S.; Yang, S.; Yoon, D. K. Fabrication of Periodic Nanoparticle Clusters Using a Soft Lithographic Template. *J. Mater. Chem. C* **2015**, *3*, 4598–4602.

(139) Ung, T.; Liz-Marzán, L. M.; Mulvaney, P. Gold Nanoparticle Thin Films. *Colloids Surfaces A Physicochem. Eng. Asp.* **2002**, *202* (2-3), 119–126.

(140) Liu, K.; Resetco, C.; Kumacheva, E. Salt-Mediated Kinetics of the Self-Assembly of Gold Nanorods End-Tethered with Polymer Ligands. *Nanoscale* **2012**, *4* (20), 6574–6580.

(141) Cant, N. E.; Zhang, H.-L.; Critchley, K.; Mykhalyk, T. a.; Davies, G. R.; Evans, S. D. Fabrication and Characterization of Self-Assembled Nanoparticle/Polyelectrolyte Multilayer Films. *J. Phys. Chem. B* **2003**, *107* (49), 13557–13562.

(142) Yoo, D.; Shiratori, S. S.; Rubner, M. F. Controlling Bilayer Composition and Surface Wettability of Sequentially Adsorbed Multilayers of Weak Polyelectrolytes. *Macromolecules* **1998**, *31* (13), 4309–4318.

(143) Shiratori, S. S.; Rubner, M. F. pH-Dependent Thickness Behavior of Sequentially Adsorbed Layers of Weak Polyelectrolytes. *Macromolecules* **2000**, *33* (11), 4213–4219.

(144) Ariga, K.; Hill, J. P.; Ji, Q. Layer-by-Layer Assembly as a Versatile Bottom-up Nanofabrication Technique for Exploratory Research and Realistic Application. *Phys. Chem. Chem. Phys.* **2007**, *9* (19), 2319–2340.

(145) Ahn, H.-Y.; Lee, H.-E.; Jin, K.; Nam, K. T. Extended Gold Nano-Morphology Diagram: Synthesis of Rhombic Dodecahedra Using CTAB and Ascorbic Acid. *J. Mater. Chem. C* **2013**, *1* (41), 6861–6868.

(146) Ghosh, S.; Pal, T. Interparticle Coupling Effect on the Surface Plasmon Resonance of Gold Nanoparticles: From Theory to Applications. *Chem. Rev.* **2007**, *107*, 4797–4862.

(147) Wang, D.-S.; Lin, C.-W. Density-Dependent Optical Response of Gold Nanoparticle Monolayers on Silicon Substrates. *Opt. Lett.* **2007**, *32* (15), 2128–2130.

(148) Bohren, C. E.; Huffman, D. R. *Absorption and Scattering of Light by Small Particles*; John Wiley & Sons, 2008.

(149) Swinehart, D. F. The Beer-Lambert Law. *J. Chem. Educ.* **1962**, *39* (7), 333–335.

(150) Ricci, R. W.; Ditzler, M.; Nestor, L. P. Discovering the Beer-Lambert Law. *J. Chem. Educ.* **1994**, *71* (11), 983–985.

(151) Niklasson, G. a; Granqvist, C. G.; Hunderi, O. Effective Medium Models for the Optical Properties of Inhomogeneous Materials. *Appl. Opt.* **1981**, *20* (1), 26–30.

(152) Zhang, H.; He, H. X.; Wang, J.; Mu, T.; Liu, Z. F. Force Titration of Amino Group-Terminated Self-Assembledmonolayers Using Chemical Force Microscopy. *Appl. Phys. A Mater. Sci. Process.* **1998**, *66* (SUPPL. 1), 269–271.

(153) Choi, J.; Rubner, M. F. Influence of the Degree of Ionization on Weak Polyelectrolyte Multilayer Assembly. *Macromolecules* **2005**, *38* (1), 116–124.

(154) Bieker, P.; Schönhoff, M. Linear and Exponential Growth Regimes of Multilayers of Weak Polyelectrolytes in Dependence on pH. *Macromolecules* **2010**, *43* (11), 5052–5059.

(155) Notley, S. M.; Biggs, S.; Craig, V. S. J.; Wagberg, L. Adsorbed Layer Structure of a Weak Polyelectrolyte Studied by Colloidal Probe Microscopy and QCM-D as a Function of pH and Ionic Strength. *Phys. Chem. Chem. Phys.* **2004**, *6*, 2379–2386.

(156) Burke, S. E.; Barrett, C. J. Acid-Base Equilibria of Weak Polyelectrolytes in Multilayer Thin Films. *Langmuir* **2003**, *19* (8), 3297–3303.

(157) Schönhoff, M. Layered Polyelectrolyte Complexes: Physics of Formation and Molecular Properties. *J. Phys. Condens. Matter* **2003**, *15* (49), R1781–R1808.

(158) Zhang, S.; Liu, W.; Liang, J.; Li, X.; Liang, W.; He, S.; Zhu, C.; Mao, L. Buildup Mechanism of Carboxymethyl Cellulose and Chitosan Self-Assembled Films. *Cellulose* **2013**, *20* (3), 1135–1143.

(159) Heinze, T.; Koschella, A. Carboxymethyl Ethers of Cellulose and Starch - A Review. *Macromol. Symp.* **2005**, *223*, 13–39.

(160) Moskovits, M.; Hulse, J. E. The Ultraviolet–visible Spectra of Diatomic, Triatomic, and Higher Nickel Clusters. *J. Chem. Phys.* **1977**, *66* (9), 3988–3994.

(161) Kuzman, T.; Kutija, M. B.; Juri, J.; Jandroković, S.; Škegro, I.; Olujić, S. M.; Kordić, R.; Cerovski, B. Lens Wearers Non-Compliance-Is There an Association with Lens Case Contamination? *Contact Lens Anterior Eye* **2014**, *37* (2), 99–105.

(162) Kilvington, S.; Shovlin, J.; Nikolic, M. Identification and Susceptibility to Multipurpose Disinfectant Solutions of Bacteria Isolated from Contact Lens Storage Cases of Patients with Corneal Infiltrative Events. *Contact Lens Anterior Eye* **2013**, *36* (6), 294–298.

(163) Furuhata, K.; Ishizaki, N.; Kawakami, Y.; Fukuyama, M. Bacterial Contamination of Stock Solutions in Storage Cases for Contact Lens, and the Disinfectant-Resistance of Isolates. *Biocontrol science*. 2010, pp 81–85.

(164) Chae, E. J.; Lee, J. H.; Oh, B. K.; Choi, J. W. Label-Free Nanobiosensor to Detect Infectious Bacterica Based on SERS. *J. Biomed. Nanotechnol.* **2013**, *9* (4), 659–663.

(165) Wang, L.; Wei, Q.; Wu, C.; Hu, Z.; Ji, J.; Wang, P. The Escherichia Coli O157:H7 DNA Detection on a Gold Nanoparticle-Enhanced Piezoelectric Biosensor. *Chinese Sci. Bull.* **2008**, *53* (8), 1175–1184.

(166) Peeters, E.; Nelis, H. J.; Coenye, T. Comparison of Multiple Methods for Quantification of Microbial Biofilms Grown in Microtiter Plates. *J. Microbiol. Methods* **2008**, *72* (2), 157–165.

(167) Kim, J. Y.; Lee, J. S. Synthesis and Thermally Reversible Assembly of DNA - Gold Nanoparticle Cluster Conjugates. *Nano Lett.* **2009**, *9* (12), 4564–4569.

(168) Mendelsohn, J. D.; Barrett, C. J.; Chan, V. V.; Pal, A. J.; Mayes, A. M.; Rubner, M. F. Fabrication of Microporous Thin Films from Polyelectrolyte Multilayers. *Langmuir* **2000**, *16* (11), 5017–5023.

(169) Bridier, a.; Briandet, R.; Thomas, V.; Dubois-Brissonnet, F. Resistance of Bacterial Biofilms to Disinfectants: A Review. *Biofouling* **2011**, *27* (9), 1017–1032.